Fourier Transform Ion Cyclotron Resonance Imaging Mass Spectrometry

Development of instrumentation, data acquisition software and data processing methods

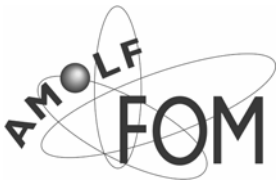

The work described in this thesis was performed at the FOM Institute for Atomic and Molecular Physics, Kruislaan 407, 1098 SJ Amsterdam, The Netherlands.

ISBN: 978-90-77209-20-2

Fourier Transform Ion Cyclotron Resonance Imaging Mass Spectrometry
Developments of instrumentation, data acquisition software and data processing methods

2008 © Ioana Mihaela Barbu (iomiba@yahoo.com)

Fourier Transform Ion Cyclotron Resonance Imaging Mass Spectrometry

Development of instrumentation, data acquisition software and data processing methods

Fourier Transform Ion Cyclotron Resonance afbeelding massa spectrometrie
Ontwikkeling van instrumentatie, data acquisitie software en data verwerking methoden
(met een samenvatting in het Nederlands)

Proefschrift
ter verkrijging van de graad van doctor aan de Universiteit Utrecht
op gezag van de rector magnificus, prof. dr. J. C. Stoof, ingevolge het besluit
van het college voor promoties in het openbaar te verdedigen
op woensdag 9 april 2008 des middags te 14.30 uur

door

Ioana Mihaela Barbu
geboren op 10 januari 1979, te Roemenie

Promotor: Prof. dr. R.M.A. Heeren

Co-promotor: Dr. L.A. McDonnell

Part of this work was carried out in the context of the Virtual Laboratory for e-Science project (www.vl-e.nl) and was supported by a BSIK grant from the Dutch Ministry of Education, Culture and Science (OC&W), part of the ICT innovation program of the Ministry of Economic Affairs (EZ).
The Netherlands Proteomics Centre and Bruker Daltonics financially supported this project.
The imaging MS studies are part of research program of the "Stichting voor Fundamenteel Onderzoek der Materie (FOM)", which is financially supported by the "Nederlandse organisatie voor Wetenschappelijk Onderzoek (NWO)".

It would be possible to describe everything scientifically, but it would make no sense; it would be without meaning, as if you described a Beethoven symphony as a variation of wave pressure.

Albert Einstein

Contents

1. Introduction **11**

1.1 Challenges in proteomics 12
1.2 Imaging mass spectrometry 14
1.3 Ionisation techniques in IMS 19
1.4 Mass analysers and hybrid mass spectrometers used in IMS 23
1.5 Data acquisition and processing 25
1.6 FTICR-MS and molecular imaging 26
1.7 Scope of the thesis 27

2. Fourier Transform Ion Cyclotron Mass Spectrometry and imaging basic concepts **20**

2.1 FTICR-MS principles of operation 21
2.1.1 Ion motion in the cell 30
2.1.2 Ion excitation and detection 34
2.1.3 Fragmentation techniques 38
2.2 Experimental description of the instrument 41
2.3 FTICR-MS in imaging mass spectrometry 46

3. A novel workflow control system for FTICR-MS allows for unique on-the-fly data-dependent decisions **55**

3.1 Introduction of the workflow-based method 56
3.1.1 Materials and methods 58
3.1.2 Description of the modules used in the workflow-based method AWG3 65
3.1.3 Results and discussion 69
3.1.4 Conclusions and outlook 79

3.2 On-the-fly data-dependent decisions in quantitative proteomic studies 80
3.2.1 Materials and methods 82
3.2.2 Results 84
3.2.3 Discussion and conclusions 88

4. Imaging of peptides in rat brain tissue using MALDI-FTICR mass spectrometry 89
4.1 Introduction 90
4.2 Experimental 92
4.3 Results and discussion 94
4.4 Conclusions 100

5. Parallel processing of large datasets from FTICR-MS measurements 103
5.1 Introduction 104
5.2 Methodology 107
5.3 Experimental 112
5.3.1 NanoLC-FTICR-MS 112
5.3.2 Samples and protein identification 113
5.3.3 Programming software: PP-VLAM and parallel Processing 114
5.3.4 Computer hardware 115
5.4 Results and discussion 116
5.4.1 Evaluation of the PP-VLAM algorithm using protein standards 116
5.4.2 Scan precision and mass accuracy 117
5.4.3 Visualization of peptide profiles from CSF samples: "a real life example" 119
5.4.4 Speed benefits of distributed computing of

large mass spectral datasets 122
5.5 Conclusions 123

Appendix 1 Design and results of a high performance linear accumulation octopole with enhanced ejection capabilities 125
A1.1 Introduction 126
A1.2 Description of the simulated accumulation octopoles 129
A1.3 SIMION simulations 130
A1.4 Results and discussion 133
A1.5 Conclusions 141

Bibliography 142

Summary 161

Samenvatting 166

Acknowledgments 170

Curriculum Vitae 174

List of publications 175

1

Introduction

Imaging mass spectrometry (IMS) is a technique that can provide both chemical specificity and spatial localization of molecules directly from tissue sections, single cells and other surfaces. Developments in sensitivity, mass resolution, and spatial resolution have been the main focus of several research groups. Now, the use of hybrid instruments allows ion fragmentation for molecular identification as well as distinguishing between isobaric ions. Developments of instrumentation, acquisition software and data processing of Fourier transform ion cyclotron mass spectrometer that extend experimental possibilities in the field of imaging mass spectrometry will be described in this thesis.

Chapter 1

1.1 Challenges in proteomics

Proteomics deals with proteins, the products of the genome that contain the whole hereditary information encoded in DNA[1-3]. Proteins are organic compounds made of amino acids. The sequence of amino acids in a protein is defined by a gene and encoded in the genetic code. While the genome is a rather constant entity, the proteome differs from cell to cell and is constantly changing through its biochemical interactions with the genome and the environment. Any organism has radically different protein expression levels in different parts of its system, in different stages of its life cycle and influenced by different environmental conditions. Furthermore, a single complex organism such as a human being contains a very high number of different proteins, each having different functions. Not genes but their products, proteins, are directly involved in almost all biological processes therefore sequencing the human genome is not enough to explain biological functions[4]. Here, proteomics plays an important role by giving us information about protein's localization, expression level, association with other proteins or molecules, posttranslational modifications, and splicing[2,5-10]. The latter two factors increase the number of distinct proteins and thus increase the complexity of the system when compared to the protein coding genes.

Analysing an organism's proteome is anything but simple and therefore extensive investigations of new methods and techniques are carried out by different life-science disciplines. There is still no single method or instrument that gives a final result about identification, quantification, and localization of the expressed proteins in a biological system[11]. Thus, different methods and techniques are often combined in order to get information about complex protein samples[2,11]. Analytical biochemical methods such as one or two dimensional polyacrylamide gels (separation matrices used in electrophoresis of biomolecules) were initially used to study proteins[12-14]. However, even in the case when gels were reproducible, the determination and identification of low

abundant proteins were difficult. Moreover, the lack of rapid analytical methods for peptide characterization was another drawback of the 2D gels. Now, modern mass spectrometry (MS) can rapidly identify small amounts of proteins from very complex mixtures[2]. The identification of peptides (containing a smaller number of amino acids) and proteins (containing a larger number of amino acids) generally requires the identification of the amino acids present in the sequence. Currently, most methods of protein identification involve enzymatic digestion to produce proteolytic peptides, combined with chromatographic (peptides separation) and mass spectrometric analysis of these peptides. By using mass spectrometry, the peptides can be subjected to different sort of fragmentation techniques to obtain their amino-acid sequences. The use of mass spectrometry was a major forward step in biomedical research by the increase of sensitivity, robustness and data handling. Primary sequences of proteins, post-translational modifications and protein-protein interactions have been successfully analysed by MS. Recently developed methodologies offer the opportunity to obtain quantitative proteomic information by labelling the peptides with stable isotopes. Comparing the signals from the same peptide under different conditions gives relative estimates of protein abundance. Functional information of the proteins and temporal changes can be traced in this manner[15]. In clinical research, mass spectrometry opens new ways by detecting patterns of differentially expressed proteins in blood or serum in patient and control samples. Such strategies have been exploited to determine biomarkers (indicator of a biological state) that can be correlated with certain diseases[5,11,16]. Mass spectrometry based proteomics is now one of a number of different approaches being used to investigate human biology, diseases and drug discovery. However, only identifying the proteins present in biological samples is not sufficient in the study of diseased tissue or drug discovery[5,16]. Lists of proteins that are differentially expressed do not show if the proteins are the cause of the cellular changes or if they are effects of these changes. To understand the protein function in cellular networks, the molecules playing an active role have to be locally monitored in the cell at any point in time[17].

Subcellular localization of proteins at different moments in time can often provide a better understanding of how proteins works individually and with their interaction partners[18].

Fluorescent microscopy and immunostaining are mostly used for protein localization[19-22]. The use of multiple fluorescent labels in a single experiment makes it possible to study the spatial behaviour of multiple selected molecules at the same time in one experiment. However, only a limited number of molecules can be studied. Specifying post-translational modifications can be difficult and unknown molecules cannot be detected[23]. A technique that can provide both chemical specificity and spatial localization is imaging mass spectrometry (IMS). The ability to map the distribution of hundreds of compounds in one experiment, which allows their localization to be determined in parallel, without labelling and from native samples makes imaging MS an attractive discovery technique[16,24-28]. Nevertheless, IMS is an emerging technique and challenges remain. Lately, significant progress has been made in improving the speed and spatial resolution of IMS. Now, methodological and instrumental improvements are moving towards developments that give not only information about chemical specification but also chemical identification. In this context, further in this thesis, new instrumentation and methods for IMS are described.

1.2 Imaging mass spectrometry

In standard proteomics studies, large populations of cells are harvested, a homogenate mixture prepared and subsequently analysed with MS. However, many times in the case of various diseases, only a few cells show a difference between a healthy and a diseased tissue[29]. Here, tissue homogenates analysis becomes problematic. With sufficient spatial resolution and sensitivity IMS would overcome this limitation. Moreover, spatial analysis of tissues or cells can be

investigated without removing them from their original environment. IMS can rapidly identify which proteins are associated with tumour and non-tumour tissue[30]. Information about the localization of compounds such as peptides and lipids on tissue increased the knowledge about their role in various clinical disorders such as Alzheimer's[31,32] and Parkinson diseases[33]. Furthermore, the way a drug treatment affects different parts of the body[16] or tracing an administrated drug and its metabolites are emerging an powerful applications for IMS. The fact that not only the parent molecule but also possible metabolites formed after the drug administration can be detected with IMS makes this technique attractive[31,34,35].

Mass spectrometry is an analytical technique that measures ions according to their mass-to-charge ratio. A typical mass spectrometer is composed of three parts: an ion source, a mass analyser, and a detector. IMS is a technique that is generally performed by scanning an ionising beam across a sample or moving the sample in the field of a laser beam in an organized raster. Mass spectral analysis of each localized spot of the raster provides chemical information for each position (see Figure 1.3a). Such spatially correlated datasets can be used to construct an image for each detected mass. As an example, Figure 1.1a shows molecular images from a raster over the surface of mouse brain tissue sections with consecutive laser shots. The laser position was fixed and the sample plate was repositioned for consecutive spots. Each spot (corresponding to a pixel in the images) produced a mass spectrum obtained from molecules present within the irradiated area.

Information about the distribution of different compounds in a biological system is obtained by taking advantage of both the sensitivity and specificity of mass spectrometry and the imaging capabilities. Ionisation techniques play an important role. Matrix-assisted laser desorption ionisation (MALDI)[27,28,36] and electrospray ionisation (ESI)[37-39] are soft ionisation techniques compared with earlier ionisation techniques and they are considered milestones in the field of MS for large biomolecules. The detection of large intact biomolecules, e.g. proteins, was not possible before the development of MALDI and ESI. Currently,

MALDI and ESI are the most popular ionisation techniques due to the low sample consumption (sub-femtomoles), sensitivity, speed, and wide mass range covered. These characteristics have seen them acquire dominant positions in mass spectrometry.

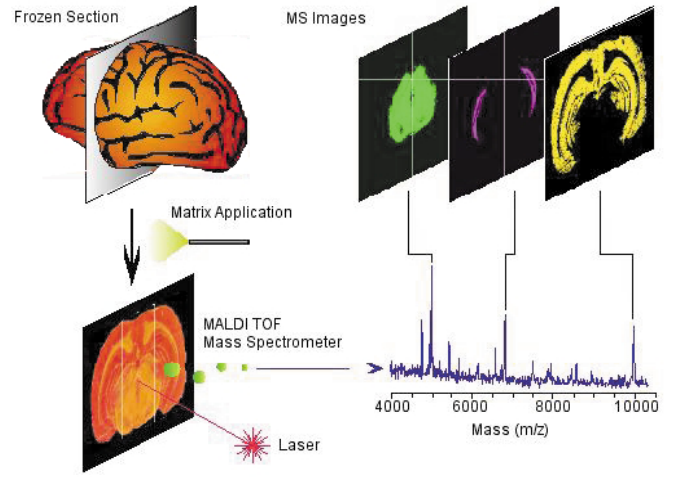

Figure 1.1. Molecular image of brain by IMS. A pulsed UV laser desorbs and ionises analytes from the tissue and their *m/z* values are determined using a time-of-flight analyser. From a raster over the tissue and measurement of the peak intensities over thousands of spots, mass spectrometric images are generated at specific molecular weight values. Taken from reference 26.

ESI ionises the analyte from the solution phase. The sample is sprayed into the mass spectrometer through a needle by applying a high potential difference between the needle and the inlet of the mass spectrometer (Figure 1.2a). Many biological applications have become possible by using ESI[40-42], however the solution phase aspect limits its imaging capabilities. It was recently shown how sample voxelization combined with cutting-edge ESI-based mass spectrometry analysis can provide the low spatial resolution distributions of a large number of proteins covering a wide dynamic range. In this experiment the sample, a mouse brain, was divided into an array of 1 mm^3 cubes. Each cube, or voxel, was then subjugated to a complete homogenisation-ESI-based proteomics

analysis. This construction of a 3D protein map of the brain is very useful for comparison with other techniques but is too slow, 71 voxels analysed in 7 days, for any practical investigation. For imaging experiments, MALDI is the method of choice. In a regular MALDI experiment the analyte is combined with a matrix, typically a small aromatic acid, which strongly absorbs the laser radiation. MALDI volatilises and ionises the sample out of the matrix by laser interaction (Figure 1.2b). Nowadays, MALDI-MS is a well-established technique for fast determination of the molecular mass of macromolecular species from biological samples. Using MALDI, many proteins can also be analysed directly from the tissue sections. Among the various imaging ionisation techniques MALDI is the one used to record macromolecular distributions directly from native sample like tissue sections[26,43]. Alternative ionisations techniques in IMS will be briefly discussed in the next section.

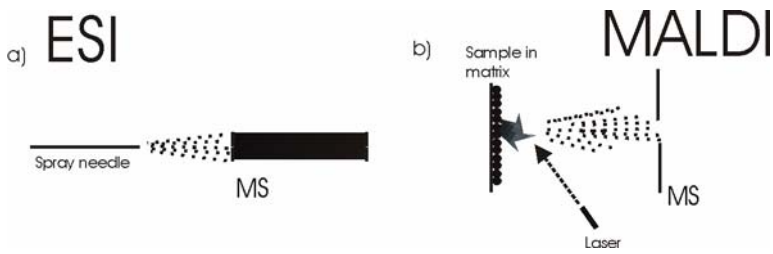

Figure 1.2. a) ESI and b) MALDI ionisation techniques.

Methods to obtain spatial information in IMS

Two mass spectrometric imaging approaches currently exist: microprobe and microscope mode imaging. In microprobe IMS experiments, the ionisation beam is rastered over the sample surface or the sample stage moved in the field of ionisation beam, and a mass spectrum recorded at each x,y-coordinate (see Figure 1.3a). Mass resolved images or spectra from regions of interest are then extracted from this dataset of position-correlated spectra. An alternative approach for high spatial resolution IMS is the mass microscope (see Figure

1.3b). Here the spatial resolution is independent of the spot size of the ionising laser beam, but solely dependent on the ion optics of the instrument and the kinetic energy distribution of the generated ions. Compared to microprobe experiments the spatial information from within the ionisation spot is not lost. The desorbed molecules retain their spatial distribution during mass analysis and are projected onto a position sensitive detector. For ionisation techniques such as MALDI, which is not compatible with a small ionisation beam, such stigmatic ion imaging is valuable.

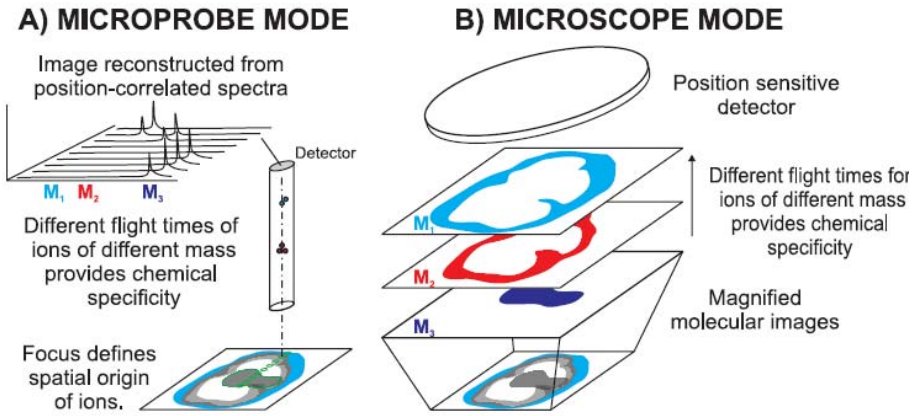

Figure 1.3. Schematics of the two different approaches to IMS a) microprobe mode b) microscope mode. Taken from reference 68.

There is no mass spectrometer that can simultaneously provide the highest sensitivity, mass resolution, accuracy, and spatial resolution. Depending on the type of information required, different combinations of ionisation techniques and mass analysers are used. Before talking more detailed about ionisation techniques and mass analysers used in IMS, a short explanation of these parameters is given below. Mass resolution represents the ability to separate two adjacent masses:

$$R = m / \Delta m \quad (1.1)$$

It measures the "sharpness" of the MS peak. The mass accuracy is the difference between the theoretical mass and the measured mass:

$$\Delta m_{accuracy} = m_{experimental} - m_{theoretical} \quad (1.2)$$

Mass accuracy indicates the accuracy of the mass information provided by the mass spectrometer. And it is linked to the mass resolution. If the peak is not "sharp" enough the difference between the measured mass and theoretical mass is more dependent on the peak-picking algorithm. A low-resolution instrument cannot provide high mass accuracy. For imaging instruments spatial resolution is an other important parameter. It is commonly defined in the IMS field as the distance between the centres of two neighbouring pixels. This simple 'pixel-size' definition is easily determined with the use of a calibration target but omits all other factors that can determine which length scales can be reliably resolved in an imaging mass spectrometry experiment, for example microscope mode imaging experiments have reported 600 nm pixel size but 4 μm resolving power.

1.3 Ionisation techniques in IMS

The first imaging mass spectrometry experiments were performed using secondary ion mass spectrometry (SIMS)[44]. However, as stated previously, IMS of large biomolecules, using their intact molecular ions, only became possible after the invention of the soft ionisation technique MALDI[28]. Since then, new ionisation techniques and instrumentation have been developed and have become interesting for different applications[26,31-33]. These developments are briefly described here and in sections 1.4 and 1.5.

MALDI is the method of choice for recording molecules at high masses, up to several hundreds of kilodaltons, such as intact proteins, oligonucleotides, and carbohydrates. The success of MALDI is due to the physics of photo-ablation of the matrix and gas-phase chemistry of the excited matrix molecules. Application of a matrix solution to a tissue section extracts the molecules from the sample and leads to the formation of analyte-doped matrix crystals. This co-crystallisation segregates the analytes from detrimental co-factors such as salts and disentangles and isolates the large molecules in a sea of matrix. Ablation of these crystals with a UV laser directs a cooperative motion of the matrix into the vacuum, in which the analyte is entrained. Ablation ejects matrix, entrained analyte, and clusters into the gas phase. Evidence for this entrainment mechanism is the near independence of the initial velocity of the analyte ions on the mass of the analyte but its dependence on the matrix and post ionisation of such clusters.

Ablation of the analyte-entrained matrix into the gas phase is the mechanism by which intact macromolecules are desorbed. Equally important is the ionisation of the desorbed species as it greatly influences which ions are seen in the mass spectrum. Proton and cation transfer reactions occur throughout the ablated plume, the final products being determined by the relative proton/cation affinities of the species present in the plume. Breuker et al. have shown that when enough material is ablated to ensure many collisions within the plume, the analytes observed in the final spectrum are largely under thermodynamic control. Karas and Knochennmus have extensively reviewed the role of these in-plume processes[45-48]. To reduce the amount of cationised peptides and proteins in imaging mass spectrometry of tissue sections, which can complicate spectral assignment as well as lower signal intensities, the tissue sections are often desalted by washing in cold ethanol solutions or other solvent mixtures.

UV and IR MALDI experiments have been performed, but UV MALDI is by far the most common due to its higher sensitivity for peptides and proteins and the lower amount of matrix removed[49,50]. However, in the case of labile

complexes, the softer ionisation method IR MALDI can be more suitable[51]. The ion signal dependence on the constituents of the plume can manifest itself as ion suppression effects, in which the presence of other analytes affects the signal of the analyte(s) of interest. Seeding tissue sections with some model peptides is normally sufficient to detect whether ion suppression is a complicating factor.

Sample preparation and matrix deposition are important parameters in MALDI imaging, thus a lot of effort is being put in to these developments. Common matrix materials are cinnamic acid derivatives (e.g. sinapinic acid (SA) and 4-hydroxy-α-cyanocinnamic acid (HCCA)) and 2,5-dihydroxybenzoic acid (DHB). The proper choice of matrix leads to more sensitive analysis and is empirically determined for different molecular classes[52]. For tissue analysis of proteins, sinapinic acid provides the best signal whereas HCCA is suitable for lower molecular weight peptides[53]. On the other hand, DHB has been found to provide better signal for lipids[54,55]. To obtain higher spatial resolution sinapinic acid is suggested[56]. For ion fragmentation, matrices that produce ions with high internal energy are used[57].

In SIMS, the sample surface is bombarded with high-energy (5-25 KeV) primary ions (single- or polyatomic) that lead to the sputtering of ions and neutral species from the upper most region of the sample (SIMS is considered a surface sensitive technique). Biomolecular analysis using SIMS has traditionally been limited to low mass molecular fragments. However modern developments have increased the sensitivity of SIMS for larger molecular ions up to 1000 Da. This has been the result several distinct strategies for increasing the molecular ion yield. This includes the development of polyatomic primary ion sources (e.g. C_{60}^+, SF_6^-, Au_n^+, Bi_n^{m+})[58,59], matrix deposition (matrix-enhanced SIMS, ME-SIMS)[52,60], and sample coating (Metal-Assisted SIMS, Meta-SIMS)[61-64] with a thin layer of gold or silver (1 nm).

The spatial resolution obtained in MALDI microprobe imaging is typically in the 100 - 200 μm range, limited by the size of the laser spot used[30,56], and 50 nm – 2 μm for SIMS[65]. Generally, SIMS provides high spatial resolution data about elements, low mass molecules and lipids while MALDI is used for low

spatial resolution peptide and protein analysis. The development of micrometer resolution microprobe MALDI imaging has been reported[66], however decreasing spot size has been found to lead to decreasing sensitivity for high mass species. A decrease in sensitivity of two orders of magnitude was observed when a regular laser diameter of 100 µm was decreased to 7-8 µm[67]. In the mass microscope mode, the spatial resolution is about 4 µm[68] and independent of the spot size of the ionising laser beam, but solely dependent on the ion optics of the instrument and the kinetic energy distribution of the generated ions. Microscope mode imaging mass spectrometry necessitates the use of time-of-flight (TOF) instruments with specifically designed ion optics and detectors. The triple ion focusing time-of-flight, TRIFT, mass spectrometer transports a magnified ion image to a position-sensitive detector and uses three hemi-spherical electrostatic analysers to provide energy focusing and thus high mass resolution. Mass spectra are recorded by measuring the time difference between pulsing of the ionisation source and arrival of ions at the detector. Recently, multi-turn time-of-flight mass spectrometers (MULTUM)[69] also proved to be suitable for imaging in stigmatic mode.

Besides MALDI and SIMS, desorption electrospray ionisation (DESI) should be mentioned here. DESI is a recent ionisation technique that can be used in imaging mass spectrometry[70]. Here, charged droplets and ions of solvent are electrosprayed onto the surface to be analysed. During their interaction with the surface the charged droplets can collect surface compounds. The resulting mass spectra are similar to normal ESI mass spectra in that they show mainly singly or multiply charged molecular ions of the analytes. DESI has attracted scientific attention from its introduction because it provides an ambient pressure technique for macromolecular analysis of different compounds on various surfaces (*e.g.* solids samples, (frozen) liquids, or biological tissues)[71,72]. This rapid and rather simple method, which can be readily implemented on existing ESI instruments, does not require any sample preparation[70,73,74] and the ambient nature of the technique means that samples can be analysed in their native environment[75]. However, compared to other ionisation techniques DESI is

less sensitive and the spatial resolution is low, since the size of the DESI ionisation beam is in the order of 0.5 to 1 mm.

1.4 Mass analysers and hybrid mass spectrometers used in IMS

Depending of the type of ionisation technique and the type of information needed, different mass analysers can be used in IMS. The 3D and 2D ion traps, Fourier transform ion cyclotron mass spectrometer (FTICR-MS), Orbitrap, and TOF-MS are five types of basic mass analysers in mass spectrometry. A schematic of these mass analysers is shown in the figure 1.4. As ionisation techniques, ESI is mostly used with ion traps. MALDI is usually coupled with TOF instruments.

The type of mass analyser used in an IMS experiment is ideally determined by the questions that need to be address but is more often limited by their availability. In this section, a brief overview over the drawbacks and advantages of the mass analysers used in IMS is sketched.

Ion traps An ion trap uses specially designed electrodes onto which a radio-frequency (RF) time varying electric field is applied, to trap ions and subject them to mass analysis or tandem mass analysis (MS and MS/MS)[76]. MS/MS is the combination of two or more MS experiments. The aim of MS/MS experiments is either to get structural information by fragmenting the ions isolated during the first MS experiment, and/or to achieve better selectivity and sensitivity for quantitative analysis.

The linear trap (two dimensional trap) uses a set of quadrupole rods to confine ions radially and a static electrical potential on end electrodes to confine the ions axially (see Figure 1.4b). 2D ion trap produces reasonable mass accuracy, mass resolution and sensitivity[77,78]. Imaging of small molecules in

tissue sections have been performed using a linear ion trap. Phospholipids and peptides in tissue sections were imaged and identified[54,79,80]. An ion trap can be a useful instrument in imaging due to its fragmentation possibilities and relative fast duty cycle. However it is limited to imaging of small molecules due to its relatively narrow mass range.

FTICR-MS is more complex: it is operated at high vacuum (10^{-9} mbar) and uses a combination of electric and a strong magnetic field, providing high mass resolution, mass accuracy, and sensitivity[81-84] (see Figure 1.4d; a detailed description can be found in Chapter 2). Up until recently, FTICR was considered by many to be expensive and not as easy to use as other instruments. The high potential of FTICR-MS has seen many improvements in the user interface, making it more accessible to non-experts as well as adding flexibility. FTICR-MS is not a very fast technique but it can be very attractive for IMS as its mass accuracy, mass resolution and many fragmentation options allow many biomolecules to be distinguished and identified. The first FTICR-MS imaging experiments have been recently shown[85].

Time-of-flight instruments

The ***TOF*** mass analyzer[86,87] can be a linear flight tube, a reflectron, TRIFT or MULTUM that separates ions based on their time-of-flight (velocity) as in Figure 1.4e. It is a sensitive detector although the mass accuracy and mass resolution is not as high as for FTICR-MS. TOF instruments are the most commonly used instruments in IMS due to their speed, high sensitivity and good mass accuracy[24]. However, ion isolation and fragmentation, to obtain the structural fragments for its subsequent identification, is not possible with a simple TOF instrument. Modern TOF instruments are mostly hybrid instruments that combine the advantages of a TOF analyser with the identification capabilities.

Hybrid mass spectrometers

Not all mass analysers have the possibility of inducing the protein/peptide fragmentation required to obtain the structural fragments used for identification.

Different instruments can be coupled to obtain the desired information about the sample by performing MS/MS. Ion traps and triple quadrupole instruments can be used for ion fragmentation[88,89]. TOF analysers need to be coupled with ion collision cells (e.g. TOF- collision cell- TOF[90]; quadrupole mass filter- collision cell- TOF[91]). Generally, the ion fragmentation technique used in collision cells is collision-induced dissociation (ions fragment by collisions with gas). Hybrid TOF instruments are widely used in proteomics due to their ease of use. Hybrid TOF instruments are also very useful for IMS owing to their combination of speed, sensitivity, fragmentation capabilities as well as ion manipulation (e.g. to select one *m/z* value before detection to enhance the selectivity of the experiment).

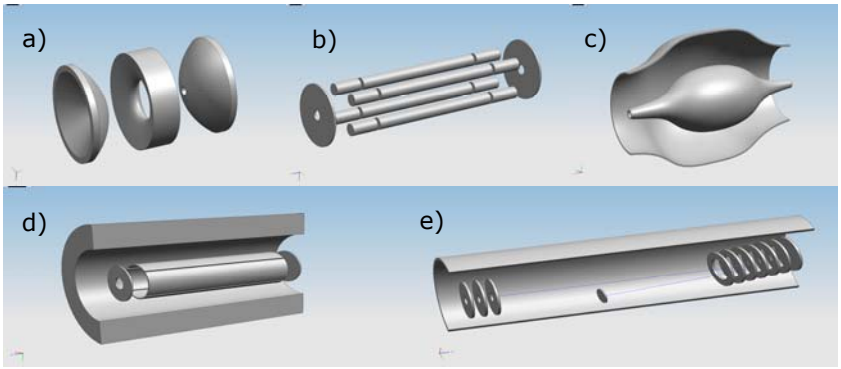

Figure 1.4. Mass spectrometers used in proteomic research. a) 3D quadrupole b) 2D quadrupole c) Orbitrap d) FTICR-MS e) time-of-flight.

1.5 FTICR-MS and molecular imaging

As stated before, imaging experiments are usually performed using a TOF instrument. They are ideally suited to the pulsed nature of the ionisation techniques most commonly used (MALDI and SIMS). Developments of sensitivity, mass resolution, and spatial resolution have been the main focus in

imaging mass spectrometry. Now, the use of TOF instruments combined with ion traps allows ion fragmentation in a collision cell, thus peptide identification is also possible[90].

By performing imaging FTICR-MS experiments it is possible to exploit the high resolving power and high mass accuracy with multistage MS/MS[75,81,92-94], which allows peptide identification directly from tissue[95]. The high mass resolution of the FTICR-MS can reveal compounds, differently localized, that cannot be distinguished with lower mass resolution TOF-based mass spectrometers[85]. Explicit examples that demonstrate the added value of FTICR-MS in imaging MS are described later in this thesis. Performing a high-resolution FTICR-MS imaging experiment is at the moment very time consuming, this being one of the aspects of FTICR-MS to be improved in the future. The instrument control methods development reported later in the thesis is an important factor in improving the speed of the experiments.

Arguably the most important benefit of the FTICR-MS for IMS is profiling and imaging small tissue areas in order to identify unknown biomolecules, thus complementing regular MALDI-TOF imaging.

1.6 Data acquisition and processing

The development of new mass spectrometry techniques together with the demand for protein discovery have led to a huge increase in the number and size of MS datasets. Data acquisition software, processing and data reduction tools have been developed in the last decade. For rapid and accurate data acquisition, analysis, and interpretation new computing methods are required. Therefore, in addition to instrumental development, data acquisition and analysis software is important to produce reliable data for database search engines. The databases are based on algorithms that perform mass

spectrometry data analysis through a statistical evaluation of observed and theoretical spectra of proteins/peptides.

To allow the new, complex mass spectrometers to be used on a large scale, the data acquisition software should be flexible and easy to use. The current acquisition software is developed to perform smart experiments and to help in the process of data analysis. On-the fly decisions can speed up the data analysis, allow new experiments, and reduce the data during measurement.

The amount and the size of the data provided by modern mass spectrometers are not compatible with manual analysis. Errors and inconsistencies that appear from manual analysis of complex data sets can be overcome by automation of mass spectral analysis and interpretation of the data. Furthermore, for imaging mass spectrometry data visualization tools need to be developed to provide an easy and rapid way to assess measurement quality and aid data interpretation.

1.7 Scope of this thesis

This thesis describes the development of FTICR-MS to study biological samples using for the first time, imaging FTICR-MS. To achieve this goal imaging experiments were performed on a (commercial) FTICR-MS and acquisition software and data processing methods were developed in-house. Furthermore, our FTICR-MS was modified to perform both ESI and MALDI imaging on the same instrument (work in progress).

Chapter 2 supplies the reader with a description of fundamental aspects of FTICR-MS in general and our instrumental set-up followed by a discussion about advantages and disadvantages of FTICR-MS in IMS.

Chapter 3 describes a workflow-based method that controls experiments on a FTICR mass spectrometer or any other type of scientific instrument and includes on-the-fly decision-making tools. The demonstrated

decision-making processes during acquisition enables new types of FTICR-experiments, which are not possible on commercially available systems. A few experimental examples (DESI and liquid chromatography (LC)-FTICR-MS experiments) demonstrate the power and the simplicity of the method.

Chapter 4 shows for the first time the results of imaging FTICR-MS experiments on a rat brain tissue section. Advantages, disadvantages and further improvements in this respect are evaluated.

In **Chapter 5** the development of a parallel processing technique for large data sets in a distributed computing environment is explained. The implementation of this novel approach, described and evaluated for LC-FTICR-MS data, is demonstrated to significantly decrease the total processing time.

In **Appendix 1** the simulations and the experimental results of a new designed ESI ion source are described. Here, our goal is to increase the detection sensitivity by designing a linear accumulation octopole with enhanced ion ejection capabilities. The octopole design and implementation was the first step in the development of the instrument in order to combine ESI with MALDI imaging.

2

Fourier Transform Ion Cyclotron Mass Spectrometry and imaging basic concepts

This chapter is dedicated to a description of the principle of operation of FTICR-MS and a depiction of our experimental set-up. Furthermore, the drawbacks and advantages of FTICR-MS in the field of imaging are described.

Chapter 2

2.1 FTICR-MS principle of operation

Fourier transform ion cyclotron resonance mass spectrometry is a technique that combines electric and magnetic fields to measure the molecular weight of ions in the gas phase. The cyclotron motion of ions in a magnetic field has its roots in 1932 when it was used for proton acceleration to high kinetic energies for nuclear physics experiments[96]. It took however a few decades before Fourier transformation algorithms for image charge detection of the cyclotron motion of the ions were reported[97,98]. This marked the beginning of a new mass spectrometer era that offered unparalleled mass accuracy and mass resolution. Furthermore, FTICR-MS was going to be known for its non-destructive ion detection, unlike previous methods (and similar to the recently introduced Orbitrap), which allows the ions to be reused after detection. More details about this technique can be found elsewhere[81,99]. In this chapter, the basic of FTICR-MS technique will be discussed.

2.1.1 Ion motion in the cell

The main component of FTICR-MS is the ICR cell, which is a Penning trap, located in the centre of a super-conducting magnet. Due to the magnetic field, considered here parallel to the z-axis, ions entering the cell follow a cyclotron motion in the x-y plane. All cell types consist of trapping, excitation and detection electrodes in various geometries[81].

An ion with charge q and speed v that enters the ICR cell experiences the combined force of the magnetic field **B** and the electric field **E**, which can be written as the Lorentz force ($\mathbf{F_L}$) equation (eq. 2.1):

$$\mathbf{F_L} = q\mathbf{E} + q(\boldsymbol{v} \times \mathbf{B}) \quad (2.1)$$

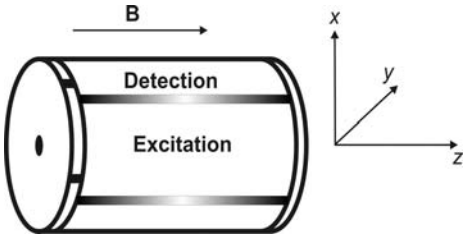

Figure 2.1. A schematic of a closed cylindrical cell. It consists of two trapping plates, two pairs of opposite electrodes for excitation and the other two for detection.

The magnitude of the Lorentz force depends only on the charge, speed and the magnetic field strength, if the electrostatic force is considered negligible. The Lorentz force is equilibrated by the centripetal force oriented in opposite direction as is shown in Figure 2.2 therefore the following mathematical equation can be written:

$$qv_{xy}\mathrm{B} = mv^2_{xy}/\mathrm{r} \quad (2.2)$$

with r the orbit radius of the ions in the cell and m, the mass of the ion. It can be seen that the Lorentz force changes just the direction of the velocity v_{xy} but not its magnitude. First, by introduction of the angular frequency ω_c as v_{xy}/r and considering the magnetic field strength constant, ω_c is dependent only the mass and the charge of the ion (eq. 2.3):

$$\omega_c = q\mathrm{B}/m \text{ or } \nu_c = q\mathrm{B}/2\pi m \quad (2.3)$$

where $\nu_c = \omega_c/2\pi$ is the cyclotron frequency. Second, the frequency of the ion is independent of the orbit radius. Moreover, ν_c is independent of the velocity of the ions and thus independent of the kinetic energy of the ions and the cyclotron

radius. This is particularly important for FTICR-MS because, contrary to other mass spectrometric methods the spread in kinetic energy of the ions does not limit the mass resolution during FTICR-MS analysis.

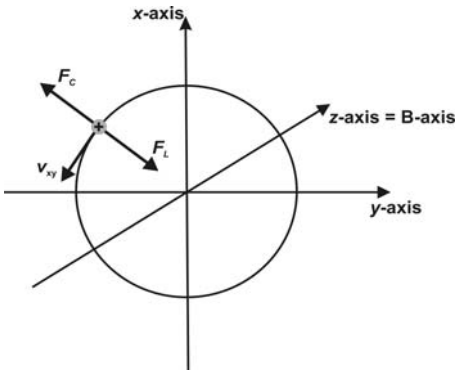

Figure 2.2. The cyclotron motion of ions in FTICR-MS. The ion velocity perpendicular to the uniform magnetic field generates a Lorentz force (perpendicular to both) that forces the ion to move in a circular orbit.

The electrical field of the trapping electrodes was neglected in eq. 2.3 but it can have a significant influence on the cyclotron motion. Positive voltages are applied to the trapping plates to trap positive ions (and negative voltages for negative ions). The ions contained by this trapping field oscillate along the axis of the cell with a trapping frequency ω_z, given by equation 2.4:

$$\omega_Z = \sqrt{\frac{qVz}{md}} \qquad (2.4)$$

where V_Z is the potential applied to the trapping electrodes and d is the length of the ICR cell. The radial field produced by the trapping potentials, $E = V_Z r/2d^2$ is opposite in direction to the inward-directed Lorentz force. With this electric field component equation 2.1 becomes:

$$m\omega^2 r = qB\omega r - q(V_Z R/2d^2) \quad (2.5)$$

which is a quadratic equation with two distinct solutions:

$$\omega_+ = \frac{\omega_C}{2} + \sqrt{\left(\frac{\omega_C}{2}\right)^2 - \frac{\omega_Z^{\,2}}{2}} \quad (2.6)$$

$$\omega_- = \frac{\omega_C}{2} - \sqrt{\left(\frac{\omega_C}{2}\right)^2 - \frac{\omega_Z^{\,2}}{2}} \quad (2.7)$$

where ω_Z is the "trapping" oscillation frequency and ω_C is the "unperturbed" cyclotron frequency. From these equations it is seen that the trapping potential has two effects on the ion motion: first, it reduces the cyclotron frequency, ω_+ is the reduced cyclotron frequency, and secondly it forces the ions to follow a periodic motion at low frequency, ω_-, called the magnetron motion. ω_+ falls in the range 5 kHz – 5 MHz for a 7T magnet (mass range between 70 kDa and 100 Da, respectively). ω_- is the magnetron frequency and is in the order of 1-100 Hz.

Several ICR traps with different geometries have been developed ranging from the trapped-ion cell (1970)[100] to the matrix-shimmed ICR trap (1999)[101]. Some of the early cells were rectangular, cubic, cylindrical, and later close-ended cylindrical[102]. Ion loss along the z-axis was one of the main disadvantages of these cells. The introduction of the infinity cell by Caravatti *et al*[103], which uses segmented end caps to approximate a linear excitation field and thus reduce z-axis losses, provided a more robust instrumental configuration. A disadvantage of the infinity cell is the limited access for ion introduction through the small hole in the first trap electrode, which can limit ion transfer efficiency into the cell. The open-cell[104] overcomes this problem. The large opening of the front trap electrode allows for efficient ion loading.

Furthermore, capacitive coupling of the open-trap electrodes to the central excitation electrodes means that the ions are excited with a near uniform excitation field thus minimizing z-axis ion losses[105]. Simultaneous trapping of positive and negative ions was achieved by so-called nested cells[81]. A more detailed description of different ICR cells can be found elsewhere[106].

Currently, in most FTICR-MS set-ups, the ions are produced in an external ion source and transported into the ICR cell. Ions have to be decelerated in the cell in order to be efficiently trapped. There are a few methods to achieved this: using the retarding field produced by the trapping plates in so called gated trapping[107,108], by sidekick trapping[109] or through multiple collisions of the ions with a neutral gas (e.g. Ar), a method known as gas-assisted dynamic ion trapping (GADT)[110]. The gated trapping is the simplest way to trap the ions, but not efficient enough to trap ions with wide energy and *m/z* ranges. To increase the trapping efficiency, GADT and sidekick trapping are used. For GADT due to the extra time required for removing the collision gas, the length of the experimental sequence is considerably increased. Sidekick trapping uses the deflection of the ion beam from the main axis of the instrument during its introduction in to the ICR cell. In this way, the ions are trapped by the higher electrostatic potential present around the cell axis. This method has the advantage of trapping ions with a wide range of energy and mass-to-charge ratios. However, the fact that the ion cloud is displaced from the axis makes ion detection less efficient.

2.1.2 Ion excitation and detection

The mass / charge ratio of the ions in FTICR-MS can be determined by measuring the cyclotron frequency (eq. 2.3 and 2.7). However, at room temperature the radius of the motion is very small and the ions move incoherently, as a result no signal can be detected on the ICR cell plates. In

order to collect a signal it is necessary to excite the ion cloud into a coherent motion and close enough to the detection plates to induce an image current. It is this image current which is then amplified and recorded that constitutes the ICR transient for subsequent Fourier transformation and conversion into a mass spectrum[81].

Ions can be coherently excited by applying a RF electric field to the two opposite excitation electrodes of the cell, prior to the detection event. The RF pulse has the form (eq. 2.8):

$$\mathbf{E}(t) = E_0 \cos\omega_C t\mathbf{j} = \frac{\alpha V_{PP}}{d} \cos\omega_C t\mathbf{j} \qquad (2.8)$$

where a is the geometrical constant of the ICR cell and V_{PP} is the peak-to-peak amplitude of the RF excitation pulse. This linearly polarised electric field can be expressed as the sum of two counter-rotating components, $\mathbf{E}_L(t)$ and $\mathbf{E}_R(t)$ (eq. 2.9 a and b):

$$\mathbf{E}_L(t) = \frac{E_0}{2} \cos\omega_C t\mathbf{j} - \frac{E_0}{2} \sin\omega_C t\mathbf{i} \qquad (2.9\ a)$$

$$\mathbf{E}_R(t) = \frac{E_0}{2} \cos\omega_C t\mathbf{j} + \frac{E_0}{2} \sin\omega_C t\mathbf{i} \qquad (2.9\ b)$$

The component, $\mathbf{E}_R(t)$, that rotates in the same sense and at the same frequency as the cyclotron motion of an ion can excite it to a higher orbit. Broadband excitation is applied to excite a wide *m/z* range and thus leads to the efficient detection of a large *m/z* window. The second component, $\mathbf{E}_L(t)$, rotates ions in an opposite sense but is 2ω off-resonance and will not have an effect on the ion's orbit. If all the excitation energy is converted into kinetic energy,

$$A(t_{exc.}) = E_0^2 q^2 t_{exc.}/4m \qquad (2.10)$$

the final radius of the ions orbit becomes:

$$r = \frac{E_0 t_{exc.}}{2B_0} \tag{2.11}$$

Equation 2.11 shows that ions are excited to the same final radius independently of their mass or charge. Most excitation methods (rectangular pulse, single frequency excitation and frequency chirp) provide an excitation power that is not entirely independent of frequency[97,98]. A uniform excitation can be achieved by applying a Stored Waveform Inverse Fourier Transform (SWIFT)[111] pulse which was introduced by Marshall in 1985[112]. In SWIFT the amplitude and frequency range is specified, and using an inverse Fourier transformation the excitation time domain pulse is calculated.

For on-resonance frequencies the ions will absorb energy and will increase their orbit radius following an outward spiral motion while the RF-excitation signal is applied. The coherent motion of the ions is detected when the cyclotron orbit radius of the ions is sufficiently large for the coherent packet of ions to induce an image charge in the detection plates. The detection plates are opposed to each other and positioned coaxially and at the same radius between the excitation plates as shown in Figure 2.1. An alternating image current is produced due to the periodical motion of the ions close to the detection electrodes. The frequency of this current matches the cyclotron frequency of the ions. This weak image current is amplified and converted into a voltage signal that gives the following time domain signal f(t):

$$f(t) = \sum_{i=1}^{M} N_i e^{-\frac{t}{\tau_i}} \cos(\omega_i t + \varphi_i) \tag{2.12}$$

where t is the length (in seconds) of the transient, ω_i is the cyclotron frequency of the ions, N_i is the number of ions i and φ_i the phase of the ions. Collisions

with the background gas and charge repulsion cause a dephasing of the coherent ion motion and a decrease of the orbit radius. As a result, the time domain signal intensity will decrease with the damping constant τ_i. The resolution of the mass spectrum is dependent on the length of the transient. An example of the time domain signal is presented in Figure 2.3.

The transient signal (Figure 2.3a) decays with time and represents the sum of the individual sinusoidal signals of all ions. A frequency spectrum is obtained after Fourier transformation of the time-domain signal. By using eq. 2.3 the mass spectrum is calibrated (Figure. 2.3b). Summing N repeated spectra improves the signal-to-noise ratio with a factor of $N^{1/2}$. For ion isolation, undesired ions can be removed from the ICR cell by applying an excitation pulse to the excitation plates to radially eject the undesired ions out of the cell.

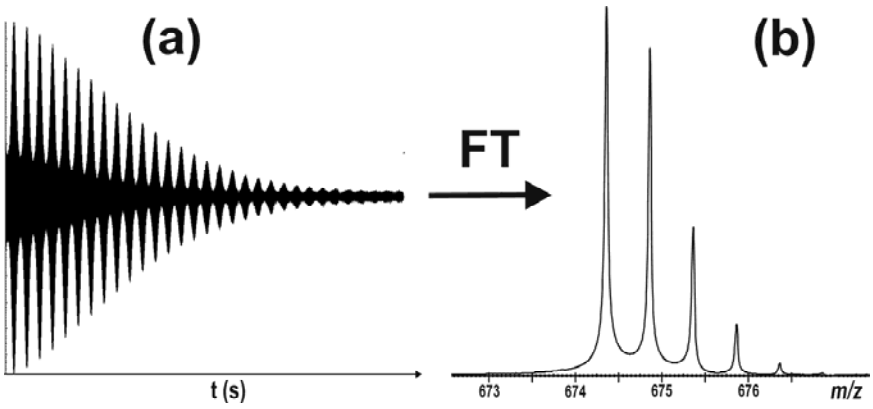

Figure 2.3. a) Time domain transient measured at a magnetic field of 7T for the isolated 2+ charge state of substance P (M = 1347.83) and b) mass spectrum of the $[M+2H]^{2+}$ isotope peaks obtained after Fourier transformation and *m/z* conversion of the time domain signal.

2.1.3 Fragmentation techniques

Structural information about peptides and proteins can be obtained by using multiple fragmentation techniques. A precursor ion is first isolated and subsequently subjected to a dissociation technique. The resulting spectra contain a collection of dissociation products at different *m/z* values and intensities.

Sequence information is obtained in MS/MS through cleavage of the peptide backbone. In Figure 2.4 the three predominant cleavages that can occur along the peptide backbone are shown. If the charge is retained on the N-terminal site the fragments are termed *a*, *b* or *c* and if the C-terminal site carries the charge, the fragments are called *x*, *y* or *z*. The fragments a/x, b/y and c/z constitute complementary information on peptide structure. This nomenclatures was proposed by Biemann[113] and Roepstorff[114] and is now the common standard (see Figure 2.4).

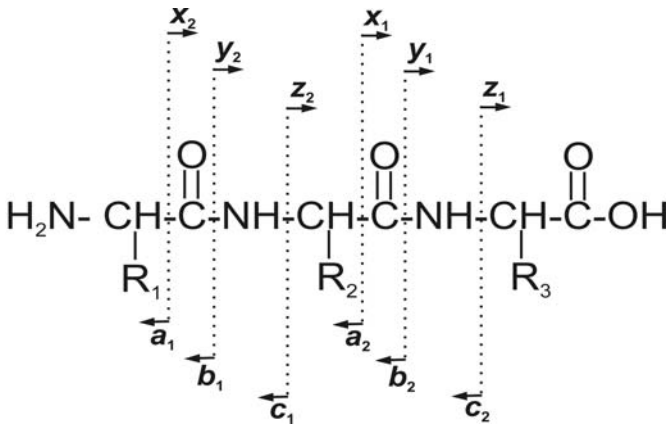

Figure 2.4. The nomenclature used for peptide backbone fragmentation. The ions containing the N-terminus are *a*, *b* and *c* and the ions containing the C-terminus are *x*, *y* and *z*.

The MS/MS techniques used in FTICR-MS are Collisionally Activated Dissociation (CAD)[115,116], Sustained Off-resonance Collision Activated Induced Dissociation (SORI-CAD)[115,117], InfraRed MultiPhoton Dissociation (IRMPD)[118,119], Surface Induced Dissociation (SID)[120,121] and Electron Capture Dissociation (ECD)[45,122-125].

With collision-based dissociation techniques the precursor ion is kinetically excited with an RF pulse, on-resonance (CAD) or off-resonance (SORI) with the cyclotron frequency of the ion, to increase the kinetic energy of the ion. A part of the kinetic energy is converted into internal energy by collisions with the collision gas. When the ion reaches the dissociation threshold fragmentation occurs.

When on-resonance excitation is used, the ions are kinetically excited to a higher orbit radius and hence a higher kinetic energy and collisions with the target gas take place. The time delay needed for relaxation of the excited ions and for pumping out the collision gas as well as the location where fragmentation occurs, far from the centre of the cell, makes detection less efficient. In addition, it has been shown that on resonance excitation distorts the ion cloud thereby reducing the time domain data and lowering the mass resolving power of the instrument[115]. Re-axialisation of the ion cloud in the cell can ameliorate this problem.

SORI-CAD uses a low amplitude RF pulse that is 1000-1500 Hz off-resonance with the cyclotron frequency of the isolated ion. The SORI pulse is alternately in- and out of phase and thus the ion is continuously (sustained) excited and de-excited, periodically expanding and contracting the cyclotron orbit (Figure 2.5).

Modulation of the kinetic energy with SORI lasts seconds whereas in on-resonance excitation this requires less then half a millisecond. A SORI excitation pulse is kept at low amplitude in order to produce fragments close to the axis of the ICR cell for efficient detection. SORI-CAD slowly raises the internal energy of the precursor ion, consequently it favours low energy fragmentation pathways.

On-resonance CAD and SORI-CAD are known to produce efficient fragmentation. However, they share some drawbacks such as introduction of a collision gas, unintentional excitation, ejection of dissociation products and distortions of the isotopic distribution.

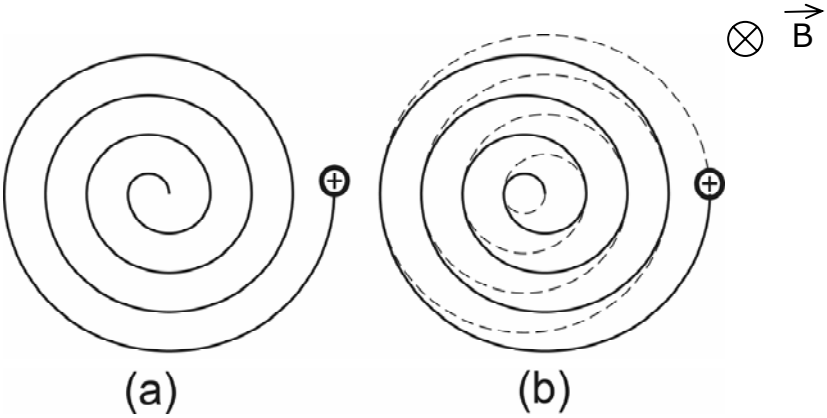

Figure 2.5. Time evolution of ion trajectory in (a) on-resonance and (b) SORI. Note that the average SORI radius is substantially smaller compared to the on-resonance excitation.

SID is another collision-based dissociation technique. This method differs from the first two (on-resonance CAD and SORI-CAD) by the fact that it is based on ion-surface impact. Using this technique the internal energy of the ions is almost instantaneously increased in a single collision[126,127] and, as no collision gas or RF excitation is used, the acquisition time for an MS/MS experiment is significantly shorter than for on-resonance CAD or SORI-CAD. However SID is only suited for small peptides, its efficiency being dependent on the size of the precursor ion.

Another way to excite and dissociate the ions is by using IRMPD. In IRMPD ion activation is established by irradiation of the ion cloud with a continuous or pulsed infrared laser beam. Multiple absorptions of infrared photons lead to an increase of internal energy until the dissociation limit is reached. The benefit of the technique is that no excitation pulse and no collision

gas are needed which considerably reduces the duty cycle. In addition, in IRMPD all selected ions can be simultaneously excited and the dissociation fragments are produced close to the cell axis.

ECD is a relatively new technique. In ECD multiply charged cations are irradiated with low energy electrons. The type of fragments produced in ECD are different than those obtained with the other techniques (c/z ions). Less backbone cleavage selectivity is observed and therefore more of the sequence is covered. The main attraction of ECD is the fact that labile post-translational modifications are retained, allowing such modifications to be identified and localized. With CAD and IRMPD the labile modifications are lost prior to backbone cleavage, thus preventing their localization. Such observations were one of the causes of the long debate as to whether ECD fragmentation occurs before intermolecular vibrational energy redistribution (so called non-ergodicity)[46]. The idea of non-ergodicity in ECD was predicated on the notion that the energetics of the gas-phase radical chemistry involved in ECD should be comparable to the closed-shell chemistry of even electron systems (as occurs in CAD and IRMPD of molecular ions)[128,129].

2.2 Experimental description of the instrument

The experiments described in this thesis were performed on a heavily modified Bruker APEX 7.0e FTICR-MS unless otherwise stated. Beside instrumental development, the electronics, computer hardware, software and data processing of the FTICR-MS experiment were developed in house and all these are subjects of the following chapters. The aim of the thesis is to show the potential of FTICR-MS in imaging mass spectrometry, in addition to its established roll in proteomics.

Figure 2.6 shows the instrumentation used in the majority of this thesis, including the nanoflow liquid chromatography system used for peptide

separation prior to electrospray ionisation in the biomarker discovery applications, figure 2.6a, and a schematic of the FTICR, figure 2.6b.

a)

b)

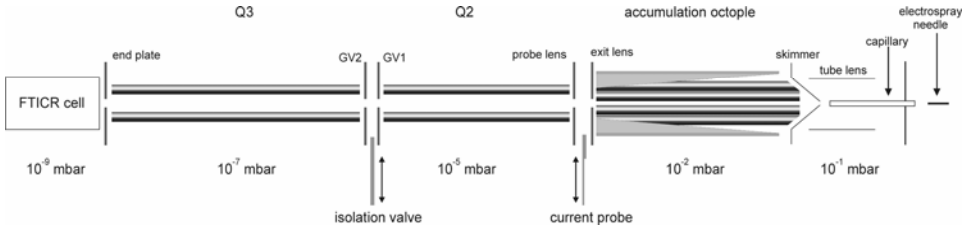

Figure 2.6. a) LC system b) FTICR-MS set-up.

The ESI source used in this thesis was designed and constructed in-house and set to work in positive and negative ion mode. Positively charged ions were obtained by applying 1000-3000 V potential difference between the spray needle (PicoTip^{TM} Emitter, New Objective Inc., Woburn, MA, USA) and the inlet of the mass spectrometer.

The nanoLC-system (LCPackings, Amsterdam, the Netherlands) consists of an autosampler, a switching unit, a nanoflow system and a UV detector (Figure 2.6a). The switching unit is equipped with a reverse-phase capillary precolumn and is used for preconcentration of the sample at a flowrate of 30

microL/min. Peptide separation is then carried out on an analytical column using nanoflow elution at 300 nL/min.

Ion transfer: The ions that emerge from the sampling capillary (stainlees steel capillary surrounded by a ceramic heated tube maintained at ~200 C to aid desolvation) are focused by a tube lens through a skimmer into an RF-only octopole (Figure 2.6b). Collisional focusing inside the octopole[130], the pressure in this region is about $\approx 10^{-2}$ mbar, provides a well-defined ion beam (in terms of spatial extent and kinetic energy distribution), necessary for high sensitivity. Ions can be accumulated and rapidly ejected by applying a pulsed axial field to the specially designed ejection rods located between the octopole rods. Ion packets are ejected with a time and energy distribution that better match the acceptance criteria of the ICR cell. A retractable current probe is situated after the octopole to enable the ion source to be tuned independently of the rest of the instrument, which significantly aids ion optical tuning. For high sensitivity it is imperative that the ions formed (and manipulated) in the source are transferred through the fringe fields of the ICR magnet[131-134] and, for ESI the pressure gradient from atmospheric to $\approx 10^{-9}$ mbar[38,130,135-137], with as high efficiency as possible[138].

FTICR-MS instruments have used electrostatic lenses[132], electrostatic ion guides[131] and radio-frequency (RF) multipole ion guides to transfer ions from an external ion source into the ICR cell[133,134]. Though new ion transport devices continue to be developed, for example the recent ion conveyor[139], multipole ion guides have been shown to provide very efficient transport[138] and kinetic energy control.

The ion guides of the instrument consist of three multipoles (see Figure 2.6). First, the octopole is 180 mm long (rod radius = 3 mm). When the current probe is retracted, three electrostatic lenses (conduction, extraction and probe lens) are used to focus the ions into the transfer quadrupoles (Q2 and Q3 in Figure 2.6b). These quadrupoles are 25.3 cm and 88.9 cm long, respectively. The cross-sections of the two quadrupoles are identical (0.25 cm rod diameter). The octopole has a separate RF power supply while the quadrupoles are

connected to one common RF power supply. Consequently, the quadrupoles always operate with identical RF voltage and frequency. All three multipoles have independent bias voltages in order to maximize sensitivity and manipulate the ions' kinetic energy. A retractable gate valve, used for isolating the high vacuum cell, separates the second and third quadrupoles. Two electrostatic lenses (GV1 and GV2) are used to ensure efficient transmission in this region. A final electrostatic lens (end plate) is used to focus the ions into the ICR cell and to terminate the RF field.

ICR cell: Two types of ICR cells were used for the work described in this thesis: a Bruker Infinity™ cell[140] and a home-build capacitively coupled open cell[141] (Figure 2.7). The end caps of the infinity cell consist of segmented plates to approximate a linear excitation potential.

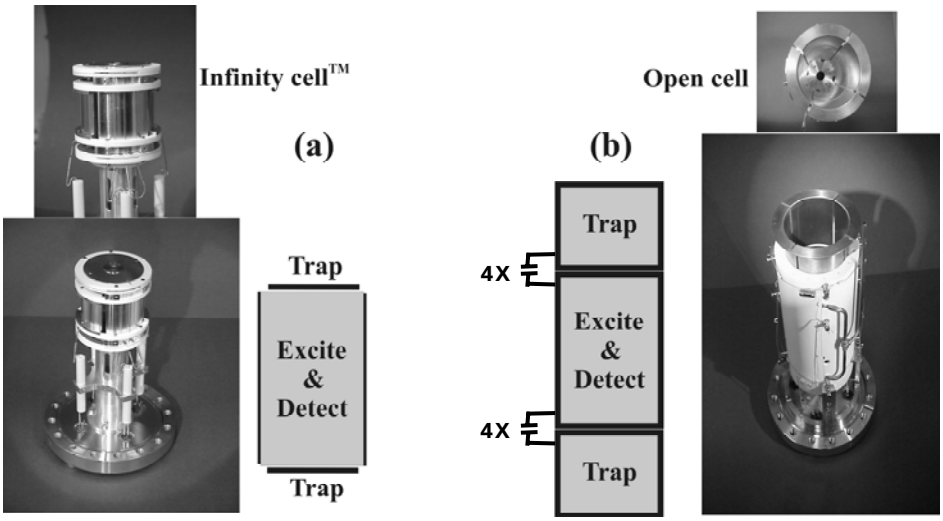

Figure 2.7. Two types of ICR cells: (a) the Infinity™ cell and (b) the in-house made capacitively coupled open ended cell.

The electrodes of the open cell are made from copper and are surrounded by a ceramic jacket embedded with a heating element and a cooling pipe. The home-built open cell allows the ions to be heated and cooled which enables the study of mechanistic aspects of ion reactions in the gas-phase.

For both ICR cells, ions can be trapped more efficiently by raising the trapping voltages during ion trapping or by introducing collision gas (e.g. Ar) to kinetically cool the ions. An example of a typical experimental sequence involving precursor ion isolation and MS/MS is shown in Figure 2.8.

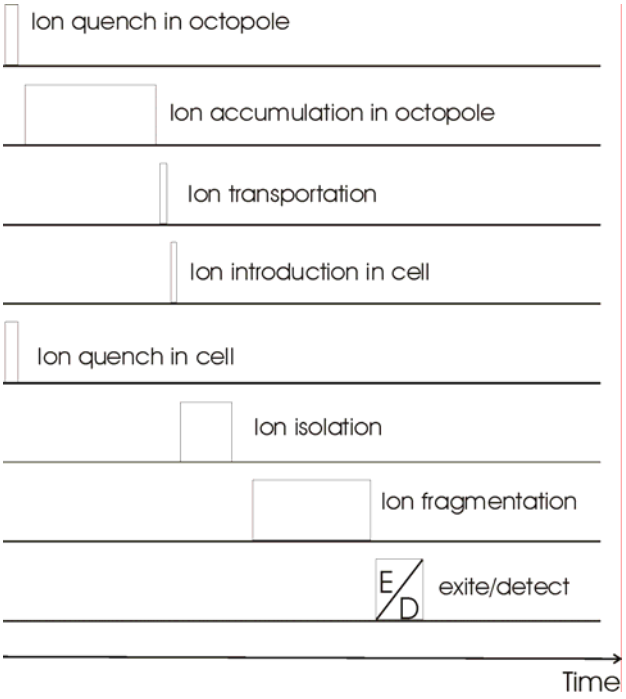

Figure 2.8. Schematic of an FTICR-MS/MS experiment. For an FTICR-MS experiment only, ion isolation and ion fragmentation are not part of the sequence.

The AMOLF FTICR-MS is equipped with a rich selection of MS/MS possibilities, including on-resonance CAD, SORI, IRMPD and ECD as well as

activated ion ECD. It had been reported that more efficient fragmentation, and thus more extensive sequence information, could be obtained by heating the ions prior to ECD. A novel set-up was implemented to enable activated ion ECD that ensured using IR and electron beams[142].

2.3 FTICR-MS in the field of imaging mass spectrometry

Imaging mass spectrometry has been performed for over 40 years. During its evolution the main developments have concerned sensitivity, mass range, spatial resolution and detection speed. Consequently, mass analysers such as TOF have been the most suitable. However, high spatial resolution is not always the highest priority. For very complex systems that possess multiple compounds of similar mass (isobaric), high mass resolution would be very advantageous.

Figure 2.9a shows an example of an imaging experiment that would benefit greatly from the high mass resolution of FTICR. In this experiment a MALDI-linear ion trap mass spectrometer was used to record the images of several lipids. The resolution of this instrument, typically nominal mass, is insufficient to distinguish between several lipids and some matrix-cluster background ions. In this example, phosphatidylcholine (16:0, 22:6) $[M+Na]^+$, phosphatidylserine (16:0, 18:1) $[M-2H+2Na]^+$, phosphatidylethanolamine (16:0, 18:1) $[M-H+Na+K]^+$, and a matrix cluster ion all have a nominal *m/z* of 828 and could not be resolved. In order to obtain images of specific lipids, MS/MS was used to distinguish the different isobaric ions. The isobaric ion, *m/z* 828, was isolated and subject to collision-activated dissociation. As the different compounds produce different fragment ions, the intensity of the fragment ions could be used to generate images of each specific compound. However this MS/MS strategy provides increased chemical specificity at the expense of two of the important advantages of mass spectrometry imaging, namely parallel

detection of multiple analytes and an non-targeted analysis. For the MS/MS strategy one needs to know which peaks can contain isobaric peaks.

a) MS/MS based imaging mass spectrometry

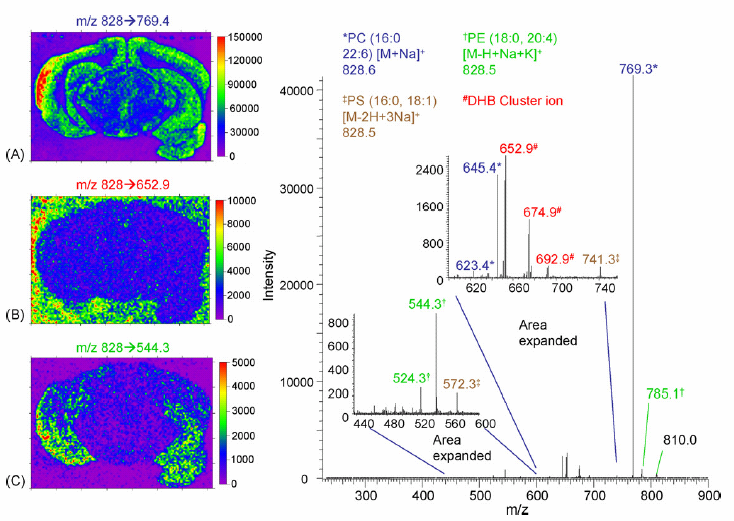

b) high mass resolution

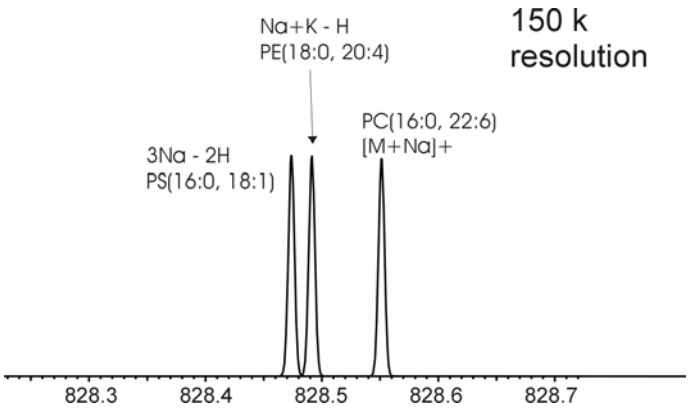

Figure 2.9. Use of MS/MS to obtain images of specific lipids a) and theoretical high mass resolution FTICR analysis of the same compounds. Note the DHB cluster ion is not in the *m/z* window of b) as its mass is too far away (easily resolvable). Taken from reference 79.

Figure 2.9b shows that with high mass resolution all of these ions would be clearly resolved and all of the chemically specific images would be obtained in a single experiment. Such high mass resolution analysis is highly advantageous for all lipid and pharmaceutical work.

The high mass resolution of FTICR-MS is typically accompanied by high mass accuracy. High mass accuracy allows the analyst to be confident about their assignments and to assign an isotopic composition to low mass peaks (mass $<$ 500) and to modifications. In addition, the FTICR-MS is equipped with a large battery of fragmentation techniques for MS/MS-based identification. Moreover, the results of MS/MS are provided with the same high mass resolution and accuracy of the regular MS analysis. The power of the FTICR-MS for obtaining structural information about biomolecules is now routine use for automated sequencing of proteins, including the identification and localization of post translational modifications.

In these respects FTICR-MS can contribute much to the field of imaging. The high mass accuracy, mass resolution and many MS/MS available techniques are highly attractive and fulfil an important niche that is otherwise missing. The FTICR mass spectrometer has some characteristics that are quite different from the more routinely used TOF analysers, which will influence how the experiments are set-up, what instrumental configurations will be required, the data-handling and even the applications that can be addressed. The salient features that need to be considered are sensitivity, mass range, detection time and mass calibration (mass accuracy).

Sensitivity - Sensitivity is crucial parameter in all biochemical analyses as it determines which problems are tractable. The TOF analyser is more sensitive than FTICR-MS. But the difference is falling. MALDI measurements on modern FTICR mass spectrometers report attomole to zeptomole sensitivity[143]. The difference is largely due to the fact that many FTICR mass spectrometers were not optimised for MALDI analysis. The multiple charging provided by ESI results in peptide and protein ions being located in the *m/z* region that can be

recorded with high mass resolution (and accuracy) with an FTICR. On the other hand the majority of ions produced by MALDI are singly charged, consequently large peptide and protein ions are located at higher *m/z*, where FTICR performance is less impressive. Consequently, a lot of the FTICR developments focussed on ESI-based applications. In turn these ESI developments have been exploited for MALDI analyses, and provide the technology behind much of today's high sensitivity MALDI measurements. For example high sensitivity MALDI-FTICR measurements are performed by trapping ions in an external ion trap. In this way signal is accumulated without the accumulation of noise, as is the case when using signal-averaging methods.

Mass Range – The mass resolution (and accuracy) of an FTICR measurement is a function of *m/z*, magnetic field strength, number of ions, and transient time. Figure 2.10 shows how the mass resolution varies as a function of *m/z*, for 1, 4.7, 7, and 9 T magnets and for transient durations of 1 ms and 1 s. It is clear that the highest resolutions are obtained in the low mass range, with a longer transient and a larger magnet. For example using a 7T magnet and a 1 s transient would provide resolution greater than 100 k for all ions less than 1 kDa, and thus would provide the performance indicated in figure 2.10.

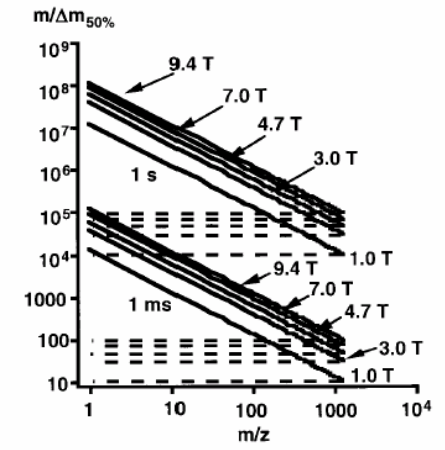

Figure 2.10. The theoretical resolving power of FTICR-MS decrease with *m/z* and increase with the magnetic field. The mass resolution can spectacularly increase if the acquisition time is longer. Taken from reference 81.

The strong reduction of resolution with increasing *m/z* is the reason MALDI of proteins is very seldom performed on an FTICR. For ions of $m/z > 5000$ the resolution and accuracy of an FTICR-MS is equivalent or less than that provided by a TOF. Consequently, MALDI-FTICR imaging mass spectrometry is best suited to low mass applications. This includes peptides, lipids, vitamins, pharmaceuticals and metabolites.

Detection Time – A typical MALDI TOF mass analysis takes less than 1 ms. In MALDI imaging mass spectrometry it is normal to accumulate the signal of 100 – 200 laser shots per pixel. Modern instruments can perform this mass analysis, data processing and data storage in 1 – 3 s per pixel. A single high mass resolution FTICR analysis can be 1 s. Some time could be gained by moving to higher magnetic field as the time needed to acquire 100 k resolution using a 14 T magnetic is half that of a 7 T magnet. In order to record images on a time-scale of 1-3 s per pixel (3 s per pixel for a 100×100 pixel image corresponds to a total experiment time in excess of 8 hours), the ions from multiple laser shots need to be accumulated in an external ion trap and then injected into the ICR cell for detection. To decrease the time per pixel further, the accumulation of ions can be performed concomitantly with the FTICR detection event of a previous bunch of ions (previously accumulated in the external trap). Figure 2.11 shows a timing diagram in which the ions from multiple laser shots are accumulated during a FTICR detection event. If the external ion trap, used for ion accumulation, has a sufficient charge capacity then the ions from the 100 laser shots used to sample each pixel can be accumulated, and a single FTICR detection event would be sufficient to detect all ions. Including the sample stage translation (movement to another pixel) within the sequence would provide an analysis time of 1 – 3 s per pixel.

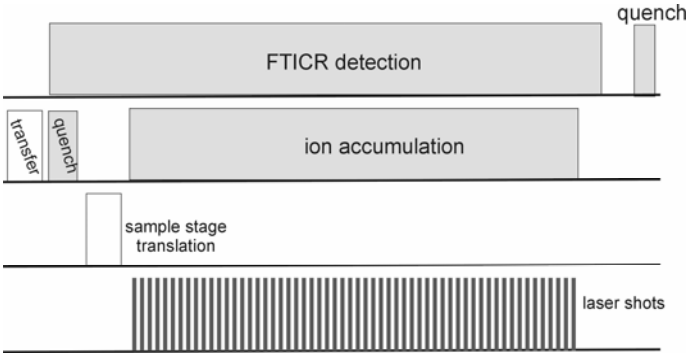

Figure 2.11. Timing diagram for multiplexed ion accumulation and detection for FTICR imaging mass spectrometry.

For this multiplexed approach to succeed, one will first need to ensure that the loss of resolution due to excessive space-charge within the FTICR cell does not undermine the performance benefits of FTICR imaging mass spectrometry. Furthermore, the external ion trap should be large enough to ensure that its charge capacity is sufficient to store all of the ions of interest and with an ejection performance to match the acceptance criteria of the FTICR cell. The results included in appendix 1 show the design and performance of an ion trap specifically made for this application[144]. Additionally, the software control system should be flexible enough as well as provide sufficient feedback as to optimise each stage of the experiment (chapter 3) and the processing fast enough to ensure that data processing is fast compared to the speed of the experiment (chapter 5).

Mass Calibration (mass accuracy) – Ion accumulation over several MALDI shots improves not only the sensitivity of the measurements but can also provide the flexibility to include internal calibrants (thus providing the highest mass accuracy). This can be easily performed if the instrument is equipped with a double source (ESI/MALDI or MALDI/MALDI) that can be rapidly switched during an imaging experiment. If the magnetic field strength is stable and high ($>$ 7 T) it is predicted that a first order calibration depends only on the density of ions (space charge) in the cell, and that the mass errors decrease with

increasing magnetic field strength[145]. Automatic gain control (AGC), high magnetic fields and designing larger ICR cells (reduced ion density) are alternative approaches to maintaining high mass accuracy. For imaging purposes AGC might not be suitable due to extensive sample consuption.

In addition, to explicitly demonstrating the high mass resolution performance advantages of FTICR imaging mass spectrometry, three of the chapters concern developments in instrumentation, data acquisition software and data processing methods that are directly applicable to FTICR imaging mass spectrometry. Intuitive and flexible software, designed to enable a simple work flow methodology for designing and implementing new experiments (combined with numerous monitors of the experiment performance) readily allows imaging and AGC experiments, as well as allowing the analyst to devise new experiments (for example searching for the diagnostic ion pairs in isotope labelling experiments for relative protein quantitation). Data processing using grid computing provides the high through put capabilities for processing the 10k + spectra in a typical imaging experiment, on a time-scale that doesn't adversely affect experiment time, and is fast enough to enable the analyst to interactively optimise the performance of the processing steps. An high capacity external ion trap allows the multiplexing of the ionisation and FTICR detection for short pixel analysis times. All of these developments are targeted at imaging mass spectrometry but are highly applicable to other areas, especially identification of the imaged molecules using the abundant MS/MS capabilities of the FTICR. Moreover, the identification capabilities of the FTICR can be utilized in isolation of its imaging capabilities, for example to complement a high spatial resolution analysis using a MALDI TOF instrument: FTICR-MS technique analysis of small tissue areas to elucidate the identification of unknown biomolecules. High spatial resolution images can be obtained with TOF instruments and after the identification of areas-of-interest, further FTICR-MS studies can be performed. High mass resolution experiments can be performed for localization of different compounds that are very close in mass. A fast, not very high mass resolution

experiments can be performed in the case MS experiments followed by of MS/MS for desired compounds. The combination of FTICR-MS and high-resolution stigmatic TOF imaging provides both high mass and high spatial resolution. The FTICR imaging strategy extends the identification possibilities in direct tissue analysis and is a valuable tool in MS imaging instrumentation (Table 2.1).

Instrument	**Mass resolution and accuracy**	**Used spatial resolution**	**Identification methods**
DESI-FTICR	High => higher chance for peptide identification	Low: 500 - 1000 µm	Multiple MS/MS techniques
MALDI-FTICR	High => higher chance for peptide identification	Low - medium: 100 - 250 µm	Multiple MS/MS techniques
MALDI-TOF	Low => lower chance for peptide identification	Medium: 1-200 µm	CAD
Stigmatic MALDI-TOF	Low => lower chance for peptide identification	High: 4 µm	-
SIMS-TOF	Low => lower chance for peptide identification	The highest: 50 nm - 1 µm	CAD

Table 2.1. Identification methods, mass resolution, accuracy and localization for the currently most used instruments in imaging mass spectrometry compared to FTICR-MS.

A SIMS-FTICR-MS that combined a TOF analyser and an FTICR mass spectrometer in a single instrument has been reported, thus making the FTICR analysis of the areas selected in a SIMS imaging experiment more straightforward[146]. A single instrument approach is highly useful for SIMS analysis as surface contaminants can make sample transfer between different instruments problematic. For MALDI, surface contaminants are not a problem and so existing FTICR and TOF instruments can be combined provided a suitable position registration system is used.

The advantage of IMS is that molecular measurements can be performed closer to the primary disease by examining different cellular areas. Spatial localization of peptides has to be combined with their identification to contribute to the biomedical field. In this context, FTICR-MS is an instrument that can bring important information about peptide structure by using its high mass accuracy and resolution and by making use of its multiple types of fragmentation methods.

3

A novel workflow control system for FTICR-MS allows for unique on-the-fly data-dependent decisions

In this chapter a novel workflow-based data acquisition and control system for FTICR-MS is presented that facilitates a fast on-the-fly decision making process for a wide variety of data dependent experiments. Several new workflow implementations demonstrate the flexibility and benefit of this approach for rapid dynamic experimental design on a chromatographic timescale. The different sequence, evaluation, decision and monitoring modules are described using a selected set of examples. During a tandem LC-FTICR-MS experiment the system is used to dynamically switch between various dissociation techniques such as ECD and SORI depending on the charge state of a tryptic peptide peak. The use of this workflow based system for imaging FTICR-MS using a DESI source demonstrates the possibility of external control of the workflow (e.g. the control of the sample stage). Moreover, this on-the-fly decisions method is used in LC-MS-based quantitative proteomics, e.g. the selection of labeled peptides followed by targeted fragmentation of the peptides that exceed a user-defined abundance ratio.

Ioana M. Taban, Yuri E.M. van der Burgt, Marc Duursma, Zoltán Takáts, Marco Seynen, Marco Konijnenburg, Anton Vijftigschild, Idsart Attema, Ron M.A. Heeren, *Rapid Comm. Mass Spectrom.*, accepted for publication, **2008**
Ioana M. Taban, Bas van Breukelen, Yuri E.M. van der Burgt, Marc Duursma, Albert. J. R. Heck, Ron M.A. Heeren and Jeroen Krijgsveld*, in preparation*

Chapter 3

3.1 Introduction of the workflow-based method

FTICR-MS is an ion trapping technique that has become an important technique for studying complex biological systems[11,81,84,147]. Technical developments of the instrumentation and improvements in instrument control software over the past few years have resulted in an increased popularity of FTICR-MS. Proteomics studies greatly benefit from the unique features of FTICR-MS. Its high mass resolution[148,149] combined with high mass accuracy makes the FTICR-MS ideally suited for rapid analysis of complex mixtures[42,150-153]. Resolving peptides of similar mass[149] and the higher confidence related with an accurate peptide mass determination are clear advantages of FTICR-MS. Mass spectrometry based proteomics experiments often incorporate a liquid separation technique, such as liquid chromatography, to reduce the complexity of the sample prior to ionisation and mass analysis[153-155]. Nevertheless, it is common to find coeluting peptides of similar mass that can only be distinguished with the high-resolution of FTICR mass spectrometry. Another advantage of FTICR-MS is related to the number of tandem mass spectrometry techniques (MS/MS) available, such as SORI-CAD[115,117], ECD[46,122-125], and IRMPD[118,119]. Often these different fragmentation techniques result in complementary peptide sequence data. Thus, a combination of these MS/MS-methods is attractive, especially when they can be carried out in one single experiment. This latter aspect stimulated us to design and develop a workflow-based method that provides the user with the freedom to build experiments by making decisions on-the-fly, i.e. within one single experiment, and that integrates all the features of FTICR-MS. This development included both the implementation of new hardware, software and user interfaces. This method is aimed to be user-friendly and flexible, and package some of the complexity and instrumental expertise required to run modern FTICR instruments.

One of the major benefits of the workflow-based approach is the modular structure of instrument acquisition and control elements. As such, a

workflow-based method is an important tool for the automation of MS/MS-experiments. The number of applications of bottom-up proteomics (identification of proteins through the positive identification of their tryptic peptides) has increased with the advent of instrument decision-making algorithms that can automatically perform MS/MS-experiments on a selected precursor ion. These decisions are based on information obtained from a previous acquisition. Such algorithms are powerful and widely used in LC-MS experiments. Here, eluting peptides are analyzed continuously and based on full mass scan spectra the instrument switches automatically to MS/MS-mode and selects, for example, the most intense ion. These on-the-fly data-dependent experiments (DDE) are possible with commercial instruments from Thermo Finnigan (Intelligent Data-Dependent tools, San Jose, CA), Bruker (SmartSelect^{TM}, Bruker Daltonics, Inc., Billerica, MA), Waters/Micromass and Applied Biosystems (Information Dependent Acquisition, Foster City, CA). However, the criteria for selection of precursor ions are still limited, as well as the flexibility to select the type of follow-up MS/MS-experiment. To overcome some of these limitations we have chosen to develop a workflow-based method. It will be shown that this approach allows unique types of data-dependent experiments. In addition to the control of MS/MS-experiments, the workflow-based method is developed such that previously reported data-dependent features can be readily implemented.

In this chapter the development and establishment of a workflow-based acquisition and control method for FTICR-MS is presented. This method both controls FTICR mass spectrometer in a flexible and user-friendly way and includes on-the-fly decision-making possibilities. The ability to make decisions *during* acquisition enables new types of FTICR-experiments, which are not yet possible or difficult to realize on commercially available systems. Moreover, a workflow-based method makes the operation of a complex system such as an FTICR-MS more intuitive and thus makes it more amenable to non-FTICR experts. The hardware implementation and the workflow-based acquisition and control software are described in this chapter. Different experimental workflows are presented and discussed. The implementation of one LC-FTICR-MS/MS

experiment and one DESI[73,75] imaging experiment are shown to demonstrate the strength of our workflow- based method.

3.1.1 Materials and methods

Hardware

Fast and flexible control of instrument parameters is important to take advantage of the FTICR-MS capabilities. Also, a modular design is necessary to allow fast integration of new features. The electronics and computer hardware of our FTICR-MS experiment consists of a PC host system, a PXI chassis with several commercially available data-acquisition boards, a wiring- and breakout box and in-house designed high speed, high quality signal amplifiers with various output levels.

The host system is an Intel Pentium™ 4 (2.4GHz / 2 GB RAM) based computer. The PXI chassis is connected with a National Instruments MXI-3 interface to the host PC. The PC system has a direct, high speed, fibre optical link to an 8 TB online storage system, using a fibre channel protocol. Furthermore we use a CCD camera, supplying close up images of the spray needle or a solid sample surface within the AWG3 (Arbitrary Waveform Generator version 3) control program. A schematic of the hardware layout is depicted in Figure 3.1.

The control boards in the PXI-chassis (United Electronics Industries, Canton, MA; National Instruments, Austin, TX; ViewPoint, Rochester, NY) provide 40 analog outputs, 64 digital outputs as well as 8 analog inputs. The PXI chassis contains a NI 5411 Arbitrary Waveform Generator (40MS/s, 16MB) for RF excitation connected to a power amplifier - T&C AG 1021 for amplification of the excitation waveforms and a NI 5620 Transient Digitizer (64Ms/s 64MB) for detection connected to an in-house developed differential low noise signal amplifier. To eliminate spectral noise during detection the output of the ICR

excitation amplifier is only connected to the cell plates during excitation. This is achieved with a precisely timed fast relay switching circuit that was designed specifically for this purpose (see Figure 3.2a). A Time Frame Generator (Viewpoint DIO-64), two analog output boards (UEI, PDXI-AO-32/16 and NI 6733) and a 400 kHz 14-bit multifunctional board (PDXI-MF-14/400H) are also located in this PXI rack.

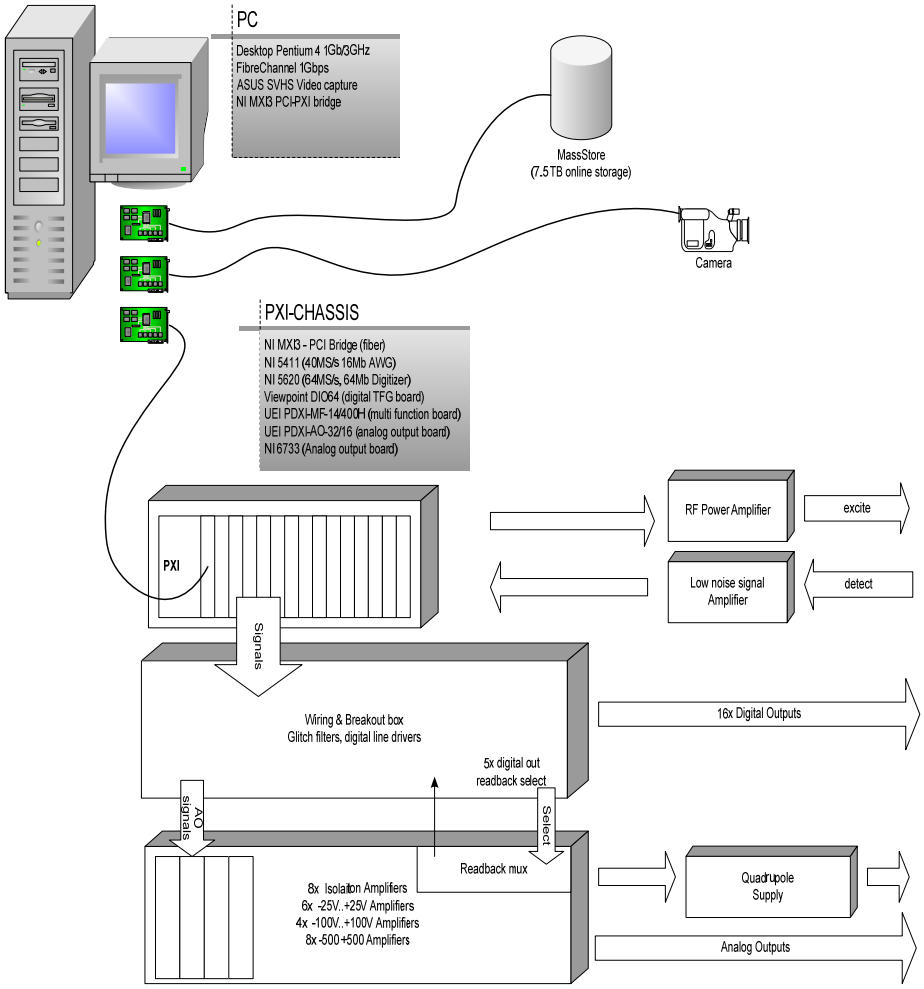

Figure 3.1. Block diagram of the FTICR-MS controller.

The wiring- and breakout box contains screw terminals that connect the analogue output signals from the Digital-to-Analogue Converter (DAC) -boards to the amplifiers. In this way the system can be easily expanded and or signals can be rerouted if necessary. Furthermore the analogue outputs have RC ((ow-pass R=1kΩ, C=3.3nF) filters to reduce DAC glitches. 16 digital outputs (TTL logic level) are available for the instrument, e.g. gas-valves, probes, shutters. These outputs are buffered with line drivers (high impedance driver partno. 74ALS541, low impedance driver partno. 74F3037) providing good signal quality over 10 – 15 m of cable.

In the Amplifier rack there are 8 isolation amplifiers, 12 amplifiers with a -25 V to +25 V output range and 8 with a –100 V to +100 V output range. The outputs of these amplifiers connect to different parts of the instrument, e.g. trap-electrodes, ion optics, source-voltages, etc. The isolation amplifiers drive the high voltage amplifier (500 V output) as well as the quadrupole power supply.

The ejection electrodes of the linear octopole ion trap in the system have to be switched on and off very fast to get the desired sensitivity increase[144]. A new octopole switching circuit was required, as the high-voltage power supplies do not provide a pulse rise time that was sufficiently short. The octopole ejection electrodes can be now switched on and off in less than 500 ns to the maximum value ± 500 V, depending on the capacitance of the cable using the in house developed switching circuit presented in Figure 3.2b. This fast switch from 0V used during ion accumulation in the octopole to ± a few hundreds volts at ejection time (for positive and negative ions, respectively) is needed to maintain the time and energy distribution of the ion packet as compact as possible. A compact ion cloud at the ejection time assures the optimum sensitivity (see appendix 1 for more details regarding the ejection electrodes).

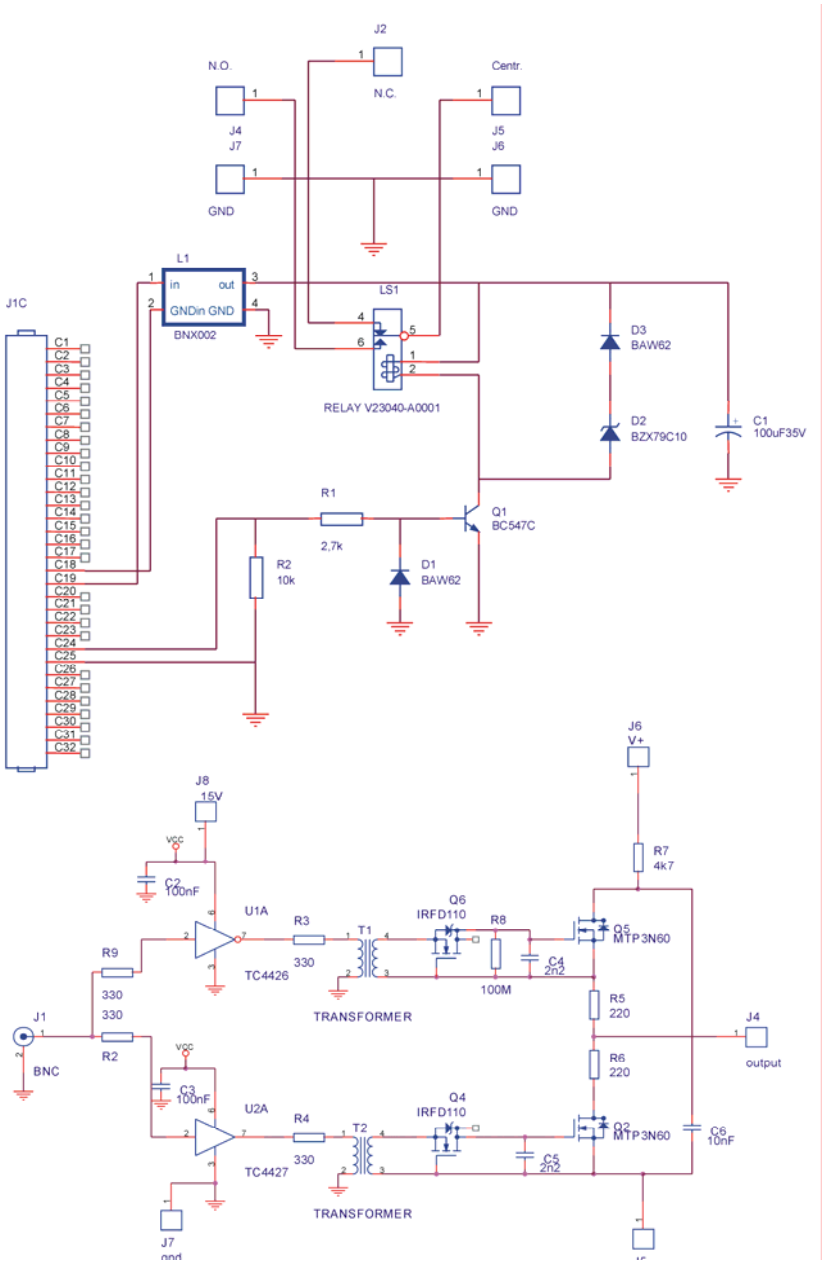

Figure 3.2. a) Schematic of the switching relay circuit connected to the cell plates during excitation b) schematic of the fast switch circuit for the ejection rods of the octopole.

Workflow architecture and software

The term "workflow" has been used in various fields and often refers to a sequence of data handling events. The use of a data workflow in MS-experiments and related data processing has been reported earlier[156,157]. Our acquisition and control software is markedly different and based on a flow control oriented model that is further referred to as AWG3. The workflow represents the actions that are required to complete an experiment, where the links between modules describe the order in which the actions are carried out. Underlying the workflow is a tree-based data-structure that contains all the settings and actions for a particular experiment. The nodes, represented by the modules of the workflow (see Figure 3.3), are object oriented in design, allowing for easy, modular expansion with new features, reuse of experimental settings (copy/paste functionality) and unlimited workflow configurations. The ease of expanding the workflow is an important characteristic that gives freedom to users to implement any new features they need to make their experiments possible.

Data-dependent decisions are implemented using a combination of data acquisition, control, evaluation and decision modules. The recorded data are first evaluated in an *evaluation* module (described later) resulting in a "true/false" decision which determines which of two output links becomes active. The following sequence of events can be controlled through decision modules (described later). These modules employ user-defined expressions to decide which subsequent module will be used. The expressions can be simple boolean equations like "variable 'x' greater than / less than / equal to a value" but can also include complex mathematical functions with multiple variables, using the built-in formula parser. This allows for a greater variety of experiments and instrument control.

All workflow properties are stored in variables, such as the initial voltages of the analog outputs, the width of a trigger pulse, charge of an ion-cluster, and mass and intensity of a peak in a spectrum. This provides the user with the freedom to design wide varieties of workflows, and enables new types

of FTICR experiments. The modular implementation of the workflow allows fast integration of new features. The design of AWG3 supports a plug & play-model, which allows control of other external hardware parts such as an LC system or a sample stage. The user can change or add modules at any point in time even during acquisition. Similarly, the order of the modules and the different actions taken after the *evaluation*- or *decision* modules are controlled by the user by making the appropriate links.

The workflow based AWG3 acquisition and control software is written in C++ with Microsoft Visual Studio. The previous version of[158] is based on a pulse-design system and is fully incorporated in the workflow approach. It is now the basis of the acquisition modules. The software uses several external libraries for hardware control, user interfacing and mathematical functions (National Instruments NI-DAQ, UEI PowerDaq, Rogue Wave Stingray Studio 2003, Intel® Signal Processing Library 4.5). Fourier transformations are performed with the freely available FFTW library version 3.1.2. It is one of the faster, highly optimized transformation libraries available for general purpose CPUs. For example: a 1M double precision floating point transformation takes little less than 100ms on a standard Intel™ Pentium4 3GHz processor[159].

AWG3 controls all the hardware timing and output signals. It provides the user-interface and stores/retrieves all data required to carry out FTICR-MS experiments. It runs on Microsoft Windows 2k or XP platform ensuring a familiar and intuitive environment for novice users.

The analog and digital output signals to the FTICR-MS hardware, the output range, name, type and secure limits of the signal are defined in a configuration file (awg.INI) allowing an experienced user to easily add or modify system signals. In this way the user can customize the organization of the signals and settings. The GUI (graphical user interface) provides different tabbed pages that display the static state of the output signals, the workflow diagram and the state of the other modules. The user can modify and arrange this tabbed lay-out to his/her own specifications using a simple configuration file.

All experiments, workflows and settings are stored on a high capacity network drive in a custom defined XML format (http://www.w3.org/XML), an open standard ideal for future data extensions and data exchange. The transient (raw) data is stored in a binary format without any header information. With each acquired measurement an entry is made in a database with experimental metadata, including information about the sample, the user name, storage location, date/time and measurement name. This database allows for easily searching and indexing experiments, retrieving their settings and/or viewing the results. The acquired data are inspected or post processed with the in-house developed software AWE (Arbitrary Wave Editor) described earlier[158]. A link to a knowledge exchange database, developed in our group, enables geographically separated researchers to store all metadata belonging to their experiments/research projects, including the necessary links to the existing storage facility to raw and processed data (knowex.amolf.nl)[160].

Samples preparation

Acetonitrile (BioSolve, the Netherlands) and acetic acid (JT Baker, Phillipsburg, USA) were used without prior purification. A tryptic digest of savinase (Sigma, USA) was prepared using trypsin (Promega, USA) at a concentration of 20 nmol/mL. Typically, 2 microliter of this solution was injected on the LC-system for analysis. The nanoLC-system (LCPackings, Amsterdam, the Netherlands) consists of an autosampler, a switching unit, a nanoflow system and a UV detector. The switching unit is equipped with a reverse-phase capillary precolumn (C18 PepMap 100, internal diameter 0.3 mm, length 1 mm) and is used for preconcentration of the sample at a flowrate of 30 microL/min. Peptide separation is subsequently carried out on an analytical column (C18 PepMap 100, internal diameter 0.075 mm, length 15 cm) using nanoflow elution at 300 nL/min. The eluents used were 1% acetic acid and 5% acetonitrile in water (A) and 1% acetic acid and 10% water in acetonitrile (B The gradient used for the separation of peptides was 0-30 min 0-50% B, followed by 30-35 minutes 50-90% B. The nanospray source connecting the LC-system to the mass

spectrometer was built in-house and equipped with New Objective Picotips™. The nanospray source connecting the LC-system to the mass spectrometer was built in-house and equipped with New Objective Picotips™.

Two standard peptides in 1 mg/ml concentration, Val5-Angiotensin II and Lys-des-Arg9-Bradykinin (Sigma, Germany) were manually applied on sandblasted plexiglass for desorption electrospray ionisation DESI experiments. Methanol/water 1/1 and 0.1 % acid acetic was sprayed at 3 µl/min.

All the peptide mass measurements were performed in the positive ion mode using a modified Bruker APEX 7.0 T FTICR-MS equipped with a 7 T superconducting magnet and an infinity cell[161]. The ions generated by the electrospray ion source are externally accumulated in a linear octopole ion-trap[144] (typical accumulation time 0.4 seconds) prior to transfer to the ICR cell via two RF-only quadrupole ion guides. The ions were trapped in the ICR cell using gas assisted dynamic trapping. DESI nozzle pressure was 9 bars for all experiments. The spray impact angle was 60° and the spray tip-to-stage distance was 1-3 mm.

3.1.2 Description of the modules used in the workflow-based method AWG3

The workflow consists of *modules* and *links*. Each module represents an action or combined actions in a measurement. Different sequential actions are connected through links in the workflow. A general workflow is depicted in Figure 3.3 This schematic provides a presentation similar to that of the user interface. Additional details are accessed by opening the module of interest. A basic workflow contains a *start*- and *stop* module, at least one acquisition and control *sequence*, and one or more *evaluation*- and *decision* modules. These latter two modules have two outputs that influence the order of actions in the

workflow. An *event viewer* module visualizes the status of any variable in the data tree. It monitors and records all actions during an experiment and is not linked to any other module. Depending on the type of results expected from an experiment, different types of modules can be added or designed to the workflow. Screenshots of AWG3 workflow and modules can be found on www.amolf.nl/fticrms.

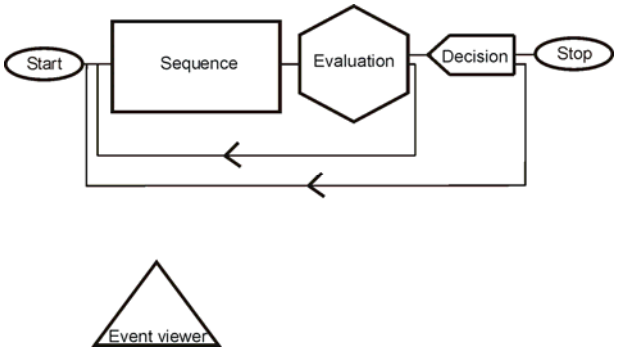

Figure 3.3. General workflow-based experiment.

The *sequence* module contains all time-dependent outputs of the instrument. The sequence shows all the signals in a timeline representation. This timeline resembles the GUI sequence from the previous AWG[158] system. Apart from the analog and digital signals there is a special signal called "AWG/transient digitization" (AWG/TD) for the excitation and detection of the ions in the cell. Here one or more excitation pulses or combined excitation and transient detections can be inserted. Any type of excitation waveforms can be generated and modified on-the-fly for the manipulation of ions. A *sequence* module can either contain an FTICR-MS experiment (*i.e.* a survey scan) or an MS/MS-experiment using a certain fragmentation method.

Each sequence is followed by an *evaluation* module that extracts a wide range of information from a recorded mass spectrum on-the-fly. The input and output variables of the *evaluation* modules are given in Table 3.1. The information is passed on from one module to another to facilitate the decision making process. When this evaluation process results in no information ("no

signal in the mass spectrum"), this module is linked back to a previous sequence module (see Figure 3.4). Based on different criteria, the user defines which signals are considered for further experiments. This is useful for example in LC-MS applications, in which only a certain amount of masses need to be selected for MS/MS-experiments due to a continuously changing elution profile. Different types of *evaluation* modules are available, which are described further in the next sections.

In the *PeakPicker* evaluation module ions are annotated using the in-house developed algorithm based on criteria such as mass range, neighbouring data points, mass window, and peak threshold[162]. The obtained peak list is sorted based on its *m/z* or intensity values (either in ascending or descending order). A mass exclusion list can be implemented to exclude calibration compounds, interferences or other undesired mass regions. From a peak list the total ion current of a mass range above a set threshold can be recorded in the so-called *IonCurrent* module. Alternatively, in a *ClusterList* module all detected peaks are clustered together using a peak clustering algorithm[162], based on parameters such as mass precision, charge range, maximum number of peaks in one cluster, and the isotopic ratios. Other *evaluation* modules are the so-called *TargetList*, used to include predetermined specific *m/z*-values for an experiment. The *ListTest* module can be used to dynamically add (automatically) *m/z* exclusion values during the experiment. The latter is of particular use for LC-applications, in which previously sequenced peptides are bypassed. The *AnalogInput* module is a different type of *evaluation* module, in which one or more external voltages can be monitored. The voltage is sampled with a 14bit ADC (analog to digital conversion) and its value can be used in the workflow, as a parameter to control and modify instrument settings or to facilitate the decisions making process. For example, the signal from the UV detector of the LC can be sampled and can be used to make decisions in the workflow.

Either evaluation modules or decision modules can establish branching in the workflow. The main difference between the evaluation modules and the decision modules is that the evaluation module passes on information (i.e.

metadata) to the next module whereas the decision modules merely provides a true/false decision. All the different *evaluation* modules have two output links in order to facilitate on-the-fly decisions. When the user wants the program to make a decision based on the value of a variable, an additional *decision* module is needed, which operates by evaluation of a user-defined expression. Different variables such as the charge of a cluster, the peak- or cluster intensity or the number of peaks in a cluster are extracted from one or more *evaluation* modules. Algorithmic expressions are employed by the *decision* modules to make a decision how the workflow proceeds. For example, a second *sequence* module containing an MS/MS experiment can be started after the initial MS sequence. The output of an *evaluation* module is used to provide a list of *m/z*-values that is passed on to the next *sequence* module to enable automatic generation of SWIFT pulse for the isolation of the precursor ions[111]. Also more trivial decisions can be made on-the-fly: is it necessary to repeat the measurement, or should it be carried out using different instrumental settings? The broad potential of this workflow will be discussed in the results section, followed by a typical LC-MS/MS and DESI imaging example.

Module	**Input**	**Output**
PeakPicker	Mass spectra acquired in *Sequence*	Peak list of m/z and intensity values.
IonCurrent	Peak list	Total ion current/selected ion current
ClusterList	Peak list	Cluster list of monoisotopic peak values of isotopic clusters and their charge state, intensity and peak resolution
TargetList	User defined m/z values prior experiments	m/z values
ListTest	m/z values dynamically added during experiment via *PeakPicker* or *ClusterList*	m/z values
AnalogInput	External input	Recorded external input values

Table 3.1. Input and output information used for different evaluation modules in AWG3.

All workflows contain one or more *event viewer* modules. The information in this viewer can be considered as a "system log" of all recorded values during the execution of the workflow. For example, in a typical MS/MS-experiment this module logs all the clusters observed in full mass survey scans, and logs, which clusters are selected for further fragmentation analysis. Using this module any variable can be graphically shown and stored in the course of the experiment. More variables can be plotted either in the same or different graphs by opening different tab pages.

3.1.3 Results and discussion

The workflow concept allows new features to be easily designed and implemented taking full advantage of the on-the-fly evaluation and decision making possibilities. We tested a great variety of different workflows in AWG3 and used these for various different applications, ranging from simple data-dependant MS/MS, LC-FTICR-MS/MS to imaging mass spectrometry. It is however not the purpose to discuss here all these workflows in detail, or to show all possible examples. Some of the data-dependent experiments described can also be carried out on commercial instruments such as Thermo's LTQ-FT or Bruker APEX Ultra. The examples shown here will demonstrate the extended capabilities of the innovative workflow approach described in this section compare to the commercial instruments. In Table 3.2, an overview of different types of experiments already implemented using AWG3 is presented, showing the versatility and potential of this workflow-based approach. A more detailed description of selected experiments is provided in the next section and is referenced to the corresponding numbers in this table.

One of the advantages of AWG3 is that it allows easy implementation of automatic gain control (exp. (1) in Table 3.2). It has been shown that accumulation of an excessive charge in the FTICR cell results in decreased mass accuracy[163]. Highest mass accuracy is achieved when a well defined number of ions is loaded into the ICR cell for analysis[107,164]. This keeps the effects of space charge constant throughout the experiments and leads to an improvement in the magnitude and stability of the mass accuracy. In addition internal reference masses are required to correct for the space charge related frequency shifts[165]. The internal calibrant can be mixed with the analyte before entering the MS[145,166] or it can be sequentially accumulated using different procedures[167-170]. However, such experiments alone are not sufficient to obtain optimal mass measurements accuracy (MMA) during LC-FTICR-MS experiments. It has been shown that internal calibration combined with adjustment of the accumulation time in an external linear quadrupole trap (to control the amount of ions entering the cell) improves mass accuracy down to 2 ppm[171]. Therefore, the adjustment of the amount of ions in the ICR cell leads to an improvement of mass accuracy. The augmentation of mass accuracy increases the resulting database query scores for peptide and protein identifications[153]. In our instrument, the amount of ions in the FTICR cell is controlled by adjusting the ion accumulation time in the linear octopole trap, based on the total ion current determined in a survey scan. The workflow is used to adjust the number of ions in the ICR cell to the desired constant amount. In an LC-MS experiment it was verified that the total ion current determined in a high-resolution scan was constant compared to the ion current detected in survey scan.

Set-up	Experiment using on-the-fly decisions in AWG3	Experiment using AWG3
FTICR-MS	*Survey scan followed by high-resolution scan* **1.** Implement automatic gain control **2.** Select peaks for accurate mass determination **3.** Start high-resolution scan when a compound enters the system (*e.g.* loop-injection)	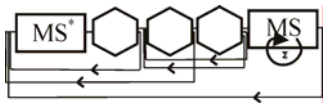
FTICR-MS/MS	*Survey scan followed by one or multiple MS/MS scans* **4**. Add masses to an inclusion- or exclusion list **5.** Precursor isolation using an automatically generated SWIFT excitation pulse **6**. Neutral loss triggered MS/MS **7.** Apply different MS/MS-methods on one species **8.** Dynamically switch between different MS/MS-methods (IRMPD, ECD, SORI-CAD) depending on peak properties **9.** Variable number of selected peaks for MS/MS (*e.g.* three most abundant for ECD and one for SORI-CAD) **10**. Vary the number of accumulated scans for MS/MS **11**. Carry out additional MS/MS scan based on evaluation of the first MS/MS-spectrum **12**. Carry out "quick" survey scans in irrelevant parts of LC **13.** Monitor specific mass differences (*e.g.* characteristic for a post-translational modification or isotopically labeled peaks)	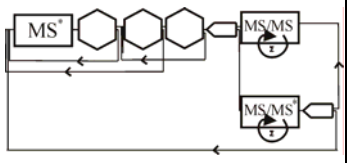
Miscellaneous	**14.** FTICR-MS coupled with matrix-assisted laser desorption ionisation (MALDI) source **15.** FTICR-MS coupled with desorption electrospray ionisation (DESI) source **16.** External signal from *xy*-stage controller is used to trigger data acquisition **17.** Record external signal from LC (*e.g.* UV detector) and use as an control variable **18.** MS and MS/MS in imaging combines with all previous possibilities	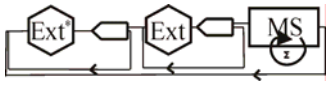

Table 3.2. Different types of FTICR-MS experiments using AWG3 for on-the-fly decisions based on different evaluation modules.

The selection of a certain peak for accurate mass determination (exp. (2) in Table 3.2) has been reported by Olsen *et al.*[172] using the so-called SIM option in the LTQ-FT[172]. With AWG3, the same result can be obtained in multiple ways, *i.e.* the accurate mass analysis of a single peak (or isotope cluster) in the ICR-cell can be carried out either after SWIFT-isolation or after isolation in a quadrupole or ion trap in a hyphenated system.

Many different data-dependent MS/MS-experiments have been established in the field. Clearly, the generation of a dynamic inclusion- or exclusion list, and the automatic isolation of a precursor ion are pivotal (as exp. (4) and (5) in Table 3.2). Examples have been shown on data-dependent CAD and ECD triggered by a neutral loss (exp. (6) in Table 3.2)[173,174]. One of the unique features of AWG3 is the ability to apply different MS/MS-methods on one species and dynamically switch between these methods based on on-the-fly decisions (exp. (7), (8) and (9) in Table 3.2). These decisions are either based on total ion intensity, on precursor ion abundance or on charge state or a combination of these variables. The number of selected peaks from a survey scan may vary for each method (exp. (10) in Table 3.2). The number of MS/MS-experiments (accumulation of spectra) that can be carried out on an eluting LC-peak depends on the type of fragmentation method. For instance, SORI-CAD requires more time than ECD due to pumping requirements. During an LC-experiment it is convenient to shorten the FTICR acquisition time as much as possible in irrelevant parts of the chromatogram. With the LTQ-FT this can be done by using different *segments*, provided the analyst knows already which time parts of the LC-run contain the relevant peaks. AWG3 is demonstrated to switch automatically between different FTICR acquisition methods based on information obtained in a "quick" survey scan (exp. (12) in Table 3.2).

An additional new feature is the on-the-fly screening for specific mass differences between different clusters in a survey scan. This information is used to monitor isotopically labeled peptides for quantitative proteomics and to trace post-translationally modified peptides through specific in-source neutral mass losses (exp. (13) in Table 3.2). Finally, the combination of hardware and

software described in this chapter is used for the implementation of new experimental FTICR-MS scenarios such as the automated MS and MS/MS imaging using the possibility to control a *xy*-stage with AWG3[85] (exp. (18) in Table 3.2). In these experiments an external status signal coming from the *xy*-stage controller was monitored and employed to start and stop data acquisition (exp. (16) in Table 3.2.). Two examples will be shown in the next paragraphs of experiments (8) and (15) from Table 3.2.

LC-MS/MS dual MS/MS workflow

In this section the results from a LC-MS/MS workflow are discussed to illustrate the strength of making on-the-fly decisions with the AWG3 workflow control system. Clearly, it is advantageous to have automated tandem mass spectrometry for nanoLC-FTICR experiments. Moreover, making on-the-fly decisions during peptide elution regarding which MS/MS technique should be used on each eluting peptide improves the quality of MS/MS-spectra and thus identifications in automated high-throughput approaches.

A tryptic digest of savinase was used to test the workflow-based method for applying either SORI-CAD or ECD. The workflow of the LC-MS/MS experiment is shown in Figure 3.4a. Executing the workflow starts with recording a single mass spectrum in the module called *SurveyScan* (approximately 2 seconds). Then, the signals in the spectrum are peak-picked and clustered on-the-fly in modules called *PeakPicker* and *ClusterList*, respectively. Note that if no peaks or no clusters are found another *SurveyScan* is recorded. In principle, a cluster list can contain multiple mass values from different co-eluting peptides. All these masses in the cluster list are compared with those already present in the module *ListTest*. This ensures that no time is wasted on repeated MS/MS of previously analysed peptides. A new *SurveyScan* is recorded if no additional masses are present in the cluster list compared with the *ListTest*. When a new peptide mass is detected the workflow enters a new decision module. In this example, based on the charge state of the cluster, it is decided whether this peptide is selected for ECD (charge state > 1) or SORI-

CAD (charge state = 1). This on-the-fly decision process takes just a few milliseconds. After an ECD-experiment has been carried out in the module *Sequence_ECD,* it is in principle possible to select a second peptide from *ListTest* for fragmentation. However, in this case ECD consumed a considerable amount of time (approximately 3 seconds per scan, 10 spectra were recorded and summed) so we decided to start a new *SurveyScan* after each MS/MS-experiment. Similarly, for time consumption reasons after each SORI-CAD experiment a new *SurveyScan* was acquired. At the end of the workflow the user defines the maximum number of experiments to be carried out in a simple *decision* module.

The analysis of the data from this example is shown in Figures 3.4b-d. In Figure 3.4b the contour plot of the mass spectra of all *SurveyScans* is shown. The numbers in this plot indicate eight *m/z*-values of five different tryptic peptides that are in agreement with the molecular masses of the theoretical digest of savinase. These five different peptides are sufficient for identification of savinase, however in more complex protein mixtures such peptide mass fingerprinting methods are insufficient and MS/MS experiments are needed for protein identifications. From the data recorded with *event viewer* module it was confirmed that the five multiply charged savinase peptide peaks were selected for ECD MS/MS. The singly charged *m/z*-values 1100.6 and 1200.6 (corresponding to peaks 6 and 8 in Figure 3.4b) were selected for SORI-CAD fragmentation.

As an example of peak selection after on-the-fly evaluation, *SurveyScan* number 35 is shown in Figure 3.4c. From this spectrum *m/z* = 911.0 was selected for ECD. The resulting ECD-spectrum is shown in Figure 3.4d, which is in excellent agreement with the doubly charged peptide "VAVLDTGISTHPDLNIR". Nine *z*-fragments and one *c*-fragment are assigned, resulting in 63 % peptide sequence coverage. It is evident that such high quality MS/MS spectra add to the confidence of protein identifications in more complex mixtures.

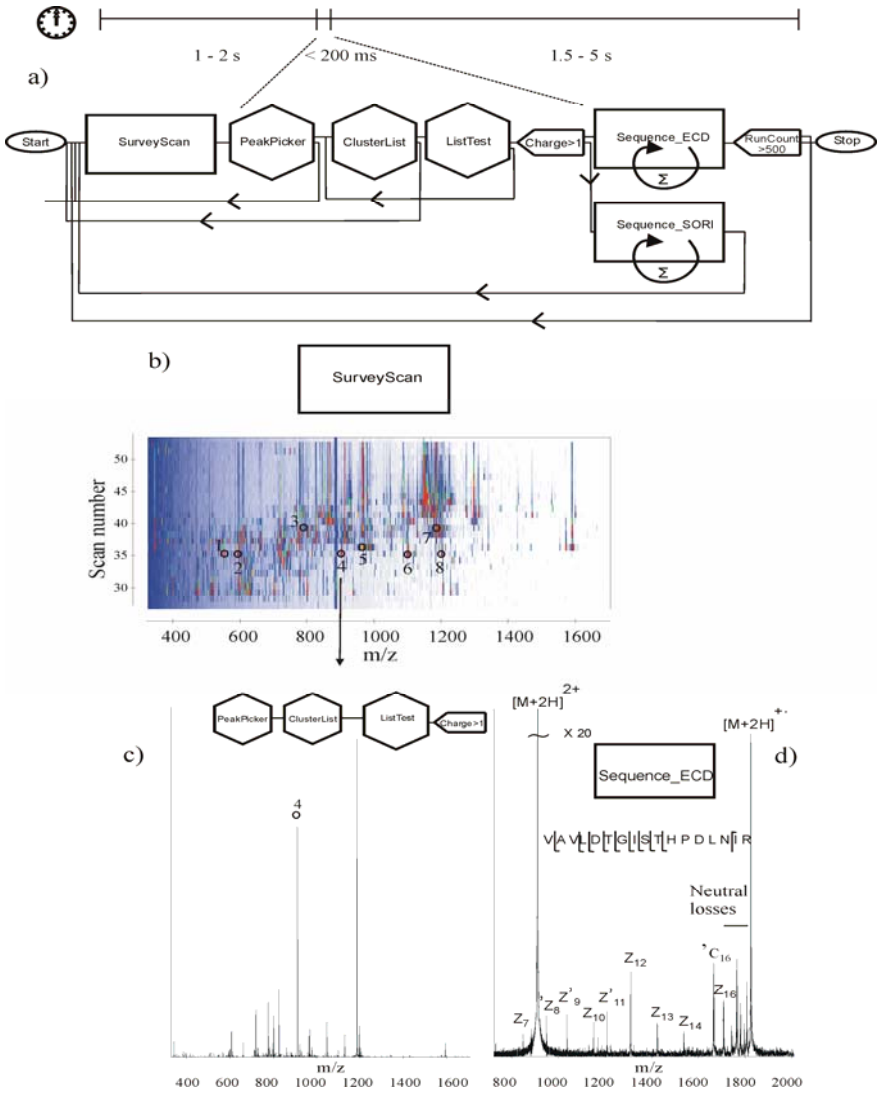

Figure 3.4. a) Workflow of automated ECD experiment b) 3D visualization of the *SurveyScan* for tryptic digested savinase (x = m/z, y = scan number, z = intensity);1-AQSVPWGISR (z = +2) 2-NPSWSNVQIR (z = +2) 3-NTATSLGSTNLYGSGLVNAEAATR (z = +3) 4-VAVLDTGISTHPDLNIR (z = +2) 5-GVLVVAASGNSGAGSISYPAR (z = +2) 6-AQSVPWGISR (z = +1) 7-NTATSLGSTNLYGSGLVNAEAATR (z = +2) 8-NPSWSNVQIR (z = +1) c) selected spectrum –of 61 recorded- from *SurveyScan* d) selected ECD spectrum 4-VAVLDTGISTHPDLNIR (z = +2).

This LC-MS/MS workflow demonstrates the power of on-the-fly decisions. Precious sample and analysis time are saved compared to first measuring a full LC-MS trace, then creating a list of peaks-of-interest, and then running the sample again targeting these peptides for ECD. Previously, Cooper and co-workers[175] reported data-dependent LC-MS/MS (ECD) experiments on proteomic samples. Using an LTQ-FT instrument, they recorded high-resolution MS- and MS/MS scans in an alternating way in the ICR cell. Singly charged peptides were dynamically excluded from ECD-experiments. The two most abundant peaks from each survey scan were selected, on-the-fly, for ECD fragmentation by first using the ion trap for isolation of the precursor ion, and then carrying out ECD in the ICR cell. Using the approach presented in our work, the singly charged species are not lost but subjected towards SORI-CAD. In addition, in AWG3, the type of MS/MS-experiment may vary from species to species depending on the user-defined selection and decision criteria. In this way complementary MS/MS information is automatically provided. An experiment were the compounds of interest were subjected to ECD and SORO-CID with LTQ-FT was performed by Koekher et. all[176]. In their work, if the ion of interest was multiply charged, ECD followed by SORI-CID was performed for all peptides. Compared with this experiment, we can make now the decision when do we want to perform ECD or SORI-CID, in this way saving time and sample.

DESI-FTICR imaging workflow

A workflow was designed for a DESI-FTICR-MS imaging experiment to demonstrate how external signals can be used to control a complex experiment. The workflow is shown in Figure 3.5a. In this case external input monitoring and evaluation modules are used to determine when the sample stage has arrived at a certain position and then triggers FTICR data acquisition. Upon completion of the DESI-FTICR-MS scan at one position the workflow directs the sample stage to the next position.

Figure 3.5 additionally demonstrates the utility of the high mass resolution of FTICR mass spectrometry in imaging mass spectrometry[85]. Three

droplets containing nominally isobaric peptides were spotted on sandblasted plexiglass: Val5-Angiotensin II (m/z = 1032.5261), Lys-des-Arg9-Bradykinin (m/z = 1032.5625) and a mixture of these two peptides. From Figure 3.5 it follows that the peptides were present in a very narrow mass range but with different spatial distributions (as expected from spotting of three droplets). The images were composed and visualized by using in-house software[177]. The pixel size of the image is 1 × 1 mm, the image containing 6 × 25 pixels. The selected mass window was 0.01 Da. The lower mass resolution of TOF mass spectrometers cannot resolve these components and so the distinction cannot be made. This example clearly demonstrates the advantage of high mass resolution FTICR in imaging mass spectrometry and the flexibility of AWG3 in accommodating very different types of experiments.

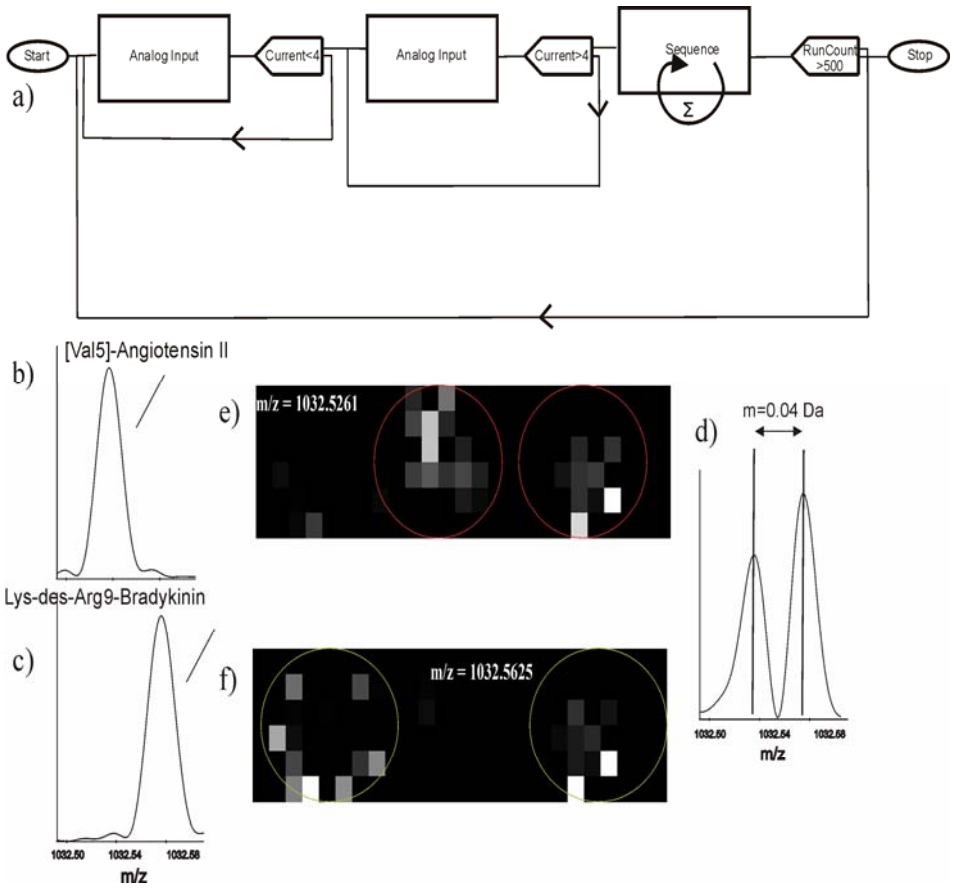

Figure 3.5. a) Workflow of an automated DESI experiment b) selected spectrum of m/z = 1032.5261 c) selected spectrum of m/z = 1032.5625 d) selected spectrum from the region with both peptides e) DESI-image of m/z = 1032.5261 f) and m/z = 1032.5625.

3.1.4 Conclusions and outlook

The implementation of the workflow-based method AWG3 has shown its importance of making decisions on-the-fly. This FTICR acquisition software is easy to use and to adjust owing to the modular design. We tested and established a wide variety of workflow control scenarios on our 7T FTICR-MS instrument. Two different workflows are presented to exemplify the functionality of our control system. The first workflow describes automated ECD- and SORI-CAD experiments. Based on information resulting from a survey scan, peaks are selected on-the-fly for one of these fragmentation methods. ECD was performed only on ions with a charge state higher than 1+ and the singly charged ions were fragmented using SORI-CAD. The flexibility in choosing MS/MS method increases the information from each LC-run. As an example, one of the ECD spectra obtained from an automated LC-FTICR-MS/MS (ECD) experiment of trypsin digested savinase was shown, including nine *z*-fragments and one *c*-fragment (63 % peptide sequence coverage). The second workflow exemplifies a DESI experiment for imaging MS purposes. The external information from a moving *xy*-stage was used to ensure the position of the sample stage is fixed at the subsequent raster position before initiating the next DESI mass analysis.

The AWG3 workflow control system enables both MS- and MS/MS-experiments to be performed on FTICR mass spectrometers in one single experiment or workflow. Based on decisions on-the-fly, the system can dynamically switch between different fragmentation methods within one workflow (*e.g.* SORI-CAD, ECD and IRMPD), and the parameter settings of each MS/MS-experiment may vary from scan to scan (*e.g.* the number of accumulated scans or number of selected peaks). AWG3 is already used to control imaging FTICR experiments demonstrating the system's experimental flexibility. Although this chapter deals with workflow based control of FTICR-MS experiments the system described can be readily employed for the control of

many other scientific instruments ranging from mass spectrometers and ion beam lines to high end UHV compatible scanning probe systems.

3.2 On-the-fly data-dependent decisions in quantitative proteomic studies

In proteomics, quantitation of proteins is important to determine the difference in protein composition of samples obtained under different experimental conditions. To date, several methods for protein quantification have been developed[178]. The most common are based on staining intensity of proteins after gel separation (e.g. difference gel electrophoresis-DIGE[179]), or on ion intensities of peptides analysed by mass spectrometry[180]. The latter approach is often used in combination with liquid chromatography mass spectrometry where the task is to find quantitative differences in highly complex mixtures. This can be achieved by comparing ion chromatograms of samples run in parallel, which requires time alignment correction for any experimental differences that might occur between the separate runs. The alignment issue is avoided using isotope labeling approaches developed over the past couple of years, such as stable isotope labeling with amino acids in cell culture (SILAC)[181] or even the whole animal, stable isotope labelling in mammals (SILAM)[182] and isotope-coded affinity tags (ICAT)[183] which incorporate heavy isotopes (^{13}C, ^{15}N) into proteins. When these proteins (or their digests) are mixed with an unlabeled reference sample and analysed by LC-MS, labeled and unlabeled peptides can be distinguished by a characteristic mass difference, while their ion intensities directly reflect their relative abundance in the original samples.

Although quantitation in isotope labeling and label-free approaches is different, they have in common that protein identification depends on mass spectrometric fragmentation. A typical mass spectrometric workflow consists of

MS scans detecting chromatographically separated peptides, triggering intermittent MS/MS events for peptide fragmentation. From these fragmentation spectra peptides are identified, which are subsequently quantified from MS intensities in the same run. In this scenario, the problem is in the time constraint in the acquisition of a maximum number of MS/MS spectra for sufficient depth in peptide identifications. Sacrificing too many data points in the MS scans would prohibit proper quantitation. This dilemma relates to the phenomenon that in data-dependent triggering of MS/MS often the highest peaks are selected for fragmentation, which are not always of high biological interest and relevant for quantitative studies. Maximizing the number of MS/MS scans then is a way to drill down to the lesser abundant peaks, but compromises quantitation. Yet another aspect often encountered in comparative proteomics studies is that the vast majority (>90%) of all identified proteins do not change in abundance. Thus, these proteins are mostly of limited value to biologically explain the difference between the samples, and it could be argued if the MS/MS-time needed to identify them is well spent.

One solution to these issues is in the decoupling of quantitation and identification in two consecutive runs of the same sample. The first run would then consist of MS scans only which would be used for quantitation purposes, resulting in an inclusion list of only those features that seem of interest for identification in the second run. This is in fact common practice in the case of 2D gel electrophoresis, where only those spots are selected that show a difference in abundance, which can then be analysed by mass spectrometry for protein identification. This two-step process can also be applied to (multidimensional) LC-MS experiments if many samples can be compared before peaks that meet certain criteria are selected for identification. This has been done by label-free approaches[180,184] and there are no fundamental reasons why this could not be applied to experiments utilizing stable-isotope labeling as well. The major bottleneck however is the time needed to analyse multiple MS ion chromatograms, e.g. from a 2D LC-MS experiment, and proper bioinformatic and statistical tools for time-alignment, peak extraction and peak integration.

Consequently, the time between the first (MS) and second (MS/MS) run may be considerable, potentially giving rise to changes in experimental conditions, which may affect the experiment.

Here we describe an efficient method to circumvent most of these issues. It comprises the quantitation of labeled peptides on-the-fly, followed by targeted fragmentation of only those peptides that are labelled and exceed a user-defined abundance ratio. In short, MS (survey) scans are processed on-the-fly including automatic peak picking and detection of peptides pairs with an expected (user-specified) mass difference corresponding to the isotope label used. Subsequently the software determines the peak ratio and only those peptide (feature) pairs that exceed a specified difference in abundance are selected for fragmentation (MS/MS). This is a time-efficient approach where only those peptides are fragmented that are of potential biological interest, thereby liberating time for MS detection and quantitation purposes. This approach is highly flexible because it accommodates any mass difference introduced by the isotope label in the same time, and a combination of mass criteria when multiple labels are used. Also, thresholds can be set to trigger different type of MS/MS methods. Furthermore, it circumvents the need to repeat the experiment thereby reducing consumption of (biological) material and experiment time. All together, this provides a time-efficient tool to quantify labeled peptides on-the-fly in quantitative proteomic studies with novel flexibility in making intelligent data-dependent decisions.

3.2.1 Samples and methods

Sample preparation

Acetonitrile (BioSolve, the Netherlands) and acetic acid (JT Baker, Phillipsburg, USA) were used without prior purification. All the lysines and all N-termini of the peptides in a tryptic BSA-digest (Sigma) were dimethylated using

formaldehyde[185]. The dimethylation was performed by using either "normal" or "deuterated" formaldehyde (CH_2O and CD_2O, respectively, both from Sigma) through reductive amination, resulting in "light-labeled" and "heavy-labeled" BSA-peptides (4 Da mass difference between them).

5 microliter of this solution was injected on the LC-system for analysis. The nanoLC-system (LCPackings, Amsterdam, the Netherlands) consists of an autosampler, a switching unit, a nanoflow system and a UV detector. The switching unit is equipped with a reverse-phase capillary precolumn (C18 PepMap 100, internal diameter 0.3 mm, length 1 mm) and is used for preconcentration of the sample at a flowrate of 30 microL/min. Peptide separation is subsequently carried out on an analytical column (C18 PepMap 100, internal diameter 0.075 mm, length 15 cm) using nanoflow elution at 300 nL/min. The eluents used were 1% acetic acid and 5% acetonitrile in water (A) and 1% acetic acid and 10% water in acetonitrile (B). The gradient used for the separation of peptides was: 0-30 min: 0-50% B, followed by 30-35 minutes: 50-90% B. The nanospray source connecting the LC-system to the mass spectrometer was built in-house and equipped with New Objective Picotips™.

All the peptide mass measurements were performed in the positive ion mode using a modified Bruker APEX 7.0eT FTICR-MS equipped with a 7 T superconducting magnet and an open cell[161]. The ions generated by the electrospray ion source are externally accumulated in a linear octopole ion-trap[144] (typical accumulation time 0.4 seconds) prior to transfer to the ICR cell via two RF-only quadrupole ion guides.

Experimental

A pool of heavy and light peptides was injected in a ratio of 5:3 into a LC-FTICR-MS system. First, a mass spectrum is recorded in the module *SurveyScan*. Then, the signal is peak picked above a certain threshold and clustered by using the evaluation modules *PeakPicker* and *ClusterList*, respectively. If no peaks or clusters are found in these modules a new mass spectrum is recorded. Further, in the *Labeling* module, pairs of heavy labeled- light labeled peptides with a

mass difference of 4 Da are found and recorded. A user-defined expression takes care of selecting m/z values only if they differ in intensity in a certain percentage that can be defined by the user. To make this decision, a *decision* module is implemented. For every new cycle, the added masses are compared with the one found in *ListTest* module. For peptides recorded and analysed in a previous experiment, the workflow starts again with a survey scan. For new-recorded values, a SORI experiment is carried out by automatic selection of the m/z value that corresponds to the highest intensity of the peak pair. In this experiment the heavy-labeled peptide is selected, due to the original mixing ratio. Again, a user-defined experiment is defined for performing MS/MS only for the highest m/z value. The whole experiment is performed for a pre-defined numbers of runs that cover the period when the peptides are eluted, and then the experiment is automatically stopped. Optionally, if the signal persists for a sufficiently long time, additional MS/MS experiments with different dissociation techniques can be used to provide further information about the peptide sequences.

3.2.2 Results

The acquisition and control software is markedly different and based on a flow control oriented model[186] and it is described in Section 3.1.

In the workflow presented in Figure 3.6 the mass spectrum recorded in the *SurveyScan* is passed to the *evaluation* modules for further processing. Then, in a *decision* module a decision is made on-the-fly which way the experiment continues. In this example, when a pre-defined difference of 4 Da between the first monoisotopic peaks of two different clusters is detected, the experiment continues with an MS/MS experiment of the peak of interest. If no pairs with the specific mass differences of 4 Da is found, a new mass spectrum in *SurveyScan* is recorded.

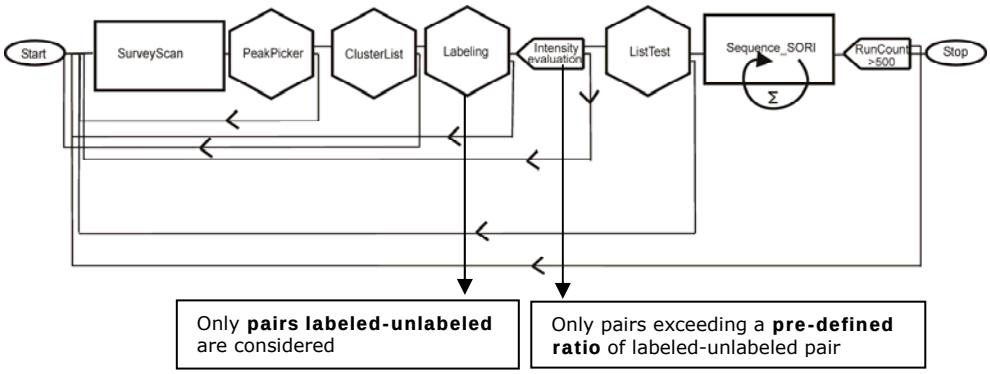

Figure 3.6. Workflow of automated targeted on-the-fly selection of labeled peptides.

In Figure 3.7a, a contour plot is shown of the mass spectra from all survey scans of the experiment. As an example, in Figure 3.7b a zoom-in is shown of the detected heavy labeled – light labeled pair from survey scan experiment number 64. A more extensive description of the workflow method modules and their use are described in a previous paper. In this work, we implemented a new *Labeling* module. By using this module pairs of ions or clusters that differ in mass with one or more pre-defined values, Δm, are searched during an on-line LC experiment. To calculate this difference, different criteria such as the monoisotopic peaks, the most intense peak of a cluster are used. Δm is given with a certain precision and can be varied by the user depending on the precision and resolution of the mass analyser.

A variable is included to define a maximum multiplicity of the number of labels. In addition, multiple Δm values can be included in the *Labeling* module, when more than one type of label has been used in the experiment. After processing of the incoming information, the output of this module is a list with m/z values and other characteristic values of the heavy labeled compounds with their light labeled counterparts (see Table 3.3).

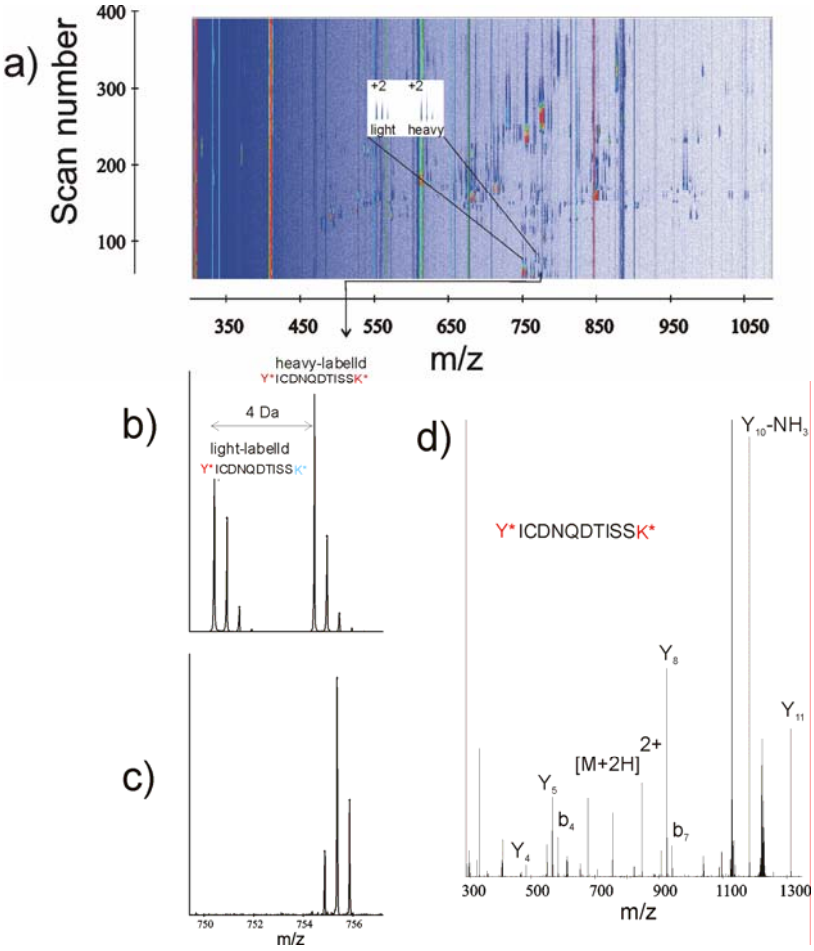

Figure 3.7. a) 3D visualization of the *SurveyScan* for tryptic digested BSA (x = m/z, y = scan number, z = intensity) b) selected spectrum –of 64th recorded- from *SurveyScan*; Y*ICDNQDTISSK* (z = +2) and Y*ICDNQDTISSK* (z = +2); c) zoom of the labeled ion selected for SORI experiment d) selected SORI spectrum of Y*ICDNQDTISSK* (z = +2); Y* = tyrosine containing two methyl-groups (163 + 28 Da), K* = lysine containing two methyl-groups (128 + 32 Da), K* = lysine containing two heavy methyl-groups (128 + 28 Da).

Module	Input	Output
Labeling	m/z values and intensity values recorded in *PeakPicker* or *ClusterList* modules (charge state and peak resolution are added if input is given by this module)	list of m/z values, intensity values, charge and number of peaks of labelled and unlabelled species and the multiplicity of the labelled species per spectrum

Table 3.3. Input and output information for *Labeling* module.

Compared to the commercial systems, our workflow-based system offers more flexibility as well as the possibility to design new experiments that are not possible otherwise[186]. Recorded parameters such as charge, number of peaks, intensities can be readily used in the decision-making. Decisions can be made by user-defined logical expressions if the most intense, the less intense or both selected masses (heavy-light labeled) are selected for MS/MS. In Figure 3.7c, the isolation spectrum is shown followed by the SORI experiment of the most intense peptide of the pair, Y*ICDNQDTISSK* (z = +2). In this way, five more heavy labeled – light labeled peptides (12 % coverage) of BSA were found and the heavy labeled peaks were automatically subjected to MS/MS and identified, without any time-losses in selection of the light labeled lower-intensity counterparts.

Additionally, a pre-defined ratio between the intensity of the heavy labeled – light labeled pair can be set in such a way that in complex biological samples only if this ratio exceeds a certain value further analysis is performed. Furthermore, the implementation of the *ClusterList* module is very important for labeling experiments. Using the decharged masses in the decision making process, prevents the analysis of the same peptide multiple times.

Another unique feature of this workflow-based approach is the possibility of carrying out different MS/MS methods on one species and dynamically switch in one experiment between these methods based on decisions on-the-fly[186]. For instance, based on charge state, it can be decided if the m/z value is subjected to different dissociation techniques, such as SORI or ECD. SORI experiments can

be performed for peptides with charge +2 and ECD experiments can be performed for peptides of high charge state. Thus, by making on-the-fly decisions using recorded parameters from any module implemented in the workflow, relevant information can be obtained and time and sample is saved.

3.2.3 Discussion and conclusions

We demonstrated here how our software works for experiments of labeled peptides. Certainly, biological applications would benefit from our acquisition software based on a workflow method. It is a flexible and user-friendly method that allows on-the-fly selection of labeled peptides followed by targeted fragmentation of the peptides that exceed a user-defined abundance ratio. Only in this way automatic analysis of differences in protein expression of low abundant species is now possible. Moreover, different on-the-fly fragmentation methods can be used in one single experiment, thus increasing the chance of peptide identification.

4

Imaging of peptides in the rat brain using MALDI-FTICR mass spectrometry

Analytical methods are pursued to measure the identity and location of biomolecules down to the subcellular (μm) level. Available mass spectrometric imaging methods either compromise localization accuracy or identification accuracy in their analysis of surface biomolecules. In this study imaging FTICR-MS is applied for the spatially resolved mass analysis of rat brain tissue with the aim to optimise protein identification by the high mass accuracy and online MS/MS capabilities of the technique. Mass accuracies of 6 ppm or better were obtained in the direct MALDI-analysis of the tissue together with a spatial resolution of 200 μm. The spatial distributions of biomolecules differing in mass by less than 0.1 Da could be resolved, and are shown to differ significantly. Online MS/MS analysis of selected ions was demonstrated. A comparison of the FTICR-MS imaging results with stigmatic TOF imaging on the same sample is presented. To reduce the extended measuring times involved it is recommended to restrict the FTICR-MS analyses to areas of interest as can be pre-selected by other, faster imaging methods.

Ioana M. Taban, A.F. Maarten Altelaar, Jens Fuchser, Yuri E.M. van der Burgt, Liam A. McDonnell, Gökhan Baykut, Ron M.A. Heeren**,** *J. Am. Soc. Mass Spectrom.*, **2007**, 18, 152-161

Chapter 4

4.1. Introduction

In several diseases like Alzheimer's, cancer, obesity, etc., malfunctioning proteins or protein fragments (i.e. peptides) plays a crucial role. Changes in protein function can be caused by a number of events such as altered localization[23,187,188], posttranslational modifications[189-192], or expression levels[23,193]. Studying these events is a challenging area because of the dynamics of the cellular proteome and the sensitivity of the molecules of interest to fluctuations in their natural surroundings. Recently imaging mass spectrometry (IMS) has been recognized as a proteomic tool for in situ spatial analysis of (diseased) tissue[6,11]. MALDI-MS has been shown to be able to determine the localization of native biomolecular components like proteins and peptides in tissue[32,33,194-196]. Often, the data includes several unknown species with a spatial distribution that indicates it is associated with a disease or biochemically-altered region of the tissue. A strategy that combines high mass resolution mass spectrometry with imaging has the potential to directly identify these unknown compounds. In addition to the high mass resolution online tandem mass spectrometry further can aid in compound identification.

In most laboratories, TOF is used for peptide imaging directly from biological tissues. Both, MALDI[27,36] and SIMS [197-199] approaches can provide good mass resolution images (~10^4). MALDI can be used for the analysis of high mass species (up to 100 kDa) at low spatial resolution (pixel size > 25 μm)[32]. Very high spatial resolution is obtained using SIMS (pixel size < 1μm[198], however its sensitivity rapidly decreases with increasing mass, making the technique less suited for protein analysis. Surface modification techniques such as Metal Assisted SIMS or Matrix Enhanced SIMS can be used to extend the useable mass range to small peptides and proteins[25,64,196,200-207].

Two mass spectrometric imaging approaches currently exist: microprobe and microscope mode imaging. In microprobe IMS experiments, the ionisation beam is rastered over the sample surface acquiring a mass spectrum at each

x,y-coordinate. Mass resolved images or spectra from regions of interest are then extracted from the dataset. The spatial resolution obtained in MALDI microprobe imaging is typically in the 100-200 μm range, limited by the size of the laser spot used[30,56]. The development of micrometer resolution has been reported[66], however decreasing spot size has been found to lead to decreasing sensitivity for high mass species. An alternative approach for high spatial resolution IMS is the mass microscope. Here the spatial resolution is about 4 μm[68] and independent of the spot size of the ionising beam, but solely dependent on the ion optics of the instrument and the kinetic energy distribution of the MALDI-generated ions. The desorbed molecules retain their original spatial distribution during the TOF analysis and are projected onto a position sensitive detector. The mass microscope can record the spatial information from within the spot of the MALDI laser beam with 4 μm spatial resolution (600 nm pixel size). By using laser spots of 200 μm diameter, a high-resolution image is obtained with each laser shot. Because the mass microscope is also a TOF mass analyzer, an image is obtained for each analyte. In a microprobe experiment, this spot would constitute a single pixel for each analyte[68].

By using MALDI-FTICR-MS it is possible to combine high resolving power, high mass accuracy, and the possibility of performing multistage MS/MS experiments[81,92-94] allows peptide identification directly from tissue[95]. The FTICR imaging strategy extends the identification possibilities in direct tissue analysis and is a valuable tool in MS imaging instrumentation.

For the first time, MALDI-FTICR-MS was used for imaging of rat brain tissue sections. In the study described in this chapter, the left half of a rat brain tissue section was imaged with FTICR-MS and the right half with the mass microscope MALDI-TOF. The resulting images were compared to demonstrate the strength of the high mass resolution, accurate mass measurements made with the FTICR-MS and its added value to imaging experiments. In addition on-line FTICR-MS fragmentation techniques were used to identify a neuropeptide found during the tissue analysis.

4.2 Experimental

Tissue sections

Experimental procedures were in accordance with the European directives (86/609/EEC) and approved by the Commission on Laboratory Animal Experiments of the University Medical Centre Utrecht. Male Wistar rats (Crl:WU) weighing 350 g were obtained from Charles River. Rats were decapitated without prior anesthesia, and brains were dissected and frozen in liquid isopentane, cooled to -50 ºC on dry ice, and then stored at -80 ºC until sectioning. The 10-μm-thick rat brain tissue sections were cut at Interaural 7.2/Bregma -1.8 mm[208], using a cryomicrotome. Sections were thaw-mounted on Indium-Tin-Oxide-coated glass slides and were stored at -80 ºC until use. Prior to mass spectrometry, tissue sections were slowly brought to room temperature in a desiccator.

The rat brain tissue sections were washed twice in 70% cold ethanol (Biosolve, Valkenswaard, The Netherlands) for 1 minute. After washing the tissue sections were allowed to dry for 30 min after which the matrix was applied[53] using a TLC sprayer[209,210] (30 mg/ml of 2,5-dihydroxybenzoic acid in 50:50 ethanol/water and 0.1% trifluoroacetic acid). The sample was then covered with a 3 nm layer of gold using a plasma sputter coater (Quorum Technologies, Newhaven, U.K.).

Mass spectrometry

FTICR-MS FTICR-MS experiments were performed on an APEX III FTICR mass spectrometer (Bruker Daltonics, Billerica, MA, USA)[211] equipped with a 7 T superconducting magnet and a combined Electrospray/MALDI source ("CombiSource").

During FTICR-MS experiments, collision gas was pulsed into the medium pressure chamber housing a hexapole ion trap before firing the nitrogen laser (λ = 337 nm, laser repetition rate = 20 Hz, laser spot diameter 200 μm on the

target). The ions, cooled by collisions, were captured and accumulated in the hexapole (10 laser shots per spectrum) located in the front of the target and then further guided to the cell for mass analysis or tandem MS experiments. Isolation and fragmentation were performed in different sections of the ion guides before ions enter the ICR cell for some of the MS/MS experiments presented in the chapter.

Compass^{TM} software was used to control the instrument. Atlas Control software was additionally used to control the sample stage. This enabled an accurate setting of the step size for the imaging experiments. Each image of half a brain section spans an area approximately 7.2 × 8.4 mm and comprises 24 × 42 pixels of 300 × 200 μm dimensions.

TOF MALDI-TOF experiments were performed on a heavily modified TRIFT II (Physical electronics, Eden Prairie, MN) instrument incorporating an ion optical microscope[68,212,213]. The TRIFT II mass spectrometer is equipped with a Nd:YAG laser (λ = 355 nm, repetition rate = 10 Hz, oval spot = 150 × 200 μm). The data recording for the microprobe and microscope analysis is done simultaneously in this TRIFT set-up. The sample stage was continuously moved at 100 μm/s while recording 150 × 200 μm TIC (total-ion-count) images and full spectra with each laser shot. To cover half of the rat brain tissue section 65 line scans (the distance between two line scans is 120 μm), each containing 850 individual single-shot images were acquired. The size of each pixel for the TOF microprobe images overlaying the TIC stigmatic image was chosen to be 10 × 120 μm.

Data processing The visualization software, DataCubeViewer, allows the generation of selected ion images from the FTICR-MS data set. The minimum mass window that can be selected is 0.1 Da. This value was used for all images shown in this chapter. The intensities of the selected mass range are binned together. In the resulting image white represents the highest relative

intensity. The spectra of individual linescans can be examined with the in-house AWE and AWE3D software[158].

For the TOF images, the individual TIC single-shot images were combined to form a linescan and subsequently all linescans were assembled to construct the total image, using in-house software (Spatial Image Composer)[177]. The position-correlated TOF mass spectra were used to generate microprobe images of specific peaks using the same software.

4.3 Results and discussion

Imaging

In this study a comparison between microprobe MALDI-FTICR-MS imaging and microscope TOF-MS imaging is made. The symmetry of a rat brain tissue section makes it an ideal sample for such a comparison. In order to ensure a fair comparison, the two techniques were applied to opposing halves of a single tissue section and multiple replicates made for confirmation. Two different brain tissue sections were imaged and different areas of interest on other brain tissues sections and pituitary gland sections were studied. An optical inspection of the sample during the various stages of the experiment ensured that the transfers between mass spectrometers did not lead to the loss of matrix material. All the analyses were performed within 48 hours from their preparation.

The use of DHB matrix provides more intense signals in MALDI FTICR-MS of neuropeptides and less fragmentation of the ions compared to other matrices. Figure 4.1 shows the total mass spectrum of the MALDI-FTICR-MS analysis of the left side of the rat brain tissue section together with some representative images of the selected ions. It is clear from the figure that this approach can provide a wealth of biochemical information and that various

biomolecules have significantly different spatial distributions. The selected ion images show the distribution of the mono-isotopic peak of the compounds.

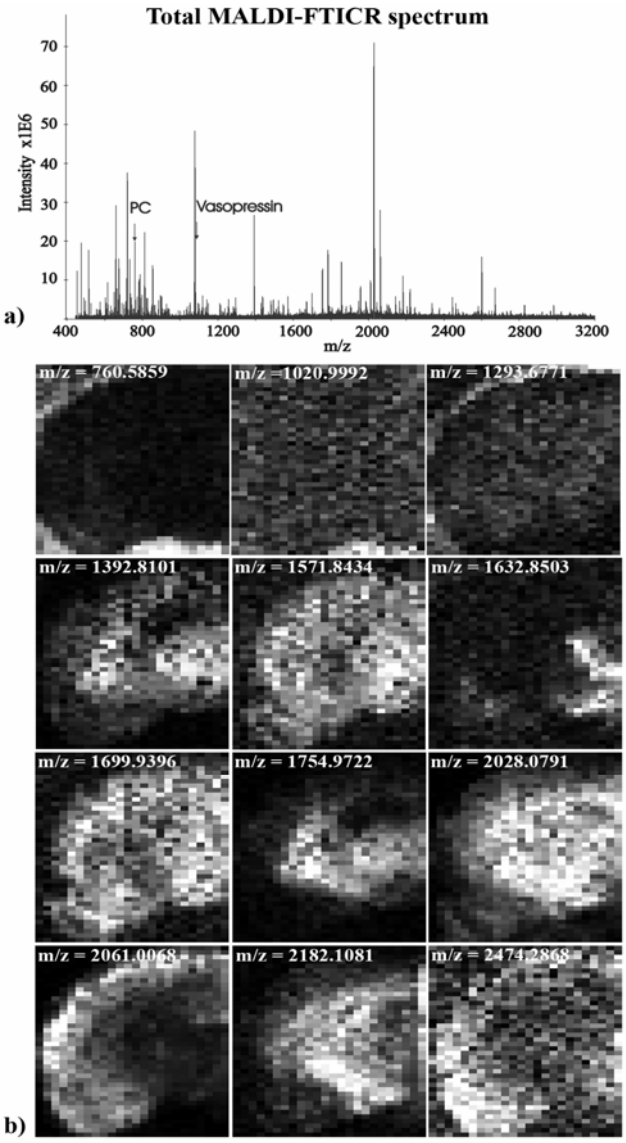

Figure 4.1. a) Total MALDI-FTICR spectrum of the left side of the rat brain tissue b) the rat brain with white representing the highest relative intensity for each *m/z* value.

Peptide identification is greatly facilitated using accurate mass FTICR-MS, even allowing positive identification if the proteome is small and the mass accuracy sufficiently high[42]. Variation in the total number of ions entering the ICR cell will affect the mass accuracy, thus calibration of the spectra with an internal calibrant is required for such peptide identification. Alternatively, known lipids located in the brain can be used as internal calibrants as these lipids are present in all spectra. Here we have restricted ourselves to external calibration.

The observed variation of the mass accuracy of phosphatidylcholine (*m/z* = 760.5856) and vasopressin are shown in Figure 4.2a,b for this externally calibrated imaging dataset.

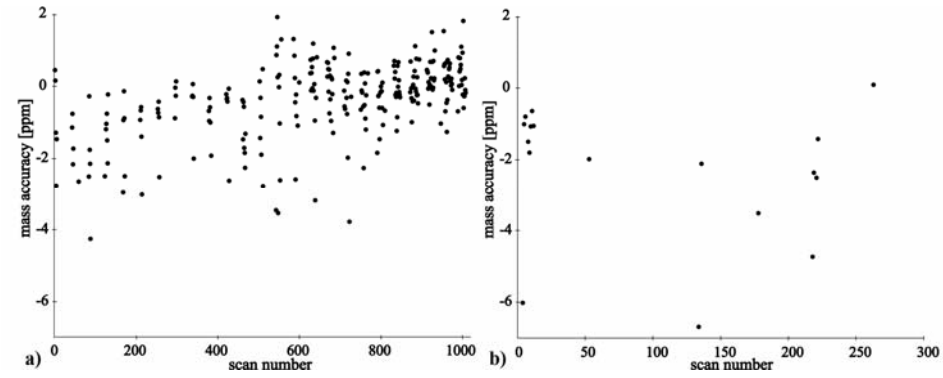

Figure 4.2. Mass accuracy of PC and vasopressin for the FTICR image of the left side of the rat brain tissue section. Neutral masses were used for calculations.

This figure was generated by examining the mass accuracy of the selected peaks above a set noise threshold for all linescans contained in the image. The number of points in Figure 4.2b is limited because vasopressin is present in a limited number of locations in the tissue. The mass accuracy of these compounds after external calibration is found to be approximately 6 ppm or lower. The number of laser shots was chosen so that the number of ions trapped in the ICR cell was not excessive, thus ensuring high mass accuracy. Internal calibration would improve the accuracy even further.

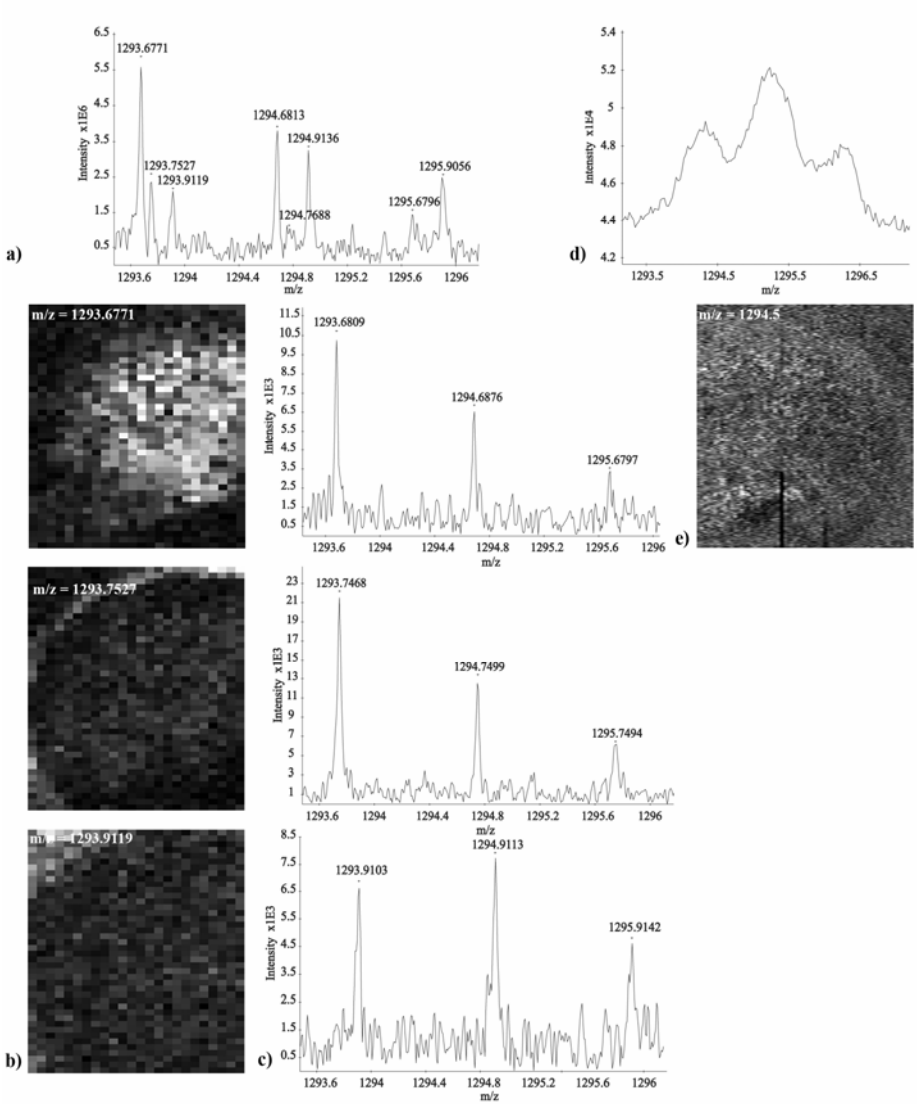

Figure 4.3. a) Selected region of the FTICR summed spectrum of half of the rat brain tissue section b) FTICR selected ion images of the first isotope of three different compounds c) Region of interest analysis reveals the spectrum of each individual component d) Selected region of the summed spectrum of half of the rat brain tissue section e) The TOF selected ion image of *m/z* = 1294. Due to a technical problem a part of a line scan of TOF experiments is not present in the selected ion images.

Figure 4.3 demonstrates the utility of high mass resolution FTICR mass spectrometry. Figure 4.3a shows a selected region of the total mass spectrum. The three different compounds and their isotopes, *m/z* = 1293.6771, 1293,7527, 1293.9119, present in this very narrow mass range show the high-resolution and quality of the FTICR-MS data. Moreover these three species exhibit a different spatial distribution in the rat brain as shown in the images in Figure 4.3b. Figure 4.3c shows the corresponding region-of-interest spectra, providing spectral information on the three individual components (Note the small differences in mass reflect the different number of ions generated in different positions, the cause of the 6 ppm mass errors). The lower mass resolution of the TOF imaging, which requires a constant extraction field, cannot resolve these components and so this distinction cannot be made and the image combines the spatial distribution of each component (Figures 4.3d and 4.3e). This example clearly demonstrates the advantage of high mass resolution FTICR in imaging mass spectrometry over medium mass resolution TOF.

Figure 4.4a shows a comparison of MALDI-FTICR (left side of the brain) and MALDI TOF imaging experiments (right side of the brain), Figure 4.4b an optical image taken after the imaging experiments, and Figure 4.4c a schematic of the rat brain tissue section at Bregma –1.8 mm. The distribution of the neuropeptide vasopressin (green) is included in Figure 4.4a. As can be seen the vasopressin is localized around the third ventricle, between the supraoptic nuclei, in agreement with previous studies[214-216]. The FTICR-MS images are microprobe images, whereas the TOF images are microprobe images for selected ions overlaying the TIC stigmatic image (grey scale). This overlay allows the localization of the peptides within the brain to be readily identified. All images are not smoothed. As can be seen the vasopressin distributions acquired with the two techniques are very similar. This demonstrates that compounds of interest localized with the ion optical microscope time-of-flight can be imaged with high mass resolution on the FTICR-MS on the same tissue section.

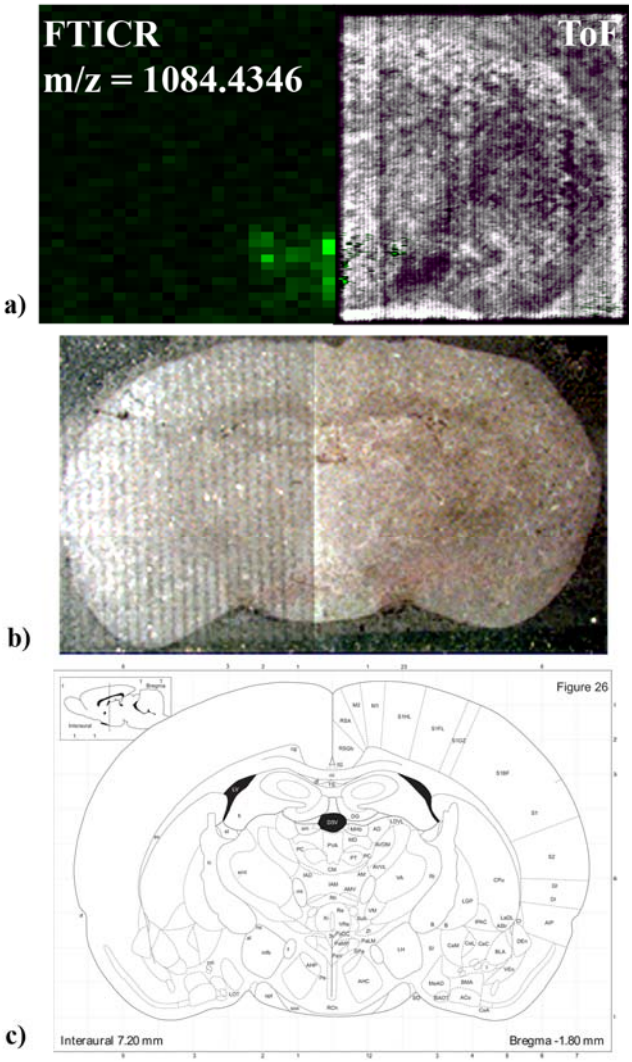

Figure 4.4. FTICR (left) and TOF (right) images of a) the distribution of Vasopressin *m/z* = 1084.44 on the brain section in green. For clarity in the right hand side TOF image the vasopressin distribution is overlain on the total ion image in black and white. b) Optical image with FTICR-MS laser tracks on the left clearly visible. c) Schematic representation of the anatomy of the rat brain tissue section with the specification where the tissue was taken from the brain.

A further advantage of using FTICR-MS for direct tissue imaging and profiling is the availability of multistage tandem mass spectrometry for peptide sequencing and identification. Different dissociation techniques such as SORI-CAD, IRMPD and CAD in an external linear ion trap are available with the FTICR set-up. Figure 4.5a shows the MS/MS spectrum of vasopressin obtained by CAD in an hexapole located prior to the ICR cell. The accurate parent ion mass and the accurate masses of the *b6* and *b*8 fragment ions were sufficient for positive identification of this neuropeptide. Only a few fragments were CAD generated (even for high collisions energies) due to the presence of a disulfide bond. Figure 4b shows the IRMPD spectrum of *m/z* = 2028, which is very abundant in the rat brain (see Figure 4.1a). Despite many fragments obtained with both IRMPD and SORI-CAD (not shown) the identity of this ion remains elusive.

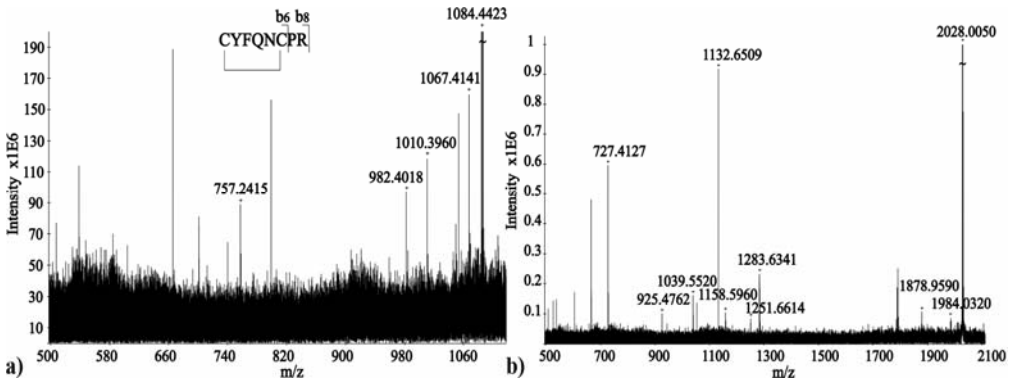

Figure 4.5. a) CAD of Vasopressin b) IRMPD for m/z = 2028.

4.4 Conclusions

For the first time, FTICR-MS imaging of endogenous neuropeptides and lipids was performed directly on rat brain tissue. The high mass resolution of the

FTICR-MS can reveal the localization of different compounds that cannot be distinguished with lower mass resolution TOF based imaging techniques. To perform a high-resolution FTICR-MS imaging experiment of an entire rat brain tissue section is very time consuming (almost 1 day for this brain tissue section). However, imaging of small-areas of interest combined with MS/MS analysis makes the approach a valuable tool. The real benefit of the technique is imaging small tissue areas to elucidate the peptide sequences of unknowns, thus complementing high spatial resolution stigmatic TOF imaging.

5

Parallel processing of large datasets from nanoLC-FTICR-MS measurements

A new approach for automatic parallel processing of large mass spectral datasets in a distributed computing environment is demonstrated to significantly decrease the total processing time. The implementation of this novel approach is described and evaluated for large nanoLC-FTICR-MS datasets. The speed benefits are determined by the network speed and file transfer protocols only and allow almost real-time analysis of complex data (*e.g.* a 3 gigabyte raw dataset is fully processed within 5 minutes). Key advantages of this approach are not limited to the improved analysis speed, but also include the improved flexibility, reproducibility and the possibility to share and re-use the pre- and post-processing strategies. The storage of all raw data combined with the massively parallel processing approach described here allows the scientist to re-process data with a different set of parameters (*e.g.* apodization, calibration, noise reduction), as is recommended by the proteomics community. This approach of parallel processing was developed in the Virtual Laboratory for e-Science (VL-*e*), a science portal that aims at allowing access to users outside the computer research community. As such, this strategy can be applied to all types of serially acquired large mass spectral datasets such as LC-MS, LC-MS/MS and high-resolution imaging MS results.

Y.E.M. van der Burgt, I.M. Taban, M. Konijnenburg, M. Biskup, M.C. Duursma and R.M.A. Heeren, *J. Am. Soc. Mass Spectrom*, **2007**, 18, 145-151

Chapter 5

5.1 Introduction

FTICR-MS in biomarker discovery

Nowadays mass spectrometry (MS) is the method of choice for the systematic analysis of a proteome[11]. Moreover, mass spectrometry-based proteomics is now one of the key-players in systems biology, *i.e.* the integrated approach of different technical disciplines to study the physiological processes in a cell or tissue[217]. The number of researchers using MS for protein and peptide analyses is still rapidly increasing. Multiple instrumental developments have made MS accessible to a broader research community and enabled automatic data acquisition. In clinical research mass spectrometry has opened new ways of (early) detection of diagnostic biomarker molecules. Their identification is done by differential analysis of protein expression patterns in patient and control samples. These patterns often change dramatically as a result of a disease and are thus helpful in early detection. Additionally, detection of such biomarkers can also play a significant role in prevention. In search for these biomarkers FTICR-MS is a powerful tool due to its distinguishing feature of ultrahigh mass resolution. In a proteomics set-up, FTICR-MS provides high mass precision and high mass accuracy of complex peptide mixtures, thus enabling peptide and protein identifications with high confidence. It is well-known that the variation in protein concentration by more than ten orders of magnitude is one of the major challenges in proteomics is in Anderson et al.[154]. The peptides that originate from high abundant proteins usually cause suppression of the low abundant peptide ions in ESI. A protein or peptide separation step such as gel electrophoresis or on-line LC is necessary to reduce the complexity of the mixture. The FTICR mass spectrometer is perfectly suited for on-line coupling to a nanoLC-system provided adequate differential pumping is applied. NanoLC-FTICR-MS runs typically take 30-60 minutes and with an ICR scan time of 1-2 seconds this results in 900-3600 individual transients. These transients occupy 4 megabytes of disk space each and Fourier transformation is required to obtain

corresponding mass spectra. The processing of these data has become a more time-consuming task than the LC-MS experiment itself and usually is carried out after the measurement. From these considerations the need for automatic processing and improvement of speed is evident. In this chapter we present new methodologies for processing large mass spectral datasets in a fully automated way. It will be shown that the total analysis time decreases dramatically upon using a flexible distributed computing environment. The increased processing speed enables on-line data analysis

Parallel processing of large mass spectral datasets

The analysis and interpretation of complex mass spectra has always been a challenging task for scientists in the field. Despite all modern computer facilities expert manual examination of a mass spectrum is still very common and necessary in an MS laboratory and thus remains an indispensable skill. However, it is evident that the amount and size of mass spectral datasets generated by modern mass spectrometers are incompatible with manual analysis. Examples of such large MS based datasets are found in high-throughput proteomics experiments[218] as well as high-resolution imaging MS experiments[219]. In a research lab real-time analysis of the experiments is pursued so that results can be used to adjust the parameters of the following experiment. Manual analysis of complex datasets is often inconsistent, incomplete and error prone. Thus, the automation of mass spectral data analysis and interpretation of peptide profiling measurements is pivotal for the extraction of valuable information from each experiment and remains a key challenge in bioinformatics. Automation not only tackles the increasing data volumes but also allows repeated use of data analysis strategies with different parameters or datasets. This automated approach improves both flexibility and repeatability of analysis of large MS based datasets.

The need for automation was already recognized after the first ESI experiments[220] and has been further developed since[221-223]. Modules for distributing the computational MS/MS data searches have been described[224].

Here we present a new approach that combines preprocessing and post-processing of serially acquired mass spectral datasets (*e.g.* LC-FTICR-MS datasets) in a distributed computing environment. The speed of processing increases by making use of multiple connected computers instead of one. This type of processing is further referred to as *parallel* processing, resulting in a decreased total analysis time. The processing of one single FT mass spectrum (in computer science referred to as a *job*) easily takes 3-4 seconds, mainly determined by the data transfer time and the peak picking algorithms. As a result, sequential processing of all jobs from one LC-FTICR-MS dataset (for example 2000 spectra) amounts to a total processing time of at least 2 hours. A parallel distribution of this workload (*i.e.* jobs) over different computers significantly decreases the total processing time. The requirements and details of a parallel set-up are described in the experimental section. In short, a computer network (cluster) usually consists of machines (*nodes*) that run the same operating system and share a data storage facility. The server starts processing the raw data using the available nodes. In the final post-processing step, the server summarizes the results and sends these to the data storage system as processed data, also referred to as metadata. Additionally, the metadata describes how, when and by whom the data set was collected. Thus, all acquisition and processing parameters are stored, enabling tracking and re-use of all such variables. It is also possible to use different computer clusters simultaneously, which are managed by a central server. In this type of data processing a so-called grid-approach is used. In a grid environment the nodes are platform independent and may be located at different geographical sites[225]. It is beyond the scope of this chapter to discuss the intricate details of data processing using a grid. Here, the processing speed of large mass spectral datasets will be evaluated on both single processors (such as a desktop PC) as well as dedicated computer clusters. The work on automated data processing of large LC-FTICR-MS datasets described in this chapter was embedded in the Virtual Laboratory for e-science (VL-*e*). VL-*e* provides a science portal for distributed analysis, *e.g.* creation and submission of jobs on a distributed

computer system in a grid. Furthermore, VL-*e* aims at allowing access to users outside the computer research community thus facilitating new scientific collaborations in grid environments.

An alternative way to speed up the processing of large data sets is reducing the data during the measurement ("on-the-fly"). This approach is implemented in the hardware of the LTQFT. Here, the original measurement (raw data) is discarded and only the reduced mass spectra are saved. Clearly the advantage is that processing of the data is finished immediately after the measurement. Unfortunately, this step is not a loss-less procedure and excludes the possibility of re-processing the raw data with a different set of parameters. Thus, the storage of all raw data is recommended, enabling future re-analysis or re-processing with a new set of parameters (*e.g.* calibration, apodisation) [226].

As an example, the parallel data processing approach described was tested using an algorithm that was developed specifically for processing datasets obtained from nanoLC-FTICR experiments. The serial mass spectra from LC-FTICR-MS are perfectly suited for parallel processing, because the spectra are (at least for the initial analysis) independent of each other, *i.e.* they can be analysed separately. The set-up of the algorithm is modular, which enables easy addition of new processing modules or change of parameters or routines. In this way the algorithm can be used for all types of LC-MS and LC-MS/MS datasets. The modular (workflow) nature of this approach also enables automated processing of other types of large mass spectral datasets such as the results obtained from high-resolution mass spectral imaging experiments[219],

5.2 Methodology

Algorithm for processing large FTICR-MS datasets

The main objective of this work is to enable processing of complex and large mass spectral datasets in a fully automated way using computational resources

in the grid. To this end, an algorithm is developed that facilitates processing of large MS datasets in parallel. Basically, this PP-VLAM algorithm (Parallel Processing Virtual Laboratory Amsterdam) consists of two parts. In the first part a mass list for each mass spectrum is generated. The subsequent second part generates a summary for the full dataset (written as an *xml* output file). The contents of the first part of this algorithm depends on the type of mass spectrometer used, whereas the latter part of the algorithm is generic and thus applies to all kinds of different LC-MS datasets (*e.g.* obtained from quadrupole, ion trap or time-of-flight instruments). Note that this approach also enables parallel processing of other two-dimensional mass spectral datasets, such as linescans in mass spectral images[219]. As an example, the PP-VLAM algorithm is described for datasets obtained from nanoLC-FTICR-MS experiments in Figure 5.1.

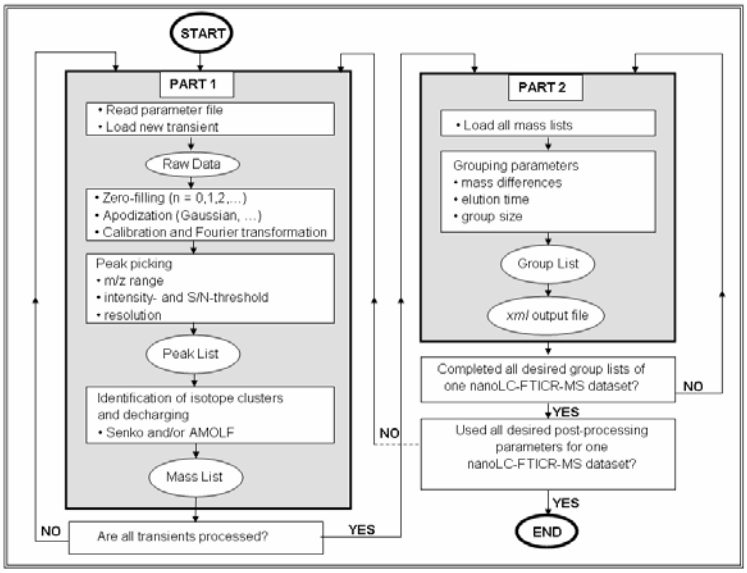

Figure 5.1. Structure and workflow of the PP-VLAM algorithms for parallel processing of datasets obtained from nanoLC-FTICR-MS experiments.

In the first part a transient file (raw data) is located and, if necessary, transferred via the network to the actual processing computer. Then the

transient is Fourier-transformed and calibrated yielding a mass spectrum. The required processing parameters such as zero-filling, apodisation, calibration and peak picking parameters have initially been user-defined. After the mass spectrum is obtained, different sets of isotopic peaks from a single molecular or fragment ion entity (*i.e.* isotopic cluster) are identified using either the Senko [221,222] or our in-house developed AMOLF routine (as described later). The monoisotopic mass of each identified isotopic cluster is calculated and summarized in a so-called mass list. These steps in the first part of the algorithm are repeated until all transients are processed and all mass lists have been completed. This approach and its corresponding algorithms is extremely suitable for massively parallel processing. The server collects all the data after processing all transients in parallel, and uses a second post-processing algorithm to group all mass lists in order to generate a so-called group list. In the following sections the design and the performance of the PP-VLAM algorithm are discussed in more detail.

Parameter file and file transfer protocols

The parameters for data processing are specified in a so-called properties file. In this file the location of the data is defined together with all user-defined parameters that are further used in the PP-VLAM algorithm (*e.g.* apodisation, threshold, mass tolerance). Different file transfer protocols were implemented, such as the *windows network protocol*, *scp*, *sftp*, *gridftp* or *mpicopy*, or by using the *grid application toolkit* (GAT, www.gridlab.org). The communication between the server and the compute nodes is via *remote method invocation* (rmi), implemented either in Java or the Ibis language.

Peak picking, noise filtering and the peak list

Peaks are identified by searching through the mass spectrum until a value is found exceeding a user-defined threshold. The area in the proximity of the *m/z* value where this occurs is subsequently searched for a local maximum (peak picking). The search area for this local maximum is defined by a mass width and

the number of neighbouring data points to check. After the local maximum is found, the peak position (*m/z*) is defined at the middle of the full peak width at half height (FWHM). When the resolution of a peak is higher than the theoretical Fourier resolution ($(f*T_{transient})/2$[227]) the peak is considered as a noise signal and discarded. Note that all peaks that are not recognized as a local maximum are not further analysed in the algorithm. It is therefore crucial to detect as many local maxima (peaks) as possible during the peak picking routine. The result of this approach is an extensive peak list.

Single processing results: Isotopic cluster identification, decharging and the mass list

The peak list contains a significant amount of redundant information. A single peptide will generate different isotopomers and can present itself in different charge states. To reduce this complexity the peak list is converted into a mass list where all redundant information is reduced to one single mass entry for each compound. To achieve this a sequence of deisotoping and decharging modules is introduced.

Decharging of the isotopic clusters after determination of their charge is performed using either the Senko[221] or the Zscore algorithm[223,228]. For the analysis of our peptide spectra, an in-house (AMOLF) developed routine was used for cluster identification and compared with the results from Senko and Zscore. The AMOLF-routine matches a specific *m/z*-distance $\Delta_{m/z}$ between two different peaks to a certain charge state q (q = 1, 2, 3…) defined as in equation:

$$\Delta_{m/z} = (M_{neutron}/q) * (1 \pm \sigma) \qquad (5.1)$$

where $M_{neutron}$ is the mass difference in Dalton between two consecutive $^{12}C/^{13}C$ isotopic peaks belonging to the same compound and q the charge state of the cluster and σ is the user specified precision with which this distance is employed.

Using different values for σ enables the analysis of mass spectra obtained from different instruments with different peak resolutions. In addition,

the ratio of the intensities of the first and second isotope is determined, and should be in agreement with expected numbers of the compounds analysed (*e.g.* for tryptic peptides this ratio is approximately between 3 and 0.3 for peptides with masses of respectively 500 Da and 5000 Da). The results from the two different decharging routines will be discussed in more detail in the section results and discussion.

After processing a certain transient (or mass spectrum) a list of masses is generated. All peaks from a spectrum are summarized in a table with their original charge state, their intensity and resolution (FWHM), and the position in the isotopic cluster. Note that at this stage a peptide (or any type of compound) that is detected with two (ore more) different charge states in one mass spectrum results in two (or more) *almost* identical peptide masses in the mass list. The user defines whether or not these different mass determinations from the same peptide are averaged. When using sub-ppm mass accuracies the consideration of two different peptide masses of the *same* peptide proved to be important, as will be exemplified in the section results and discussion.

Final processing result: Grouping and the group list

The first part of the algorithm (either sequential or parallel processing) results in a separate mass list for each spectrum. Depending on the type of experiment multiple mass lists may contain redundant information. These entries in the mass lists are grouped together to further reduce the complexity and redundancy of the parallel processing results. In this second part of the process cycle two grouping criteria are used. A scan number range is defined to ensure that the masses found belong to the same LC-peak. A mass range is defined (or tolerance) to ensure that the mass spectral peaks found belong to the same molecule. The user may additionally define a minimum amount of scans in which a certain mass was detected ("group size"). In the case of chromatographic separation prior to mass analysis the mass of each eluting peptide is measured in different (sequential) scans if the LC-peak is wide enough. Thus, different peptide masses are considered as a single eluting LC-peak provided they are

within a specific mass *and* time-range. Moreover, this algorithm enables the selection of (consecutive) scans within an eluting LC-peak and it is possible to generate a group list of a certain part from an LC-run. The resulting group list, which is actually a peak list of all eluting peptides during one specific LC-FTICR experiment, can be used for further data analysis such as database searching.

xml output file

The *xml* format is used for storage of the processed data. This format is encouraged by the HUPO Proteomics Standards Initiative (PSI) that defines community standards for data representation in proteomics (See the website: http://psidev.sourceforge.net/ms/index.html[229]). All metadata are stored in an *xml file*, *i.e.* all parameters that were used for processing the mass spectral dataset are documented. This *xml* file can be easily converted to the *mzdata* format (See the website: http://psidev.sourceforge.net/ms/index.html). Additionally, all the processing results from both the first and the second part of the algorithm (mass lists and the group list) are stored in the same *xml* file. Each time a specific dataset is processed using different parameters a new *xml* file is generated, allowing for proper comparison between different processing results.

5.3 Experimental

5.3.1 NanoLC-FTICR-MS

The nanoLC-system (LCPackings, Amsterdam, the Netherlands) consists of an autosampler, a switching unit, a nanoflow system and UV detector. The switching unit is is equipped with a reverse-phase capillary precolumn (C_{18} PepMap 100, internal diameter 0.3 mm, length 1 mm) and is used for preconcentration of the sample at a flowrate of 30 microL/min. Peptide

separation is then carried out on an analytical column (PepMap 100, internal diameter 0.075 mm, length 15 cm) using nanoflow elution at 300 nL/min. Typically, the injection volume was 2 µL. The eluents used were 1% acetic acid and 5% acetonitrile in water (A) and 1% acetic acid and 10% water in acetonitrile (B). The gradient used for the separation of peptides was: 0-30min: 0-50% B, followed by 30-35 minutes: 50-90% B. The nanospray source connecting the LC-system to the mass spectrometer was built in-house and equipped with New Objective Picotips™.

All the peptide mass measurements were performed in the positive ion mode using a modified Bruker APEX 7.0eT FTICR-MS equipped with a 7 T superconducting magnet and an infinity cell[144]. The ions generated by the electrospray ion source are accumulated in an octopole ion-trap (typical accumulation time 0.4 seconds) prior to being transferred to the ICR cell via two quadrupole ion guides. The ions were trapped in the ICR cell using side-kick. In this way, a typical scan time was 1.3 seconds. All experimental parameters were controlled using software and hardware developed in-house as part of the continual evolution of this proteomics / fundamental studies instrument.

The results of the nanoLC-FTICR-MS experiments are displayed in the AWE3D module (Arbitrary Waveform Editor), which is part of the AWTools software package[144]. This software is written in C++ and can be used for a first evaluation of chromatographic separation, mass spectral resolution and sensitivity/intensity. It displays total and selected ion currents as well as 3-dimensional representation of the data. The whole data set can be recalibrated or apodised, zero-filled in this mode.

5.3.2 Samples and protein identifications

NanoLC-FTICR-MS measurements of two different protein samples were used to check the performance and outcome of the PP-VLAM algorithm, namely a tryptic

digest of 20 μM/mL savinase (Sigma, USA) and a tryptic digest of a protein mixture (50 μM/mL BSA (Sigma, USA), 50 μM/mL ovalbumin (Sigma, USA) and 50 μM/mL lysozyme (Fluka, Germany)). For protein identification, the peptide masses were submitted to a Mascot database search (MatrixScience, UK) with a mass tolerance of 20 ppm using the SwissProt database.

Also, different clinical cerebrospinal fluid (CSF) samples from breast cancer patients with leptomeningal metastasis (brain tumor) were used. The control samples originated from headache patients without brain tumors. All samples were subjected to trypsin digestion (Promega, USA) after addition of 0.2% Rapigest (Waters, USA) in a 50 mM ammoniumbicarbonate buffer. These CSF samples were provided by the Erasmus Medical Center (EMC) in Rotterdam and have been part of a more extensive biomarker study based on MALDI-TOF measurements[230].

5.3.3 Programming software PP-VLAM and parallel processing

The PP-VLAM algorithm is written in Java and all features are Java implementations, *i.e.* the algorithm is platform independent and thus runs on every operating system. This enables in principle the use of all computers that are not used at full capacity in the laboratory. The PP-VLAM algorithm will be made available to the scientific community through the internet within the framework of the Virtual Laboratory for E-science (VL-*e*). Due to its modular setup this software is not limited to the FTICR data discussed in this chapter but can be easily adjusted for a variety of mass spectral datasets.

For parallel processing of mass spectral datasets several workers (computer nodes) request jobs (each consisting of one spectrum to be processed) upon their availability. All jobs are managed by a central server and the computational resources are linked via TCP/IP connections. The Java program code is stored centrally on a file server to ensure that every computer

node will access the same version. The properties file (containing the user-specified set of processing parameters) can be stored in any location accessible by the server. The processing details are only read by the server module, which passes them on to the worker modules. Each node transfers and processes raw data (mass spectral file) separately and returns the results to the server. The server and worker modules can run either on one or on separate computers. The server and worker programs can be started manually, in batch or by any other system that has the ability to execute programs, *e.g.* a grid job. Each worker requests the processing parameters as specified in the properties file once. On receipt of a job request the server responds with details about a job, such as the filename. Then the worker loads the corresponding mass spectrum from the data storage system. When the worker has processed the job, it returns the resulting mass list to the server and requests a new job. The server stops and compiles a concise report when all jobs have been processed. The final result list is generated as an *xml* file (as described earlier) that is stored locally or on the central data storage system.

5.3.4 Computer hardware

The measurement data is stored on a 5.5 TB storage system (SGI Origin 300) that is linked by a 2 Gigabit fibre channel connection to the acquisition computer (FTICR-MS acquisition). Different computer platforms were used to test the performance of the analysis software. The single desktop PC was a Pentium4 processor (3.2 GHz) with Hyper Threading and 1 GB RAM. The PC cluster consisted of 5 personal computers running either Windows NT, 2000 or XP, or Linux as an operating system. The internal computer cluster that was used is located at AMOLF and consists of 38 compute nodes, each equipped with dual AMD opteron 2.2 GHz processors. The nodes are internally linked via 1 gigabit Ethernet connections and externally via a 1 gigabit glass fibre connection. The

Dutch national computer cluster that was used ("Lisa") is located at SARA (Dutch Supercomputing Centre www.sara.nl. For details on the *mpicopy* protocol see www.sara.nl/userinfo/lisa/usage/progavail/index.html, "special utilities") and consists of 630 compute nodes, each equipped with dual Xeon 3.4 GHz processors. The nodes are linked via 1 gigabit Ethernet connections and run on a Debia Linux operating system.

5.4 Results and discussion

5.4.1 Evaluation of the PP-VLAM algorithm using protein standards

Two different nanoLC-FTICR mass spectral datasets were used to evaluate the performance of the described PP-VLAM algorithm. Five peptides from the resulting group list from a tryptic digest of savinase were assigned within a mass accuracy of 3 ppm after internal calibration. The total sequence coverage (s.c.) in this case is 30%. From a tryptic digest of a protein mixture (containing three well-defined proteins, see experimental section), 17 peptides from BSA (s.c.= 31%), 11 peptides from ovalbumin (s.c.= 41%) and 6 peptides from lysozyme (s.c.= 56%) from the group list were assigned all within a mass accuracy of 20 ppm. The lower mass accuracy of peptides in the protein mixture compared to savinase partly results from peptide concentration differences in the protein mixture. For example, peptides that elute in high concentration cause overloading of ions in the ICR cell and thus increased mass shifts. Moreover, in the protein mixture the relative intensity of a single peptide compared to the total ion intensity at different time points varies between 5% and almost 100% negatively affecting the mass measurement accuracy.

In conclusion, these results demonstrate the ability of the PP-VLAM algorithm to process complex nanoLC-FTICR data in an efficient way. The

application of the PP-VLAM algorithm to a peptide mixture generates a peak list that is very well suited for database searches and thus protein identification.

Evaluation of the Senko and AMOLF routine for isotope cluster identification

For cluster identification and decharging of peptide peaks the Senko and AMOLF routine both proved to be extremely powerful (in terms of computing speed and total amount of identified clusters) compared to the Zscore- and averagine-based routine[223]. The latter two methods are more suited for mass spectral analysis of intact proteins. A detailed comparison between the Senko and AMOLF routine was performed using the standard protein datasets described earlier. For savinase, all 5 identified tryptic peptides were found using either the Senko or AMOLF routine for isotope cluster identification. For the protein mixture, all 34 identified tryptic peptides were found with both the Senko and AMOLF routine. Additionally, using the AMOLF routine 2 more peptides (from BSA) were identified. In general, the mass list contained approximately 20% more peptides using the AMOLF routine compared to the Senko algorithm. This results from the less stringent requirement that only two peaks above a defined threshold are enough for an isotope cluster in the AMOLF routine, whereas in the Senko routine all other peaks in the cluster area are also taken into account.

5.4.2 Scan precision and mass accuracy

Usually, each eluting chromatographic peak is mass-analysed multiple times during an LC-MS experiment. In practice, each mass spectrum (scan) from one peptide results in a slightly different peptide mass. This variation in detected peptide mass, further referred to as *scan precision*, is dependent on different factors such as the type of instrument used, the chromatographic resolution and the ion intensities itself. As mentioned before, the high mass accuracy of FTICR-

MS is a well-distinguished feature. In modern FTICR analysers this accuracy has improved towards sub-ppm levels. Clearly, high mass accuracy improves the reliability of database searches and moreover it helps to identify peptides that are not in a database (*e.g.* unsequenced species, post translational modifications)[231,232]. The advantage of the PP-VLAM algorithm compared to other processing software packages is that all the different peptide masses are stored in the *xml* file and thus can be analysed in more detail. In this way the precision of the data can be improved significantly after data acquisition. As an example, in Figure 5.2 the elution profile of a BSA peptide (theoretical mass 688.3656 Da) in the protein mixture is shown.

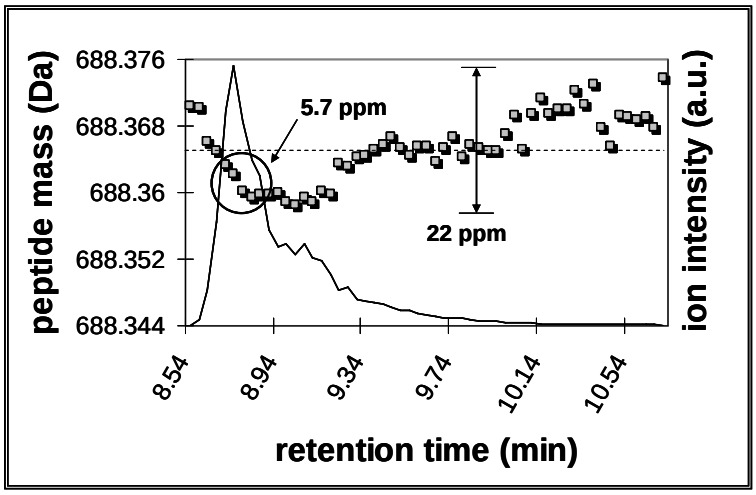

Figure 5.2. NanoLC-elution profile of a singly protonated BSA peptide. The dotted line indicates the theoretical mass of this peptide, the squares show the FTICR-measured masses in each scan. Upon post-acquisition selection of scan numbers the difference between the highest and lowest measured peptide mass decreases 4-fold, thus improving scan precision.

The peptide masses (shown as squares) are measured after external calibration. The difference between the highest and lowest measured mass is 22 ppm. Clearly, in the tail of the eluting peptide the variation increases. Upon user-defined selection of scan numbers (retention time) as indicated with the

circle the scan precision improves 4-fold. This information can be further used in an iterative way to internally re-calibrate the spectra and thus improve the mass accuracy after the data acquisition. Often a peptide is mass analysed at two (or even more) different charge states. From Figure 5.3 it can be seen that using the PP-VLAM algorithm a singly and a doubly protonated BSA peptide can be analysed separately. In this case, the scan precision of the doubly protonated species can be improved to 3.6 ppm.

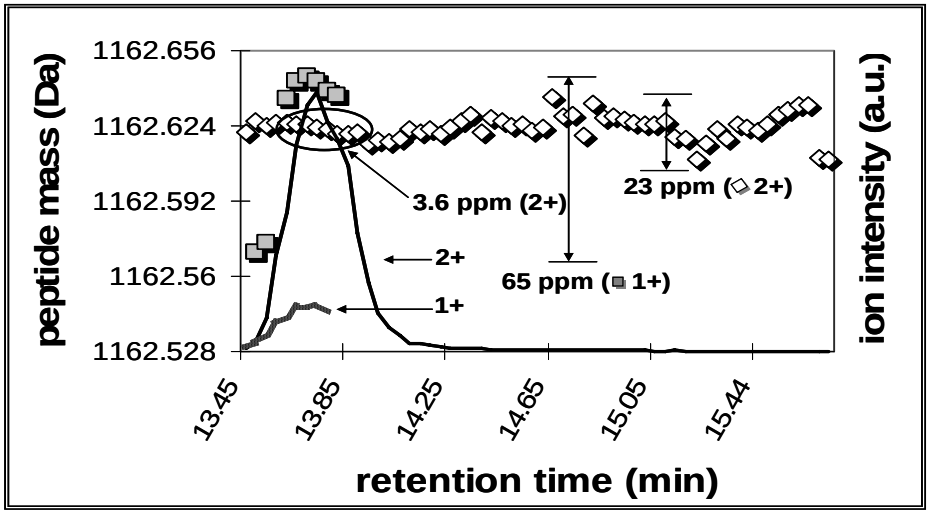

Figure 5.3. NanoLC-elution profile of a singly and doubly protonated BSA peptide. The different charge states of the *same peptide* result in different scan precisions. It is thus recommended to analyse these *different species* separately.

5.4.3 Visualization of peptide profiles from CSF samples: "a real life example"

More advantages of the here described processing and analysis tools are exemplified using a dataset obtained from nanoLC-FTICR-MS measurements of

cerebrospinal fluid (CSF) samples. The cerebrospinal fluid encloses the brain and is thus an ideal medium to investigate diseases that affect the central nervous system (CNS) such as Alzheimer disease or brain tumours. The details of the samples are given in the experimental section. In general, the objective is to compare peptide profiles of healthy and diseased individuals for detection of possible biomarkers. Each nanoLC-FTICR-MS measurement yields a large and complex dataset, and processing and visualization of each dataset is pivotal for proper comparison and thus extraction of valuable information.

As an example, all sequential FTICR mass spectra acquired during one nanoLC-experiment of a CSF sample are shown in Figure 5.4a. Obviously, the manual comparison of such plots is extremely tedious and error-prone. Application of the PP-VLAM algorithm to this specific dataset results in an *xml* output file that contains between 100 and 200 peptide masses (depending on the processing parameters). Clearly, such a list of peptide masses can be easily compared with those derived from replicate measurements (repeatability of the LC-MS measurement of one sample) or with other samples (*e.g.* patient and control comparison). For comparison of the *xml* output files we developed a tool for visualization of either the mass lists or group lists from one or multiple samples (see Figure 5.1 for explanation of the terms mass and group list). In Figure 5.4b an example is shown for a CSF sample (same as in Figure 5.4a) processed with different parameters. In this case the specific dataset is visualized for apodised and non-apodised raw data, clearly showing the similarities and differences between these two types of processing. The complexity of this plot is far less compared to the spectral data in Figure 5.4a. In addition, vertical lines that result from chemical and electronic noise in Figure 5.4a are efficiently removed in the processed data set. In a similar way, this viewer enables visual comparison of replicate measurements or of different samples.

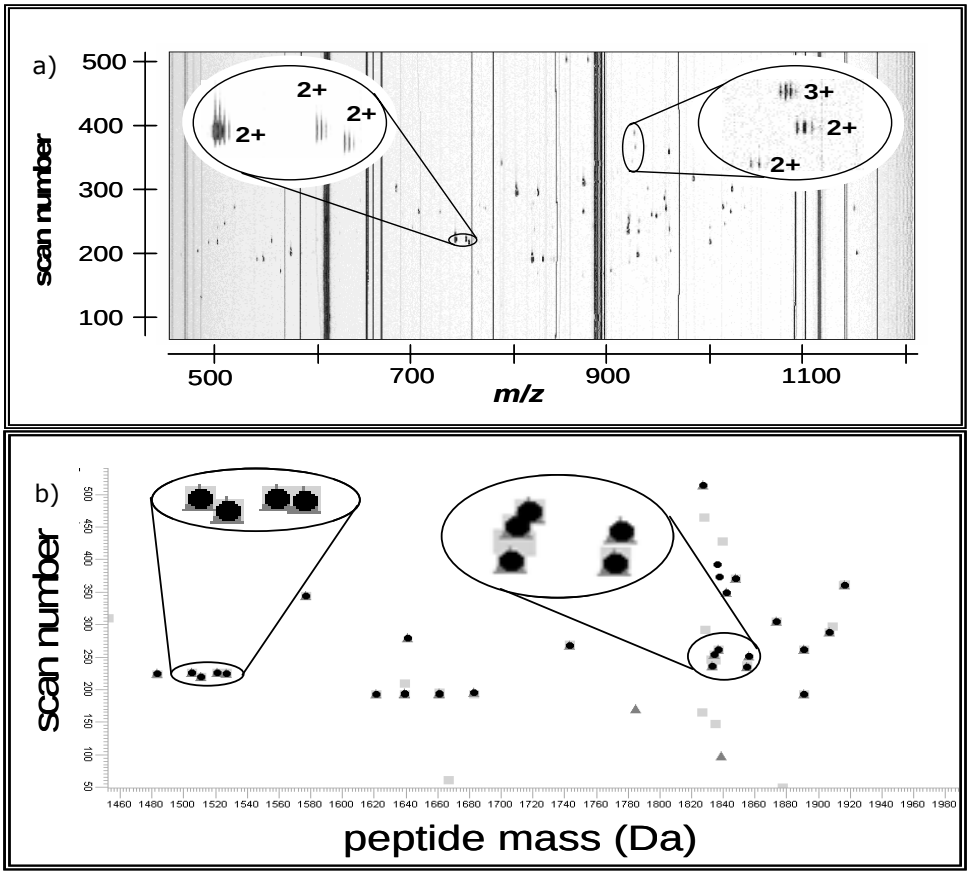

Figure 5.4. a) NanoLC-FTICR-MS measurement of a trypsin digested cerebral spinal fluid (CSF) sample displayed with the AWE3D software. The *m/z*-values are plotted on the *x*-axis, the scan numbers (linear with nanoLC retention times) on the *y*-axis and the peak intensities on the *z*-axis (out-of-plane). b) Visualization of a processed nanoLC-FTICR-MS measurement of a digested cerebral spinal fluid (CSF) sample. The peptide masses are plotted on the *x*-axis (from 1450 to 1980 Da) and the scan numbers (corresponding to retention time) on the *y*-axis (50-450). A peptide mass is visualized provided that it is detected in at least 3 sequential scans with a mass precision of 0.05 Da (see methodology). Here, different processing results are overlaid in one plot, *i.e.* no apodisation on the raw data (light grey squares), apodisation and AMOLF isotope cluster identification (grey triangles) and apodisation and Senko isotope cluster identification (black circles). The inserts show the similarity between AMOLF and Senko cluster identification results (*i.e.* each triangle is overlapped by a circle). However, without apodisation additional clusters are detected or the cluster is observed at a slightly different peptide mass.

5.4.4 Speed benefits of distributed computing of large mass spectral datasets

Several hardware configurations ranging from a single desktop computer to supercomputers (clusters) were evaluated for parallel processing of large mass spectral datasets. For a dataset obtained from nanoLC-FTICR-MS of the protein mixture (877 spectra, 3.4 gigabyte) the total processing time was more than 2 hours using a single desktop computer. Using a cluster of five desktop computers the processing time decreases to 0.5 hours, however this time is limited by the file transfer speed (*i.e.* the speed depends on the quality of the internal network between the computers and the central raw data storage). A summary of the results on different clusters is given in Figure 5.5. It is clear that even on a dedicated computer cluster the amount of spectra that are processed per minute is limited by the network speed. This limitation in speed up of distributed computing is well-known from computer sciences. The transfer of raw data from the central storage site outside the cluster to the multiple computer nodes becomes inefficient using more than seven nodes. As an alternative, the total raw dataset from an LC-MS experiment can be locally stored on the shared storage of the cluster itself or copied temporarily to all individual nodes using the *mpicopy* protocol (this takes less than 3 minutes, SARA Dutch Supercomputing Center, www.sara.nl. For details on the *mpicopy* protocol see www.sara.nl/userinfo/lisa/usage/progavail/index.html, "special utilities"). In the latter case the total 3.4 gigabyte dataset is processed on 40 computer nodes within 2 minutes, resulting in a total processing time less than 5 minutes.

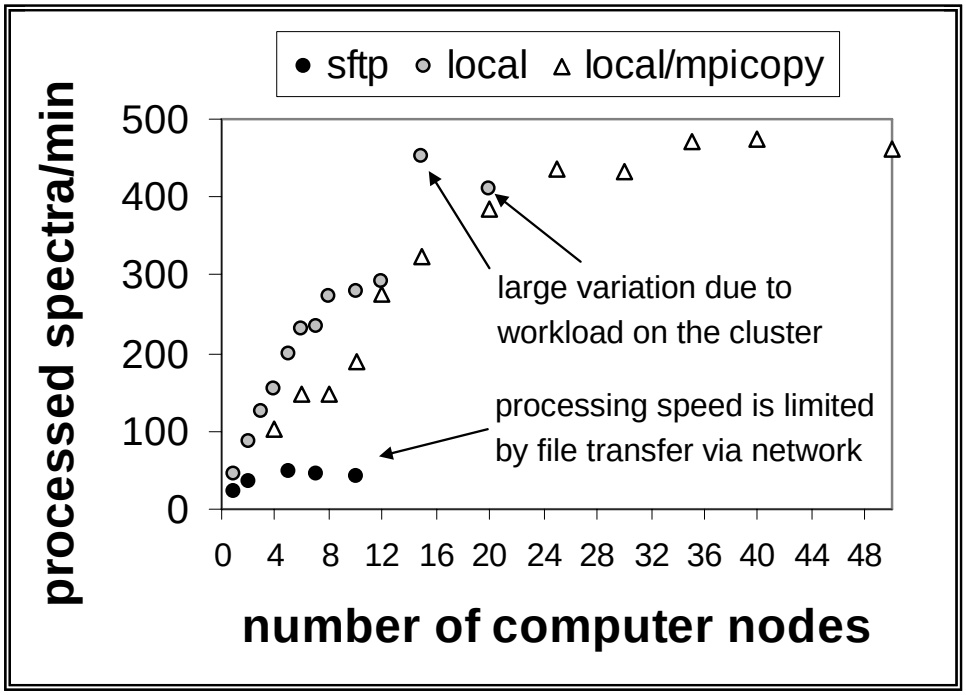

Figure 5.5. Increase in processing speed of a large mass spectral dataset using a distributed computing environment. The speed in the cluster is limited by the *sftp* transfer speed of raw data from the central storage facility to the computer nodes (black circles). The processing speed is improved up to 12 computer nodes when the raw data is stored on the cluster itself (grey circles). Note that the total processing time depends on the other activities of the cluster when using more than 15 nodes. This variation in processing time is smaller when using an *mpicopy* protocol where up to 50 computer nodes can be assigned (white triangles).

5.5 Conclusions

Automatic processing of large mass spectral datasets in a distributed computing environment allows for a substantial reduction of the analysis time. We showed

full processing of a 3 gigabyte raw dataset from a nanoLC-FTICR-MS experiment is within 5 minutes using an in-house developed algorithm on a dedicated computer cluster. Due to its modular set-up the algorithm can be applied to all other types of hyphenated or serial mass spectral datasets (*e.g.* LC-MS, LC-MS/MS, imaging MS). In our approach the storage of all data is preferred to discarding raw data during the measurement, thus enabling future re-analysis or re-processing using a new set of parameters. Furthermore, automatic processing improves the repeatability of the analysis over the more error-prone manual analysis. The ability to reuse the parallel processing modules described in this chapter in a distributed workflow environment allows for new scientific collaborations to be realized in the virtual laboratory. This in turn enables the scientists to share processing tools and strategies and enhances the quality of experimentation with large mass spectral datasets.

A1

SIMION analysis of a high performance linear accumulation octopole with enhanced ejection capabilities

Here, we present the results of extensive SIMION 7.0 modelling of a new linear octopole ion trap. The octopole was designed to increase the efficiency of an electrospray ion source coupled to a FTICR mass spectrometer. This improvement was achieved by applying a pulsed axial field to the octopole to eject the ion packet with a time and energy distribution that better match the acceptance criteria of the FTICR cell, thus increasing the trapping efficiency and sensitivity. The axial field was produced by applying a pulsed dc potential to the custom-designed ejection electrodes located between the octopole rods. The time and energy profiles of the ejected ion packets for several electrode shapes were calculated and are discussed in terms of their compatibility with efficient trapping of the ion packet in the FTICR cell. Preliminary experimental results show increased signal using the dc ejection electrodes of approximately 100 %.

Ioana M.Taban, Liam A. McDonnell, Andreas Römpp. Iliya Cerjak and Ron M.A. Heeren, *Int. J. Mass Spectrom.*, **2005**, 244 (2-3): 135-143

Appendix 1

A1.1 Introduction

The application of high performance mass spectrometric methods for biomedical analysis has increasing requirements for sensitivity. Often studies involve the analysis of low copy number molecules in a pool of high abundant proteins[42,152,233-235]. Chromatographic separation[234,236-239], capillary isoelectric focussing[240], and capillary electrophoresis[152] have all been used to reduce the complexity of the samples entering the mass spectrometer at any specific time and to concentrate each analyte. Such hyphenated experiments now permit attomole measurements. However, there are still applications where increased sensitivity is desired. High-throughput proteomics applications and specifically the search for biomarkers (up- and down-regulated proteins, post-translation modifications and point-mutations have all been associated with disease) would benefit from increased sensitivity and a higher dynamic range.

FTICR-MS is an ion trapping technique[98] that distinguishes itself from other types of mass spectrometry: high spectral resolution, for example resolving two peptides that differ in mass by less than the mass of a single electron[149], and high mass accuracy make the FTICR ideally suited for rapid analysis of complex mixtures[42,150-152,241,242]. To be compatible with fast separation techniques the ions must be trapped in the FTICR cell preferably without using a trapping gas. The acceptance criteria for the FTICR infinity cell[140] for non gas-assisted trapping with sidekick are: a trapping time window within 0.2-0.4 ms and kinetic energies of ions lower than 2 eV per charge, for ions with *m/z* lower than 2000[243].

The sensitivity of an FTICR experiment is influenced by many factors, including efficiency of ion generation, ion-transport and ion detection. Improvements in all aspects continue unabated[99,138,139,171,244-246]. Collisional cooling of ion beams in 2D-multipoles, operated in an RF-only mode, have improved the performance of FTICR mass spectrometers and are now widely used in all types of mass spectrometer[130,131,133,134,136,137,247-254]. Through

collisions, the buffer gas reduces the kinetic energy of a particle beam and focuses it on the longitudinal axis of the guiding multipole. This low-energy ion beam can then be focused and transported with high efficiency into the next region of the instrument. It has been shown that if ions are kinetically cooled and accumulated before being pulsed out of the multipole, sensitivity and dynamic range of the experiments are increased[138,249,252].

However, there is still scope for improving the performance of these linear ion traps. When many ions are present in a linear ion trap, the sensitivity of the measurement can decrease. Space-charge-induced ion discrimination in the multipole can lead to the absence of many expected analyte peaks[255] and multipole storage assisted dissociation (MSAD; space-charge-induced collision-activated dissociation inside the multipole) can lead to fragmentation of the ions of interest[256-259]. Furthermore, the trapping capability of linear ion traps is worse for native bio-macromolecules and their complexes, because their native conformations have smaller collision cross-sections than their de-natured analogues[260]. Though improved trapping has been achieved using increased collision-gas pressure, this causes MSAD to be more problematic[256].

A longer linear multipole ion-trap would alleviate many of the above problems: in a large ion-trap space charge effects occur at larger ion numbers, so the potential for MSAD and ion-discrimination is reduced, and non-covalent complexes have more time to collisionally cool, thus a greater fraction can be trapped. One drawback of a longer trap is that the time distribution of the ejected ions is larger because it takes a longer time for ions located at the beginning of the multipole to move to the end where they can experience the ejection field supplied by the exit lens (during accumulation this lens provides a trapping field). Longer multipoles can lead to lower sensitivity since only a small fraction of the ions accumulated in the multipole are trapped in the FTICR cell. Normally, the multipole length is chosen as a compromise between the ejection time distribution and space-charge considerations.

The time-distribution of the ejected ion packet can be shortened by creating an axial field in the multipole[261]. This would allow the analyst to benefit

from the advantages of a longer multipole outlined above. An axial ejection field can be created in several ways without significantly affecting the RF multipole field. Any perturbation of the RF field can reduce the *m/z* transmission window. The methods that have been used to date are:

- Segmented multipole rods – by applying a different dc bias to each segment an ejection field can be created with minimal RF-field distortion [262]. In practice, however, because alignment of the segments is key to the design, engineering must be meticulous.
- A set of rings surrounding the multipole – by applying different dc potentials to these rings, an axial field is created with low distortion of the RF field. This design is robust. However, the dc potentials that must be applied to the rings are prohibitively high[247,263].
- Tilted or conical multipole rods – perturbs the RF trapping field making trapping of the incoming ions in the multipole less efficient [263,264].
- Tilted dc wires located inside an octopole[265] – don't affect the RF field significantly, but these wires must be thin making the construction quite fragile and difficult to shape.
- T-shaped electrodes located between quadrupole rods[261] – in this case, four extra electrodes (T-shaped) were placed between the quadrupole electrodes, to which the same dc ejection voltage is applied. By shaping these electrodes, a linear axial field was created through the quadrupole. The setup is simple and the field distortion small.

To increase the efficiency of external accumulation for large ions and to minimize detrimental space-charge-induced artifacts such as MSAD and space-charge induced discrimination**,** we designed an elongated linear octopole ion trap. To ensure efficient ejection from the octopole, efficient transfer to, and trapping in the ICR cell we added eight T-shaped ejection electrodes, located between the octopole rods, to create an axial field. Extensive simulations were conducted to optimise the time and energy distributions of the ions ejected from the octopole to match the trapping characteristics of the FTICR cell.

A1.2 Description of the simulated accumulation octopoles

The octopole will be used to accumulate ions generated by ESI[37], and MALDI[27]. Consequently, ions covering a wide range of *m/z* need to be accumulated, a task best suited to a higher order multipole [266]. The wider *m/z* range and higher charge capacity of the octopole compared to that of lower order multipoles (e.g., twice higher than a quadrupole[267]) led to the decision to base our ion trap on an octopole. To increase the multipole order above eight doesn't yield improvements in performance that would justify the technological complications needed for its realization[268]. To our knowledge this is the first time a linear octopole ion trap equipped with shaped, non-linear, ejection electrodes is considered to enhance the sensitivity of the source of an FTICR-MS

The octopole is 180 mm long, made of 8 circular rods of 6 mm diameter. The field radius of the octopole was chosen such that the ratio $r_{rod}/r_0 = 0.355$. This ratio has been shown to be a good approximation for the ideal octopole field[269]. To maximize the fraction of ions trapped in the linear octopole, the beginning of the octopole was bevelled so that octopole fits inside the skimmer of the electrospray ion source. The skimmer and a single electrostatic lens at the end of the octopole provide the axial trapping field for the ions. Figure A1.1 shows a schematic of the octopole design.

Various T-shaped electrodes placed between the octopole rods were investigated. Here, the evaluations of three electrode geometries are reported. These are shown in Figure A1.1c and are:

i) Linear-positive – the stem is initially 4 mm and decreases linearly with distance to 0 mm at the end of the octopole.

ii) Linear-negative – the stem is initially 0 mm and increases linearly with distance to 4 mm at the end of the octopole.

iii) Curved – the stem of the T-shaped electrode is initially 4 mm and decreases in size non-linearly to zero.

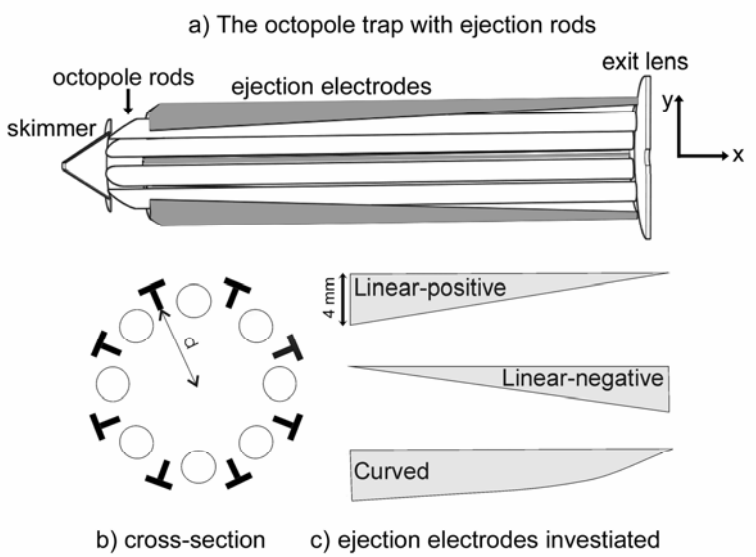

Figure A1.1. a) The ion source includes a skimmer, an accumulation octopole with ejection electrodes and an exit lens, l_e. b) cross-section of the accumulation octopole including the T-shaped ejection electrodes (at the deepest point of the stem d = 11.6 mm), and c) longitudinal view of the three ejection electrodes reported here.

The thickness of the steam is 1 mm in all situations. The two linear electrode configurations produce a non-linear ejection field, whereas the curved electrodes were designed to produce a linear ejection field. An ejection field for positive ions is produced by applying a positive potential to the linear-positive and curved ejection electrode geometries whereas a negative-potential is required for the linear-negative geometry.

A1.3 SIMION simulations

The purpose of this work was to approximate a collisionally cooled ion beam that is trapped in a long octopole ion trap and to investigate the effects of axial

ejection fields on the time and energy distributions of the ejected ion packets. These analyses were performed using SIMION 7.0[270]. The scaling used in the SIMION simulations of the octopole was 5 grid units per mm (gu/mm).

The simulation results reported here pertain only to the analysis of low abundant ions: under conditions of high space charge the ejection field will be effectively screened by the ion-cloud. Moreover, improvements in sensitivity are not required for intense ion currents. In addition, SIMION does not approximate space-charge particularly well and cannot run the groups of ions required for its space-approximations in a radio frequency device in a practical time. For these reasons, ion-ion interactions were not taken into account. These simulations were performed specifically to increase the sensitivity for the analysis of low abundance ions, to trap and transfer these ions to the ICR cell as efficiently as possible; those experiments that require improvements in efficiency and that are best described by the simulation constraints.

Ions of mass equal to that of cytochrome *c*, 12360 Da, and with charges of +1 and +15 were used in the simulations. To approximate the ion beam emitted through the skimmer of an electrospray ion source the initial positions, angles and times of the incoming ions were randomised through the ranges $0 \leq [y, z] \leq 0.5$ mm, $0 \leq \theta \leq 2°$, $0 \leq t \leq 4$ ms with an initial energy of 10 eV for +15 ions and 3 eV for singly charged ions. Note the initial energy of the ions has no effect for the evaluation of the ejection time and energy distributions because the ions are thermalised prior to the ejection pulse. For each set of parameters 1000 cytochrome *c* ions were initiated at the beginning of the accumulation octopole. The radio-frequency voltage used for these simulations was 800 V peak-to-peak and the frequency was 0.88 MHz. This voltage was sufficient to trap ions with *m/z* = 12360, but lower voltages can be used for a smaller *m/z* range.

An accumulation-ejection pulse sequence, which involves the skimmer, the dc ejection electrodes, and the exit lens, is shown in Figure A1.2. The ions were accumulated for 14 ms (thermalised) using 5 V applied to the skimmer and 10 V to the exit lens and 0 V to the ejection electrodes. To eject ions 150 V was

applied to the skimmer, – 1 V to the exit lens and 200 V to the ejection electrodes (-200 V for the linear negative configuration).

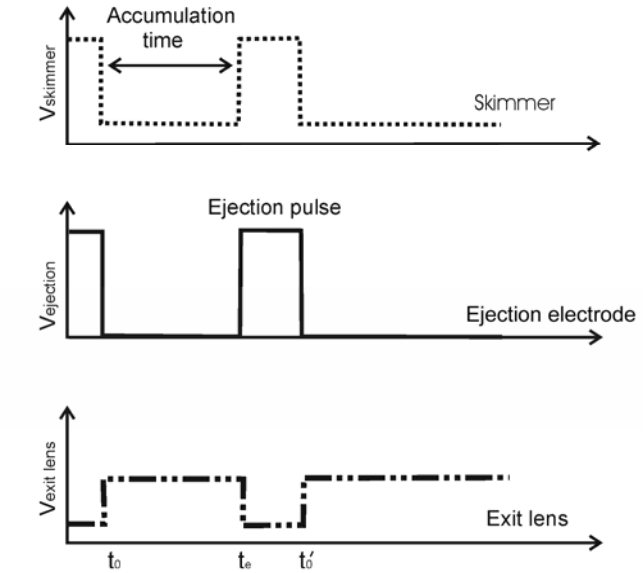

Figure A1.2. Accumulation-ejection pulse sequence used for accumulation and ejection of ions. The difference t_e (ejection) – t_0 (accumulation) represents the accumulation time. A new cycle starts at the time $t = t_0'$. The RF voltage is applied throughout simulations. $V_{skimmer\ accum}$ = 5 V, $V_{skimmer\ ejec}$ = 150 V, $V_{exit\ lens\ accum}$ = 10 V, $V_{exit\ lens\ ejec}$ = -1 V, $V_{eject\ electrodes\ accum}$ = 0 V, $V_{eject\ electrodes\ ejec}$= 200 V.

The hard spheres algorithm[267] was used in order to estimate the collisional cooling in the simulations, using the cross-section of cytochrome *c* determined from ion mobility spectrometry. The cross section of gas phase cytochrome *c* has been shown to be charge dependent[271].

This algorithm is an approximation of ion - molecule collisions that is valid for the range of kinetic energies present here. Collisional relaxation from the initial velocity to the thermal equilibrium velocity follows the law:

$$v = v_0 e^{-t/\tau} \qquad \text{(A1.1)}$$

Here, v_0 is the initial velocity of the ion, v is the velocity at a time t, and τ corresponds to the relaxation time, defined by formula:

$$\tau = 3(m+m_g)/4m_g n\sigma u_{kT}, \quad u_{kT} = (8kT/\pi m_r)^{1/2} \qquad \text{(A1.2)}$$

where m_r is the reduced mass $(m_r = mm_g/(m+m_g))$, T is the temperature of the collision gas and k is the Boltzmann constant. n is the number density of the gas molecules and σ is the collisional cross-section. m and m_g represent the mass of the ion, and the mass of the collision gas, respectively. Using a pressure of 10^{-3} mbar throughout the simulated octopole, the relaxation times were calculated to be 2.5 and 1.1 ms for +1 and +15 ions, respectively. These were implemented in SIMION through a user program that damps the ion's velocity according to the above equation but does not modify the instantaneous direction of the ions. For the pressure assumed here and the large cross-section of the analyte ions, such viscous damping is a good approximation of the large number of collisions experienced by each ion.

This simulation of an accumulation octopole enables a qualitative assessment of the performance of an octopole with ejection electrodes for the accumulation and ejection of low abundant ions. In agreement with the simulations preliminary experimental results demonstrate the higher sensitivity of this new octopole when voltage is applied to the dc ejection electrodes and an axial ejection field is generated.

A1.4 Results and discussion

The time and energy distributions of the ions ejected from the octopole are compared for the three configurations shown in Figure A1.1c and for an octopole without an axial field. These distributions were recorded at the exit of the octopole and at the FTICR entrance (quadrupole ion guides transport ions from

the octopole exit to the cell, see Figure A1.3; more details can be found in reference[161]). All three octopole configurations transported ions covering a wide *m/z* range with high efficiency (100 %), thus demonstrating that the ejection electrodes do not significantly distort the RF field of the octopole (results not shown). Note that the ion transmission through the exit lens depends on the voltage applied to the exit lens and the size of the aperture.

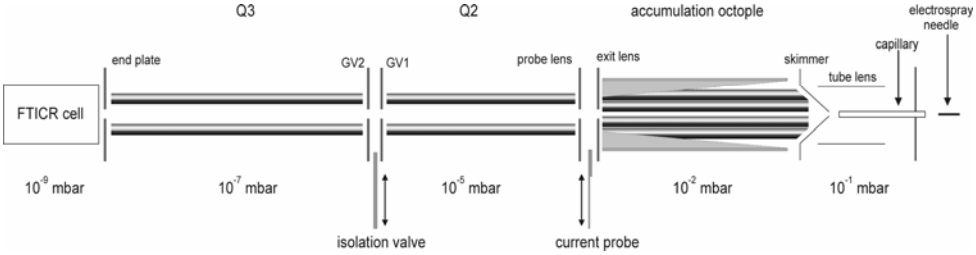

Figure A1.3. Schematic of the 7 T external electrospray FT-ICR set-up. The accumulation octopole, the following two quadrupoles and the lenses located at the entrance and exit of the multipoles were simulated using two potential arrays. A higher resolution array, 5 gu / mm, was used to model the accumulation octopole and a lower resolution array, 2 gu / mm, was used to model the two transfer quadrupoles and transfer lenses. The two arrays were joined in the middle of the exit lens, where the field lines are almost linear, and using identical potentials on the exit lens in both arrays. Due to low pressures no damping of the velocity is considered in the transfer quadrupoles. The voltages applied to the transfer optics and the two quadrupoles are: $V_{pp\ Q2,3}$ = 200 V, $V_{probe\ lense}$ = -2 V, V_{GV1} = -20 V, V_{GV2} = -70 V, $V_{end\ plate}$ = -1 V, $V_{bias\ Q2}$ = -2 V, $V_{bias\ Q3}$ = -1 V.

Figure A1.4a shows the axial dc potential gradient of the linear-positive and linear-negative designs (0 V applied to the octopole electrodes). As can be seen, the axial field is very steep in the areas influenced by the skimmer and the exit lens potentials. Between the skimmer and the exit lens the dc ejection electrodes of both configurations provide an average axial potential gradient of 0.3 V/cm (non-linear) along the octopole when 200 V is applied to the dc ejection electrodes. This potential gradient has been shown to be optimum for a segmented quadrupole linear ion trap that was used to accumulate ions for FTICR experiments, larger ejection fields decreasing sensitivity[248]. Closer examination of Figure A1.4a reveals that the linear-negative configuration has a

shallow potential gradient at the beginning of the octopole and a steeper potential gradient at the exit (in the region without influence from the skimmer and the exit lens). This profile will cause the ions located near the beginning of the octopole to be accelerated more slowly than those located near the end, a profile not favourable for a narrow time spread.

In order to investigate the performance of a linear ejection field, curved ejection electrodes were designed. The field at the centre of the octopole was measured as a function of the stem length of the ejection electrode; the stem length was then varied along the length of the ejection electrodes such that a linear ejection field was produced. Figure A1.4b shows the dimensions of these curved ejection electrodes.

Figure A1.4c shows the axial potential profiles for the curved and linear-positive geometries, resulting in linear and non-linear axial potential gradients, respectively. Energy and time distributions were recorded at the exit of the accumulation octopole for the curved and linear-positive configurations and without an axial field ($V_{dc\ electrode}$ = 0 V).

Figure A1.5 shows the time and energy distributions for z = +15 cytochrome *c* ions at the octopole exit. The ejection time spread was almost identical for the curved and linear-positive ejection electrodes (approximately 0.23 ms), whereas without an axial field the time spread was much larger, 12 ms. The time spread of 0.23 ms corresponds to approximately 3 V, z= +15 ions moving across the 180 mm length of the octopole. The analogous time spread for the singly charged ions was approximately 0.88 ms with the ejection field and 22.64 ms without the ejection field (results not shown). Though larger energies (22 - 43 eV, or 1.5 - 2.9 eV per charge) were obtained for the curved ejection electrodes than for the linear-positive configuration (19 - 36 eV, or 1.3 - 2.4 eV per charge), both energy ranges can be accommodated by the FTICR cell. However, closer examination of the energy - time distribution of the linear positive configuration reveals that the ions that are ejected first have the highest energy. The ions located at the beginning of the octopole experience a

larger ejection field and have overtaken the ions located closer to the exit. Figure A1.5 also shows the corresponding time and energy histograms.

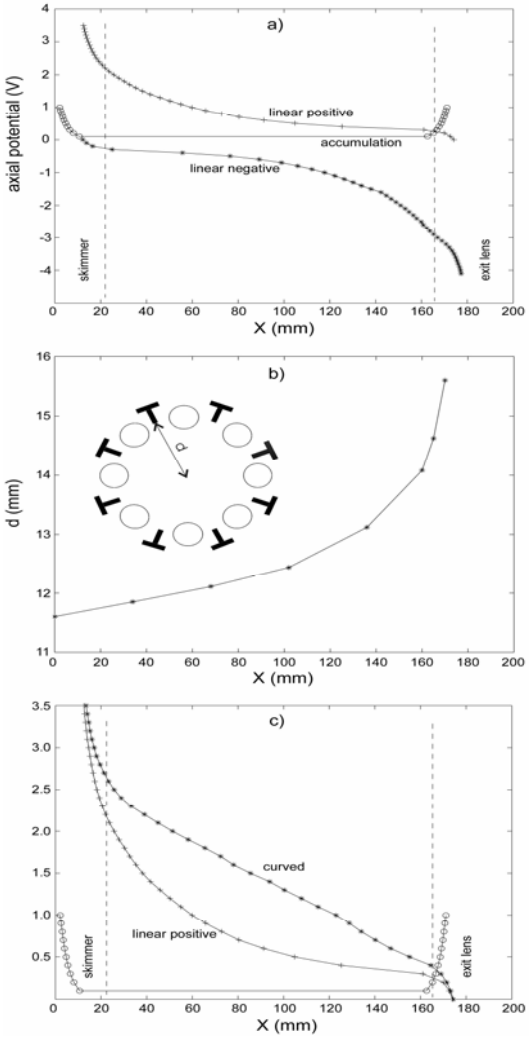

Figure A1.4. The axial dc potential along the accumulation octopoles working in ejection mode for: a) linear-positive (+) and linear-negative (∗) configurations; b) linear-positive (+) and curved (∗) configurations. The potential profile during accumulation is the same for all three configurations (o). The dashed lines show the place where the field of the skimmer and the exit lens effect the axial potential during the ejection time. During accumulation $V_{skimmer}$ = 5 V, V_{exit} lens = 10 V and $V_{eject\ electrodes}$ = 0 V. During ejection $V_{skimmer}$ = 150 V, V_{exit} lens = -1 V and $V_{eject\ electrodes}$ = 200 V for the linear-positive ejection electrodes and $V_{skimmer}$ = 5 V, $V_{exit\ lens}$ = -5 V and $V_{eject\ electrodes}$ = -200 V for the linear negative design.

It can be seen that more ions with lower kinetic energies were ejected by the linear-positive configuration than with the curved configuration. The energy distribution from the octopole without an axial field is much narrower, but has the drawback of a much larger time spread. Note the time spread isn't

thermal because the times were recorded after the ions have been ejected from the octopole and passed through the – 1 V field of the exit lens.

Simulations of the entire ion transfer system, two quadrupole ion guides and electrostatic lenses (Figure A1.3), were used to determine the time and energy distributions at the entrance of the FTICR cell. These results can be seen in Figure A1.5.

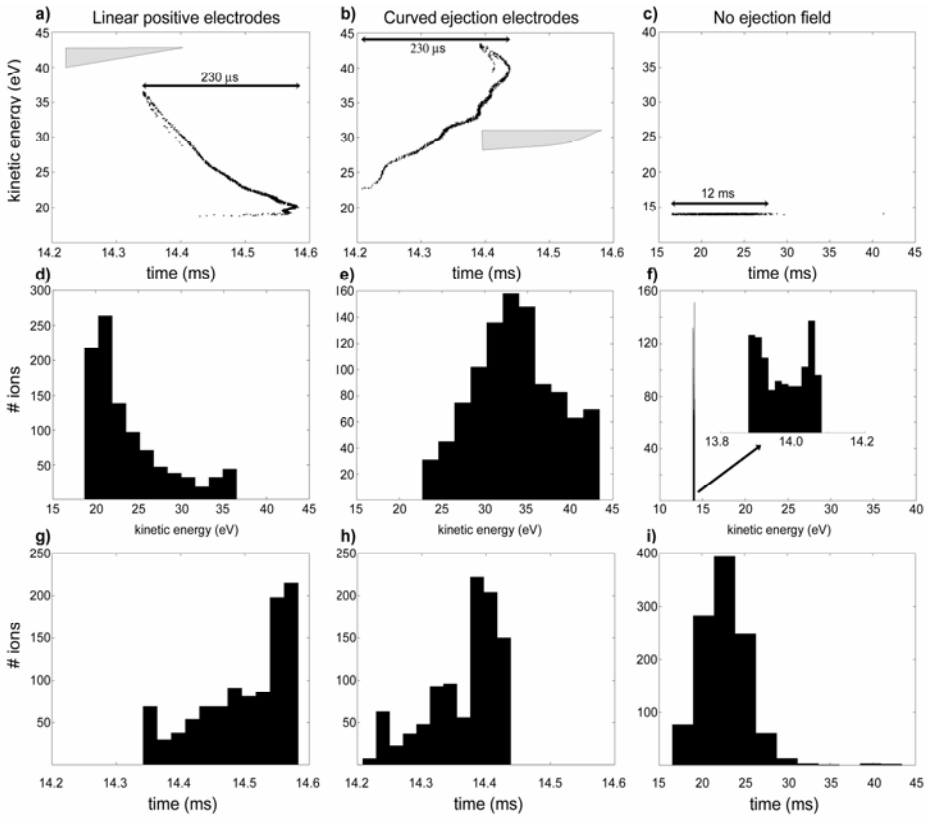

Figure A1.5. Time and energy distributions of the ion packet at the exit lens of the octopole (z = +15 ion). The first column shows a scatter plot of the time and kinetic energy distributions, and histograms of the kinetic energy distribution (middle) and the time distribution (bottom), for the ion packet ejected from the linear positive ejection electrodes configuration. The second and third columns show the results obtained for the curved electrode configuration, and with no axial field. Ions are accumulated 14 ms and then ejected. Only the period of ejection is shown in this figure (t = 0 is defined as the time when ions enter the octopole).

Because the ions with higher energy had overtaken those with lower energy for the linear-positive configuration, the time spread encompassing the majority of the z=+15 ions (90 %) at the entrance of the cell is larger than that for the curved configuration (1.17 ms and 0.77 ms, respectively). The mean and the width of the kinetic energy distributions were smaller for the linear-positive configuration, but the time spread was smaller for the curved ejection electrodes configuration at the FTICR entrance (i.e. better bunching).

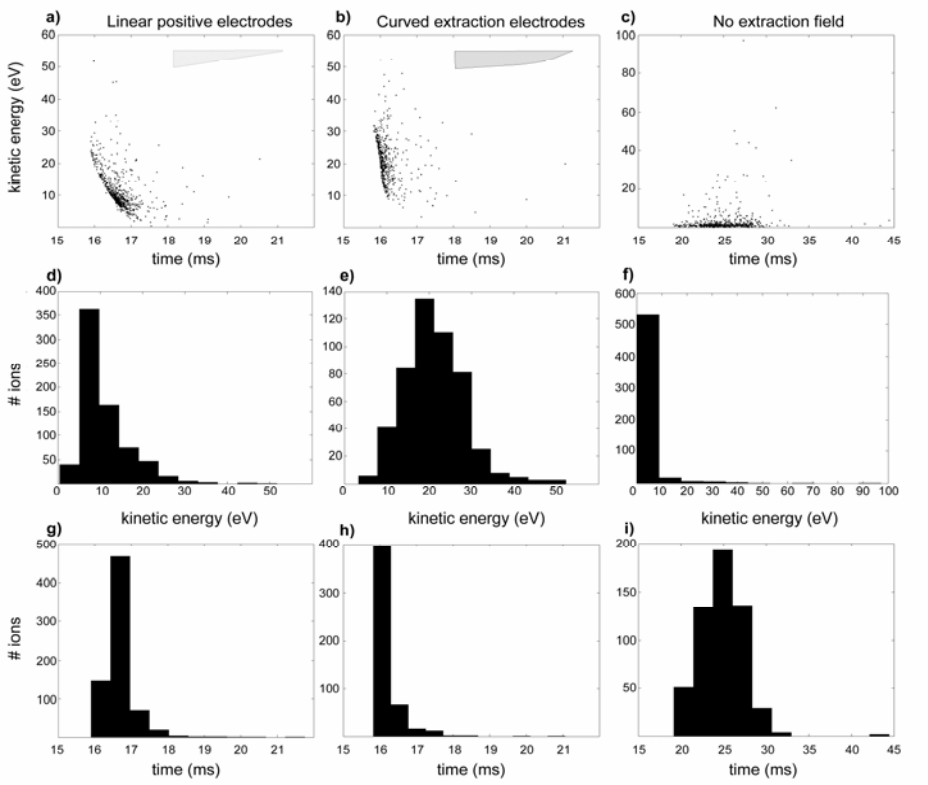

Figure A1.6. Time and energy distributions of the ion packet at the entrance of the ICR cell (z = +15 ion). The first column shows a scatter plot of the time and kinetic energy distributions, and histograms of the kinetic energy distribution (middle) and the time distribution (bottom), for the ion packet ejected from the linear positive ejection electrodes configuration. The second and third columns show the results obtained for the curved electrode configuration, and with no axial field. Only the period of ejection is shown in this figure (t = 0 is defined as the time when ions enter the octopole).

Due to the short trapping time window of the cell a more compact ion cloud at the entrance to the FTICR cell will lead to more efficient trapping, thus increased sensitivity. For both axial potential configurations the ion energy was within the acceptable limits thus the octopole that gave a shorter trapping time spread is considered to be the better choice. Again, without an axial ejection field the time spread is too large for efficient transfer and trapping of the ions in the FTICR cell (Figure A1.6).

An estimate of the increase in sensitivity for +15 cytochrome *c* ion, *m/z* = 824, was made by comparing the maximum density of ions at the cell in the time distributions of the curved- and no-ejection electrode configurations, and a trapping window of 0.2 – 0.4 ms. The octopole with the curved ejection electrodes was estimated to be 4-5 times more sensitive because of improved time-focusing at the FTICR cell.

Figure A1.7 shows preliminary experimental results obtained with an accumulation octopole of the curved electrode configuration. The ions generated from ESI of 5 μM cytochrome *c* in 69:29:2 water:methanol:acetic acid were accumulated in the octopole for 0.4 s before being transferred to the ICR cell for detection. As can be seen, the signal intensities with the ejection field, upper spectrum, were approximately 100 % stronger than that with no ejection field (0 V applied to ejection electrodes, bottom figure). Furthermore, these sensitivity improvements were observed for several charge states of cytochrome *c* indicating that sensitivity improvements can be made over *m/z* ranges compatible with LC-MS experiments of low abundance peptides, the application of interest. It also demonstrates that the time-of-flight effects of external trap FTICR experiments[243], which will be more pronounced with time-focused ejection, do not overwhelm the sensitivity gains from time-focusing of the ejected ions.

Before concluding it is pertinent to question why the experimentally measured improvement in sensitivity was less than that estimated using the simulations.

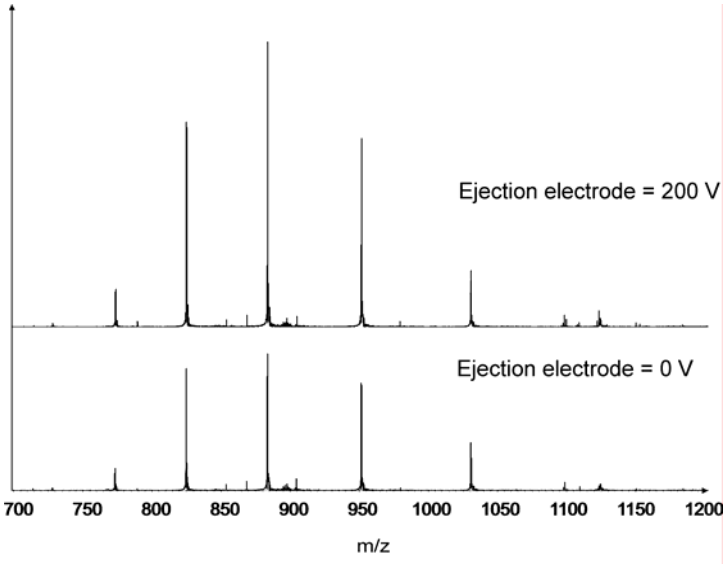

Figure A.1.7. Experimental mass spectra of cytochrome *c* when 200 V (upper figure) and 0V (lower figure) where applied to the ejection electrodes of the curved ejection electrode configuration. The arbitrary y-scales on both figures are identical.

The simulations represent an approximation of a real octopole ion trap. Uniform pressure throughout the octopole and negligible space charge effects are arguably the two most important. The pressure in an ESI experiment is not uniform. Figure A1.3 shows that the octopole ion trap is the second stage of a differentially pumped apparatus. Consequently a pressure gradient will exist along the length of the trap. Higher pressures at the beginning of the octopole will lead to greater viscous damping that can hinder ion ejection. This effect would increase the time spread of the ejected ions and thus decrease the available sensitivity gains.

As explained in the section describing the simulations, ion-ion interactions were not included for practical and reliability reasons. Space charge can shield the ions from the ejection field (higher space charge leads to a less effective the ejection field), thus reducing the time focusing at the FTICR cell and the sensitivity gains obtained. Additionally, high space charge increases the

radial size of the ion cloud in the octopole. Consequently, fewer ions might be transferred through the exit lens of the octopole accumulation device. The simulations showed that 70 % of the *m/z* = 12360 (z = +1) passed through the exit lens with a 4 mm diameter hole but 100 % of the *m/z* = 824 (z = +15) because ions of larger *m/z* (*m/z* = 12360) are less radially confined by the RF field of the octopole than ions of smaller *m/z*[267,272]. Space charge will broaden the cloud even more[272], resulting in less confined ion beams, so lowering the sensitivity compared to simulations.

The lower (but still significant) sensitivity gains of the preliminary experimental results, with respect to the simulation estimation, could reflect the pressure gradient across the octopole and / or space charge effects. While the latter will be diminished for ions of low intensity, the application of interest, an improved understanding of the physics of ion accumulation and transfer to the ICR cell could enable further sensitivity gains to be attained.

A1.4 Conclusions

Here, we have used simulations to investigate a long octopole ion trap that either has an axial potential gradient or no axial potential gradient for external accumulation and efficient transfer of ions to an FTICR-MS analyser cell. The time and energy distribution of the ions at the exit of the octopole and at the entrance of the cell show that the octopole with curved ejection electrodes (linear axial field) lead to higher sensitivity, 400-500 %. Preliminary experimental results showed that these ejection electrodes increased the ion signal from ESI of cytochrome *c* by approximately 100 % and that sensitivity improvements spanned an *m/z* range compatible the LC-MS of complex peptide solutions. The different degree of improvement between the simulations and preliminary experiments is most likely due to the approximations inherent to the simulations and will be the subject of a future experimental investigation.

Bibliography

1. Choudhary, J. & Grant, S. G. N. *Proteomics in postgenomic neuroscience: the end of the beginning*. Nat Neurosci **7**, 440-445 (2004).
2. Pandey, A. & Mann, M. *Proteomics to study genes and genomes*. Nature **405**, 837-846 (2000).
3. Tyers, M. & Mann, M. *From genomics to proteomics*. Nature **422**, 193-197 (2003).
4. Patterson, S. D. & Aebersold, R. H. *Proteomics: the first decade and beyond*. Nat Genet **33**, 311-323 (2003).
5. Stamm, S. et al. *Function of alternative splicing*. Gene **344**, 1-20 (2005).
6. Hanash, S. *Disease proteomics*. Nature **422**, 226-232 (2003).
7. Grabowski, P. J. & Black, D. L. *Alternative RNA splicing in the nervous system*. Prog Neurobiol **65**, 289-308 (2001).
8. Figeys, D. *Proteomics approaches in drug discovery*. Anal Chem **74**, 413a-419a (2002).
9. Chung, J. J., Shikano, S., Hanyu, Y. & Li, M. *Functional diversity of protein C-termini: more than zipcoding?* Trends Cell Biol **12**, 146-150 (2002).
10. Aebersold, R. *Constellations in a cellular universe*. Nature **422**, 115-116 (2003).
11. Aebersold, R. & Mann, M. *Mass Spectrometry-based proteomics*. Nature **422**, 198-207 (2003).
12. Celis, J. E. et al. *Human 2-D PAGE databases for proteome analysis in health and disease: http://biobase.dk/cgi-bin/celis*. FEBS Lett **398**, 129-134 (1996).
13. Wilkins, M. R. et al. *From proteins to proteomes: Large scale protein identification by two-dimensional electrophoresis and amino acid analysis*. Bio-Technology **14**, 61-65 (1996).
14. Anderson, N. G. & Anderson, N. L. *Twenty years of two-dimensional electrophoresis: Past, present and future*. Electrophoresis **17**, 443-453 (1996).
15. Ong, S. E. & Mann, M. *Mass spectrometry-based proteomics turns quantitative*. Nat Chem Biol **1**, 252-262 (2005).
16. Meistermann, H. et al. *Biomarker discovery by imaging mass spectrometry - Transthyretin is a biomarker for gentamicin-induced nephrotoxicity in rat*. Mol Cell Proteomics **5**, 1876-1886 (2006).
17. Andersen, J. S. & Mann, M. *Organellar proteomics: turning inventories into insights*. Embo Rep **7**, 874-879 (2006).
18. Kumar, A. et al. *Subcellular localization of the yeast proteome*. Gene Dev **16**, 707-719 (2002).
19. Wouters, F. S., Verveer, P. J. & Bastiaens, P. I. H. *Imaging biochemistry inside cells*. Trends Cell Biol **11**, 203-211 (2001).

20. Zhang, J., Campbell, R. E., Ting, A. Y. & Tsien, R. Y. *Creating new fluorescent probes for cell biology*. Nat Rev Mol Cell Bio **3**, 906-918 (2002).
21. Huh, W. K. et al. *Global analysis of protein localization in budding yeast*. Nature **425**, 686-691 (2003).
22. Bastiaens, P. I. H. & Pepperkok, R. *Observing proteins in their natural habitat: the living cell*. Trends Biochem Sci **25**, 631-637 (2000).
23. Phizicky, E., Bastiaens, P. I. H., Zhu, H., Snyder, M. & Fields, S. *Protein analysis on a proteomic scale*. Nature **422**, 208-215 (2003).
24. McDonnell, L. A. & Heeren, R. M. A. *Imaging mass spectrometry*. Mass Spectrom Rev **26**, 606-643 (2007).
25. McDonnell, L. A. et al. *Subcellular imaging mass spectrometry of brain tissue*. J Mass Spectrom **40**, 160-168 (2005).
26. Caprioli, R. M., Farmer, T. B. & Gile, J. *Molecular imaging of biological samples: localization of peptides and proteins using MALDI-TOF MS*. Anal Chem **69**, 4751-4760 (1997).
27. Karas, M., Bachmann, D., Bahr, U. & Hillenkamp, F. *Matrix-assisted ultraviolet laser desorption of non-volatile compounds*. Int J Mass Spectrom Ion Proc **78**, 53-68 (1987).
28. Karas, M. & Hillenkamp, F. *Laser Desorption Ionization of Proteins with Molecular Masses Exceeding 10000 Daltons*. Anal Chem **60**, 2299-2301 (1988).
29. Stuart, J. N., Hummon, A. B. & Sweedler, J. V. *The chemistry of thought: Neurotransmitters in the brain*. Anal Chem **76**, 120a-128a (2004).
30. Chaurand, P., Schwartz, S. A. & Caprioli, R. M. *Profiling and imaging proteins in tissue sections by MS*. Anal Chem **76**, 86a-93a (2004).
31. Rohner, T. C., Staab, D. & Stoeckli, M. *MALDI mass spectrometric imaging of biological tissue sections*. Mech Ageing Dev **126**, 177-185 (2005).
32. Stoeckli, M., Chaurand, P., Hallahan, D. E. & Caprioli, R. M. *Imaging mass spectrometry: A new technology for the analysis of protein expression in mammalian tissues*. Nat Med **7**, 493-496 (2001).
33. Skold, K. et al. *Decreased striatal levels of PEP-19 following MPTP lesion in the mouse*. J Proteome Res **5**, 262-269 (2006).
34. Khatib-Shahidi, S., Andersson, M., Herman, J. L., Gillespie, T. A. & Caprioli, R. M. *Direct molecular analysis of whole-body animal tissue sections by imaging MALDI mass spectrometry*. Anal Chem **78**, 6448-6456 (2006).
35. Belu, A. M., Davies, M. C., Newton, J. M. & Patel, N. *TOF-SIMS characterization and imaging of controlled-release drug delivery systems*. Anal Chem **72**, 5625-5638 (2000).
36. Tanaka, K. et al. *Protein and Polymer Analyses up to m/z 100 000 by Laser Ionization Time-of-Flight Mass Spectrometry*. Rapid Commun Mass Spectrom **8**, 151-153 (1988).

37. Fenn, J. B., Mann, M., Meng, C. K., Wong, S. F. & Whitehouse, C. M. *Electrospray Ionization for Mass-Spectrometry of Large Biomolecules*. Science **246**, 64-71 (1989).
38. Fenn, J. B. *Mass spectrometric implications of high-pressure ion sources*. Int J Mass Spectrom **200**, 459-478 (2000).
39. Yamashita, M. & Fenn, J. B. *Electrospray ion source. Another variation on the free-jet theme*. J Phys Chem **88**, 4451-4459 (1984).
40. Coon, J. J., Syka, J. E. P., Schwartz, J. C., Shabanowitz, J. & Hunt, D. F. *Anion dependence in the partitioning between proton and electron transfer in ion/ion reactions*. Int J Mass Spectrom **236**, 33-42 (2004).
41. Guan, Z. et al. *193 nm photodissociation of large multiply-charged biomolecules*. Int J Mass Spectrom Ion Proc **157/158**, 357-364 (1996).
42. Smith, R. D. *Evolution of ESI-mass spectrometry and Fourier transform ion cyclotron resonance for proteomics and other biological applications*. Int J Mass Spectrom **200**, 509-544 (2000).
43. Fenselau, C. & Demirev, P. A. *Characterization of intact microorganisms by MALDI mass spectrometry*. Mass Spectrom Rev **20**, 157-171 (2001).
44. Castaing, R. & Slodzian, G. *Microanalyse par émission ionique secondaire*. Journal de Microscopie **1**, 395-410 (1962).
45. Knochenmuss, R. *A quantitative model of ultraviolet matrix-assisted laser desorption/ionization including analyte ion generation*. Anal Chem **75**, 2199-2207 (2003).
46. Zubarev, R. A., Kelleher, N. L. & McLafferty, F. W. *Electron capture dissociation of multiply charged protein cations. A nonergodic process.* J Am Chem Soc **120**, 3265 (1998).
47. Karas, M., Gluckmann, M. & Schafer, J. *Ionization in matrix-assisted laser desorption/ionization: singly charged molecular ions are the lucky survivors*. J Mass Spectrom **35**, 1-12 (2000).
48. Karas, M. & Kruger, R. *Ion formation in MALDI: The cluster ionization mechanism*. Chem Rev **103**, 427-439 (2003).
49. Kampmeier, J., Dreisewerd, K., Schurenberg, M. & Strupat, K. *Investigations of 2,5-DHB and succinic acid as matrices for IR and UV MALDI. Part I: UV and IR laser ablation in the MALDI process*. Int J Mass Spectrom **169**, 31-41 (1997).
50. Fournier, I., Marinach, C., Tabet, J. C. & Bolbach, G. *Irradiation effects in MALDI, ablation, ion production, and surface modifications. PART II: 2,5-dihydroxybenzoic acid monocrystals*. J Am Soc Mass Spectr **14**, 893-899 (2003).
51. Dreisewerd, K., Berkenkamp, S., Leisner, A., Rohlfing, A. & Menzel, C. *Fundamentals of matrix-assisted laser desorption/ionization mass spectrometry with pulsed infrared lasers*. Int J Mass Spectrom **226**, 189-209 (2003).
52. Zenobi, R. & Knochenmuss, R. *Ion formation in MALDI mass spectrometry*. Mass Spectrom Rev **17**, 337-366 (1998).

53. Schwartz, S. A., Reyzer, M. L. & Caprioli, R. M. *Direct tissue analysis using matrix-assisted laser desorption/ionization mass spectrometry: practical aspects of sample preparation*. J Mass Spectrom **38**, 699-708 (2003).
54. Garrett, T. J. & Yost, R. A. *Analysis of intact tissue by intermediate-pressure MALDI on a linear ion trap mass spectrometer*. Anal Chem **78**, 2465-2469 (2006).
55. Schiller, J. et al. *The suitability of different DHB isomers as matrices for the MALDI-TOF MS analysis of phospholipids: which isomer for what purpose?* Eur Biophys J Biophys Lett **36**, 517-527 (2007).
56. Kruse, R. & Sweedler, J. V. *Spatial profiling invertebrate ganglia using MALDI MS*. J Am Soc Mass Spectr **14**, 752-759 (2003).
57. Reyzer, M. L., Hsieh, Y. S., Ng, K., Korfmacher, W. A. & Caprioli, R. M. *Direct analysis of drug candidates in tissue by matrix-assisted laser desorption/ionization mass spectrometry*. J Mass Spectrom **38**, 1081-1092 (2003).
58. Winograd, N. *The magic of cluster SIMS*. Anal Chem **77**, 142a-149a (2005).
59. Appelhans, A. D. & Delmore, J. E. *Comparison of Polyatomic and Atomic Primary Beams for Secondary Ion Mass-Spectrometry of Organics*. Anal Chem **61**, 1087-1093 (1989).
60. Wu, K. J. & Odom, R. W. *Matrix-enhanced secondary ion mass spectrometry: A method for molecular analysis of solid surfaces*. Anal Chem **68**, 873-882 (1996).
61. Delcorte, A. & Garrison, B. J. *High yield events of molecular emission induced by kiloelectronvolt particle bombardment*. J Phys Chem B **104**, 6785-6800 (2000).
62. Delcorte, A., Medard, N. & Bertrand, P. *Organic secondary ion mass spectrometry: Sensitivity enhancement by gold deposition*. Anal Chem **74**, 4955-4968 (2002).
63. Delcorte, A. & Bertrand, P. *Interest of silver and gold metallization for molecular SIMS and SIMS imaging*. Appl Surf Sci **231-2**, 250-255 (2004).
64. Adriaensen, L., Vangaever, F. & Gijbels, R. *Metal-assisted secondary ion mass spectrometry: Influence of Ag and Au deposition on molecular ion yields*. Anal Chem **76**, 6777-6785 (2004).
65. Kleinfeld, A. M., Kampf, J. P. & Lechene, C. *Transport of C-13-oleate in adipocytes measured using multi imaging mass Spectrometry*. J Am Soc Mass Spectr **15**, 1572-1580 (2004).
66. Spengler, B. & Hubert, M. *Scanning microprobe matrix-assisted laser desorption ionization (SMALDI) mass spectrometry: Instrumentation for sub-micrometer resolved LDI and MALDI surface analysis*. J Am Soc Mass Spectr **13**, 735-748 (2002).
67. Schriver, K. E., Chaurand, P. & Caprioli, R. M. *High resolution imaging mass spectrometry: Characterization of ion yields and spot sizes.* 51st

ASMS Conference on Mass Spectrometry and Allied Topics, Montreal, Canada Sci 231-232:485-489 (2003).

68. Luxembourg, S. L., Mize, T. H., McDonnell, L. A. & Heeren, R. M. A. *High-spatial resolution mass spectrometric imaging of peptide and protein distributions on a surface*. Anal Chem **76**, 5339-5344 (2004).
69. Toyoda, M. & Nishiguchi, M. *Simulation of Beam Profile of Multi-Turn Time-of-Flight Mass Spectrometers*. J Mass Spectrom Soc Jpn **55**, 17-24 (2007).
70. Takats, Z., Wiseman, J. M. & Cooks, R. G. *Ambient mass spectrometry using desorption electrospray ionization (DESI): instrumentation, mechanisms and applications in forensics, chemistry, and biology*. J Mass Spectrom **40**, 1261-1275 (2005).
71. Chen, H. W., Talaty, N. N., Takats, Z. & Cooks, R. G. *Desorption electrospray ionization mass spectrometry for high-throughput analysis of pharmaceutical samples in the ambient environment*. Anal Chem **77**, 6915-6927 (2005).
72. Wiseman, J. M., Puolitaival, S. M., Takats, Z., Cooks, R. G. & Caprioli, R. M. *Mass spectrometric profiling of intact biological tissue by using desorption electrospray ionization*. Angew Chem Int Edit **44**, 7094-7097 (2005).
73. Takats, Z., Wiseman, J. M., Gologan, B. & Cooks, R. G. *Mass spectrometry sampling under ambient conditions with desorption electrospray ionization*. Science **306**, 471-473 (2004).
74. Van Berkel, G. J., Ford, M. J. & Deibel, M. A. *Thin-layer chromatography and mass spectrometry coupled using desorption electrospray ionization*. Anal Chem **77**, 1207-1215 (2005).
75. Cooks, R. G., Ouyang, Z., Takats, Z. & Wiseman, J. M. *Ambient mass spectrometry*. Science **311**, 1566-1570 (2006).
76. March, R. E. *Quadrupole ion trap mass spectrometry: a view at the turn of the century*. Int J Mass Spectrom **200**, 285-312 (2000).
77. Schwartz, J. C., Senko, M. W. & Syka, J. E. P. *A two-dimensional quadrupole ion trap mass spectrometer*. J Am Soc Mass Spectr **13**, 659-669 (2002).
78. Hager, J. W. *A new linear ion trap mass spectrometer*. Rapid Commun Mass Spectrom **16**, 512-526 (2002).
79. Garrett, T. J. et al. *Imaging of small molecules in tissue sections with a new intermediate-pressure MALDI linear ion trap mass spectrometer*. Int J Mass Spectrom **260**, 166-176 (2007).
80. Verhaert, P. D., Conaway, M. C. P., Pekar, T. M. & Miller, K. *Neuropeptide imaging on an LTQ with vMALDI source: The complete 'all-in-one' peptidome analysis*. Int J Mass Spectrom **260**, 177-184 (2007).
81. Marshall, A. G., Hendrickson, C. L. & Jackson, G. S. *Fourier transform ion cyclotron resonance mass spectrometry: A primer*. Mass Spectrom Rev **17**, 1-35 (1998).

82. Martin, S. E., Shabanowitz, J., Hunt, D. F. & Marto, J. A. *Subfemtomole MS and MS/MS peptide sequence analysis using nano-HPLC micro-ESI Fourier transform ion cyclotron resonance mass spectrometry*. Anal Chem **72**, 4266-4274 (2000).
83. Valaskovic, G. A., Kelleher, N. L. & McLafferty, F. W. *Attomole protein characterization by capillary electrophoresis mass spectrometry*. Science **273**, 1199-1202 (1996).
84. Lipton, M. S. et al. *Global analysis of the Deinococcus radiodurans proteome by using accurate mass tags*. Proc Natl Acad Sci U S A **99**, 11049-11054 (2002).
85. Taban, I. M. et al. *Imaging of peptides in the rat brain using MALDI-FTICR mass spectrometry*. Journal of the American Society for Mass Spectrometry **18**, 145-151 (2007).
86. Weickhardt, C., Moritz, F. & Grotemeyer, J. *EMS Account: Multiphoton ionization mass spectrometry: Principles and fields of application*. Eur Mass Spectrom **2**, 151-160 (1996).
87. Guilhaus, M., Mlynski, V. & Selby, D. *Perfect timing: Time-of-flight mass spectrometry*. Rapid Commun Mass Spectrom **11**, 951-962 (1997).
88. Aebersold, R. & Goodlett, D. R. *Mass spectrometry in proteomics*. Chem Rev **101**, 269-295 (2001).
89. Krutchinsky, A. N., Kalkum, M. & Chait, B. T. *Automatic identification of proteins with a MALDI-quadrupole ion trap mass spectrometer*. Anal Chem **73**, 5066-5077 (2001).
90. Medzihradszky, K. F. et al. *The characteristics of peptide collision-induced dissociation using a high-performance MALDI-TOF/TOF tandem mass spectrometer*. Anal Chem **72**, 552-558 (2000).
91. Loboda, A. V., Krutchinsky, A. N., Bromirski, M., Ens, W. & Standing, K. G. *A tandem quadrupole/time-of-flight mass spectrometer with a matrix-assisted laser desorption/ionization source: design and performance*. Rapid Commun Mass Spectrom **14**, 1047-1057 (2000).
92. Li, Y. Z., McIver, R. T. & Hunter, R. L. *High-Accuracy Molecular-Mass Determination for Peptides and Proteins by Fourier-Transform Mass-Spectrometry*. Anal Chem **66**, 2077-2083 (1994).
93. McLafferty, F. W. et al. *Two-dimensional mass spectrometry of biomolecules at the subfemtomole level*. Curr Opin Chem Biol **2**, 571-578 (1998).
94. Castoro, J. A. & Wilkins, C. L. *High-Resolution Laser-Desorption Ionization Fourier-Transform Mass-Spectrometry*. Trac-Trend Anal Chem **13**, 229-233 (1994).
95. Kutz, K. K., Schmidt, J. J. & Li, L. J. *In situ tissue analysis of neuropeptides by MALDI FTMS in-cell accumulation*. Anal Chem **76**, 5630-5640 (2004).
96. Lawrence, E. O. & Livingston, M. S. *The production of high speed light ions without the use of high voltages*. Phys Rev **40**, 19-35 (1932).

97. Comisarow, M. B. & Marshall, A. G. *Frequency-sweep Fourier transform ion cyclotron resonance spectroscopy*. Chem Phys Lett **26**, 489-490 (1974).
98. Comisarow, M. B. & Marshall, A. G. *Fourier transform ion cyclotron resonance spectroscopy*. Chem Phys Lett **25**, 282-283 (1974).
99. Marshall, A. G. *Milestones in Fourier transform ion cyclotron resonance mass spectrometry technique development*. Int J Mass Spectrom **200**, 331-356 (2000).
100. McIver Jr, R. T. *A trapped-ion analyzer cell for ion cyclotron resonance spectroscopy*. Rev Scient Instr **41**, 555-558 (1970).
101. Jackson, G. S., White, F. M., Guan, S. & Marshall, A. G. *Matrix-shimmed ion cyclotron resonance ion trap simultaneously optimized for excitation, detection, quadrupolar axialization and trapping*. J Am Soc Mass Spectrom **10**, 759-769 (1999).
102. Lee, S. H., Wanczek, K.-P. & Hartmann, H. *Cylindrical Trap*. Adv Mass Spectrom **8B**, 1645-1647 (1980).
103. Caravatti, P. & Allemann, M. *RF Shim by Trap Segmentation*. Org Mass Spectrom **26**, 514-518 (1991).
104. Gabrielse, G., Haarsma, L. & Rolston, S. L. *Open-Endcap Penning Traps for High Precision Experiments*. Int J Mass Spectrom Ion Proc **88**, 319-332 (1989).
105. Beu, S. C. & Laude, D. A. J. *Elimination of axial ejection during excitation with a capacitively coupled open trapped-ion cell for FTICRMS*. Anal Chem **64**, 177-180 (1992a).
106. Guan, S. & Marshall, A. G. *Ion traps for Fourier transform ion cyclotron resonance mass spectrometry: principles and design of geometric and electric configurations*. Int J Mass Spectrom Ion Proc **146**, 261-296 (1995).
107. Gorshkov, M. V., Masselon, C. D., Anderson, G. A., Udseth, H. R. & Smith, R. D. *Dynamically assisted gated trapping for Fourier transform ion cyclotron resonance mass spectrometry*. Rapid Commun Mass Spectrom **15**, 1558-1561 (2001).
108. Gorshkov, M. V., Guan, S. & Marshall, A. G. *Dynamic ion trapping for Fourier-transform ion cyclotron resonance mass spectrometry: Simultaneous positive- and negative-ion detection*. Rapid Commun Mass Spectrom **6**, 166-172 (1992).
109. Rakov, V. S., Futrell, J. H., Denisov, E. V. & Nikolaev, E. N. *Instrumentation of kinetic energy-resolved surface-induced dissociation in Fourier transform mass spectrometry*. Eur J Mass Spectrom **6**, 299-317 (2000).
110. Tsybin, Y. O., Witt, M., Baykut, G. & Hakansson, P. *Electron capture dissociation Fourier transform ion cyclotron resonance mass spectrometry in the electron energy range 0-50 eV*. Rapid Commun Mass Spectrom **18**, 1607-1613 (2004).

111. Guan, S. & Marshall, A. G. *Stored waveform inverse Fourier transform (SWIFT) ion excitation in trapped-ion mass spectrometry: theory and aplications*. Int J Mass Spectrom Ion Proc **157/158**, 5-37 (1996).
112. Marshall, A. G., Wang, T. C. & Ricca, T. L. *Tailord Excitation for Fourier Transform Ion Cyclotron Resonance Mass Spectrometry*. J Am Chem Soc **107**, 7893-7897 (1985).
113. Biemann, K. *Contributions of mass spectrometry to peptide and protein-structure*. Biomed Environ Mass Spectrom **16**, 99-111 (1988).
114. Roepstorff, P. & Fohlman, J. *Proposal for a common nomenclature for sequence ions in mass spectra of peptides*. Biomed Mass Spectrom **11**, 11 (1984).
115. Senko, M. W., Speir, P. J. & McLafferty, F. W. *Collisional Activation of Large Multiply Charged Ions Using Fourier Transform Mass Spectrometry*. Anal Chem **66**, 2801-2808 (1994).
116. Dienes, T. et al. *Fourier transform mass spectrometry - Advancing years (1992 mid 1996)*. Mass Spectrom Rev **15**, 163-211 (1996).
117. Gauthier, J. W., Trautman, T. R. & Jacobsen, D. B. *Sustained off-resonance irradiation for collision-activated dissociation involving Fourier transform mass spectrometry. Collision-activated dissociation technique that emulates infrared multiphoton dissociation*. Anal Chim Acta **246**, 211-225 (1991).
118. Li, W., Hendrickson, C. L., Emmet, M. R. & Marshall, A. G. *Identification of Intact Proteins in Mixtures by Alternated Capillary Liquid Chromatography Electrospray Ionization and LC ESI Infrared Multiphoton Dissociation Fourier Transform Ion Cyclotron Resonance Mass Spectrometry*. Anal Chem **71**, 4397-4402 (1999).
119. Little, D. P., Spier, P. J., Senko, M. W., O'Connor, P. B. & McLafferty, F. W. *Infrared multiphoton dissociation of large multiply-charged ions for biomolecule sequencing*. Anal Chem **66**, 2809-2815 (1994).
120. Ijames, C. F. & Wilkins, C. L. *Surface-induced dissociation by Fourier transform mass spectrometry*. Anal Chem **62**, 1295-1299 (1990).
121. Chorush, R. A., Little, D. P., Beu, S. C., Wood, T. D. & McLafferty, F. W. *Surface-induced dissociation of multiply-protonated proteins*. Anal Chem **67**, 1042-1046 (1995).
122. Zubarev, R. A. *Reactions of polypeptide ions with electrons in the gas phase*. Mass Spectrom Rev **22**, 57-77 (2003).
123. Hakansson, K., Emmett, M. R., Hendrickson, C. L. & Marshall, A. G. *High-Sensitivity Electron Capture Dissociation Tandem FTICR Mass Spectrometry of Microelectrosprayed Peptides*. Anal Chem **73**, 3605-3610 (2001).
124. Hakansson, K. et al. *Electron Capture Dissociation and Infrared Multiphoton Dissociation MS/MS of an N-Glycosylated Tryptic Peptide To Yield Complementary Sequence Information*. Anal Chem **73**, 4530-4536 (2001).

125. Zubarev, R. A. et al. *Electron capture dissociation for structural characterization of multiply charged protein cations*. Anal Chem **72**, 563-573 (2000).
126. WysockI, V. H., Tsaprailis, G., Smith, L. L. & Breci, L. A. *Mobile and localized protons: a framework for understanding peptide dissociation*. J Mass Spectrom **35**, 1399-1406 (2000).
127. Laskin, J., Denisov, E. & Futrell, J. H. *Fragmentation energetics of small peptides from multiple-collision activation and surface-induced dissociation in FT-ICR MS*. Int J Mass Spectrom **219**, 189-201 (2002).
128. Jones, J. W., Sasaki, T., Goodlett, D. R. & Turecek, F. *Electron capture in spin-trap capped peptides. An experimental example of ergodic dissociation in peptide cation-radicals*. J Am Soc Mass Spectrom **18**, 432-444 (2007).
129. Syrstad, E. A. & Turecek, F. *Toward a general mechanism of electron capture dissociation*. J Am Soc Mass Spectrom **16**, 208-224 (2005).
130. Tolmachev, A. V., Chernushevich, I. V., Dodonov, A. F. & Standing, K. G. *A Collisional focusing ion guide for coupling an atmospheric pressure ion source to a mass spectrometer*. Nucl Instr and Meth A **124**, 112-119 (1997).
131. Limbach, P. A., Marshall, A. G. & Wang, M. *An electrostatic ion guide for efficient transmission of low energy externally formed ions into a Fourier transform ion cyclotron resonance mass spectrometer*. Int J Mass Spectrom Ion Proc **125**, 135-143 (1993).
132. Kofel, P., Alleman, M., Kellerhals, H. & Wanczek, K.-P. *Time-of-flight ICR Spectrometry*. Int J Mass Spectrom Ion Proc **72**, 53-61 (1986).
133. McIver Jr, R. T., Hunter, R. L. & Bowers, W. D. *Coupling a quadrupole mass spectrometer and a Fourier transform mass spectrometer*. Int J Mass Spectrom Ion Proc **64**, 67-77 (1985).
134. Huang, Y., Guan, S., Kim, H. S. & Marshall, A. G. *Ion transport through a strong magentic field gradient by r.f. -only octupole ion guides*. Int J Mass Spectrom Ion Proc **152**, 121-133 (1996).
135. Hunt, S. M., Sheil, M. M., Belov, M. & Derrick, P. J. *Probing the effects of cone potential in the electrospray ion source: consequences for the determination of molecular weight distributions of synthetic polymers*. Anal Chem **70**, 1812-1822 (1998).
136. Cha, B., Blades, M. & Douglas, D. J. *An Interface with a Linear Quadrupole Ion Guide for an Electrospray-Ion Trap Mass Spectrometer System*. Anal Chem **72**, 5647-5654 (2000).
137. Krutchinsky, A. N., Chernushevich, I. V., Spicer, V. L., Ens, W. & Standing, K. G. *Collisional damping interface for an electrospray ionization time-of-flight mass spectrometer*. J Am Soc Mass Spectrom **9**, 569-579 (1998).
138. Belov, M. E., Gorshkov, M. V., Udseth, H. R., Anderson, G. A. & Smith, R. D. *Zeptomole-sensitivity electrospray ionization-Fourier transform ion*

cyclotron resonance mass spectrometry of proteins. Anal Chem **72**, 2271-2279 (2000).
139. Colburn, A. W., Giannakopulos, A. E. & Derrick, P. J. *The Ion Conveyor. An ion focusing and conveying device*. Eur J Mass Spectrom **10**, 149-154 (2004).
140. Caravatti, P. & Allemann, M. *The Infinity Cell - a New Trapped-Ion Cell with Radiofrequency Covered Trapping Electrodes for Fourier-Transform Ion-Cyclotron Resonance Mass-Spectrometry*. Org Mass Spectrom **26**, 514-518 (1991).
141. Guo, X., Duursma, M., Al-Khalili, A., McDonnell, L. A. & Heeren, R. M. A. *Design and performance of a new FT-ICR cell operating at a temperature range of 77-438 K*. Int J Mass Spectrom **231**, 37-45 (2004).
142. Mihalca, R. et al. *Combined infrared multiphoton dissociation and electron-capture dissociation using co-linear and overlapping beams in Fourier transform ion cyclotron resonance mass spectrometry*. Rapid Commun Mass Spectrom **20**, 1838-1844 (2006).
143. Moyer, S. C., Budnik, B. A., Pittman, J. L., Costello, C. E. & O'Connor, P. B. *Attomole peptide analysis by high-pressure matrix-assisted laser desorption/ionization Fourier transform mass spectrometry*. Anal Chem **75**, 6449-6454 (2003).
144. Taban, I. M., McDonnell, L. A., Rompp, A., Cerjak, I. & Heeren, R. M. A. *SIMION analysis of a high performance linear accumulation octopole with enhanced ejection capabilities*. Int J Mass Spectrom **244**, 135-143 (2005).
145. Easterling, M. L., Mize, T. H. & Amster, I. J. *Routine part-per-million mass accuracy for high-mass ions: Space-charge effects in MALDI FT-ICR*. Anal Chem **71**, 624-632 (1999).
146. Maharrey, S. et al. *High mass resolution SIMS*. Appl Surf Sci **231-2**, 972-975 (2004).
147. Bogdanov, B. & Smith, R. D. *Proteomics by FTICR mass spectrometry: Top down and bottom up*. Mass Spectrom Rev **24**, 168-200 (2005).
148. Shi, S. D. H., Hendrickson, C. L. & Marshall, A. G. *Counting individual sulfur atoms in a protein by ultrahigh-resolution Fourier transform ion cyclotron resonance mass spectrometry: Experimental resolution of isotopic fine structure in proteins*. P Natl Acad Sci USA **95**, 11532-11537 (1998).
149. He, F., Hendrickson, C. L. & Marshall, A. G. *Baseline Mass of peptide isobars: A record for molecular mass resolution*. Anal Chem **73**, 647-650 (2001).
150. Hughey, C. A., Rodgers, R. P. & Marshall, A. G. *Resolution of 11 000 Oil Compositionally Distinct Components in a Single Electrospray Ionization Fourier Transfrom Ion Cyclotron Resoance Mass Spectrum of Crude Oil*. Anal Chem **74**, 4145-4149 (2002).
151. Miyabayashi, K., Naito, Y., Miyake, M. & Tsujimoto, K. *Quantitative capability of electrospray ionization Fourier transform ion cyclotron*

resonance mass spectrometry for a complex mixture. Eur J Mass Spectrom **6**, 251-258 (2000).
152. Bergquist, J., Palmblad, M., Wetterhall, M., Hakansson, P. & Markides, K. E. *Peptide mapping of proteins in human body fluids using electrospray ionization Fourier transform ion cyclotron resonance mass spectrometry*. Mass Spectrom Rev **21**, 2-15 (2002).
153. Zubarev, R. & Mann, M. *On the proper use of mass accuracy in proteomics*. Mol Cell Proteomics **6**, 377-381 (2007).
154. Anderson, N. L. et al. *The human plasma proteome - A nonredundant list developed by combination of four separate sources*. Mol Cell Proteomics **3**, 311-326 (2004).
155. Corthals, G. L., Wasinger, V. C., Hochstrasser, D. F. & Sanchez, J. C. *The dynamic range of protein expression: A challenge for proteomic research*. Electrophoresis **21**, 1104-1115 (2000).
156. Suckau, D. et al. *A novel MALDI LIFT-TOF/TOF mass spectrometer for proteomics*. Anal Bioanal Chem **376**, 952-965 (2003).
157. Graber, A. et al. *Result-driven strategies for protein identification and quantitation - a way to optimize experimental design and derive reliable results*. Proteomics **4**, 474-489 (2004).
158. Mize, T. H. et al. *A modular data and control system to improve sensitivity, selectivity, speed of analysis, ease of use, and transient duration in an external source FTICR-MS*. Int J Mass Spectrom **235**, 243-253 (2004).
159. Frigo, M. & Johnson, S. G. *FFTW:an adaptive software architecture for the FFT.* (IEEE Computer Society, Seattle, WA, 1988).
160. Kharchenko, A., Merkulov, A., Konijnenburg, M., Eijkel, G. B. & Heeren, R. M. A. *manuscript in preparation*. (2007).
161. Rompp, A. et al. *Examples of Fourier transform ion cyclotron resonance mass spectrometry developments: from ion physics to remote access biochemical mass spectrometry*. Eur J Mass Spectrom **11**, 443-456 (2005).
162. Van der Burgt, Y. E. M. et al. *Parallel processing of large datasets from nanoLC-FTICR-MS measurements*. J Am Soc Mass Spectrom **18**, 152-161 (2007).
163. Belov, M. E., Anderson, G. A. & Smith, R. D. *Higher-resolution data-dependent selective external ion accumulation for capillary LC-FTICR*. Int J Mass Spectrom **218**, 265-279 (2002).
164. Qian, W. J., Camp, D. G. & Smith, R. D. *High-throughput proteomics using Fourier transform ion cyclotron resonance mass spectrometry*. Expert Rev Proteomic **1**, 87-95 (2004).
165. Mitchell, D. W. & Smith, R. D. *Cyclotron Motion of 2 Coulombically Interacting Ion Clouds with Implications to Fourier-Transform Ion-Cyclotron Resonance Mass-Spectrometry*. Phys Rev E **52**, 4366-4386 (1995).

166. O'Connor, P. B. & Costello, C. E. *Internal calibration on adjacent samples (InCAS) with Fourier transform mass spectrometry*. Anal Chem **72**, 5881-5885 (2000).
167. Hannis, J. C. & Muddiman, D. C. *A dual electrospray ionization source combined with hexapole accumulation to achieve high mass accuracy of biopolymers in fourier transform ion cyclotron resonance mass spectrometry*. J Am Soc Mass Spectrom **11**, 876-883 (2000).
168. Cao, P. & Moini, M. *Capillary electrophoresis electrospray ionization high mass accuracy time-of-flight mass spectrometry for protein identification using peptide mapping*. Rapid Commun Mass Spectrom **12**, 864-870 (1998).
169. Flora, J. W., Hannis, J. C. & Muddiman, D. C. *High-mass accuracy of product ions produced by SORI-CID using a dual electrospray ionization source coupled with FTICR mass spectrometry*. Anal Chem **73**, 1247-1251 (2001).
170. Palmer, M. E., Clench, M. R., Tetler, L. W. & Little, D. R. *Exact mass determination of narrow electrophoretic peaks using an orthogonal acceleration time-of-flight mass spectrometer*. Rapid Commun Mass Spectrom **13**, 256-263 (1999).
171. Belov, M. E. et al. *Automated Gain Control and Internal Calibration with External Ion Accumulation Capillary Liquid Chromatography-Electrospray Ionization-Fourier Transform Ion Cyclotron Resonance*. Anal Chem **75**, 4195-4205 (2003).
172. Olsen, J. V., Ong, S. E. & Mann, M. *Trypsin cleaves exclusively C-terminal to arginine and lysine residues*. Mol Cell Proteomics **3**, 608-614 (2004).
173. Sweet, S. M. M., Creese, A. J. & Cooper, H. J. *Strategy for the identification of sites of phosphorylation in proteins: Neutral loss triggered electron capture dissociation*. Anal Chem **78**, 7563-7569 (2006).
174. Schroeder, M. J., Shabanowitz, J., Schwartz, J. C., Hunt, D. F. & Coon, J. J. *A neutral loss activation method for improved phosphopeptide sequence analysis by quadrupole ion trap mass spectrometry*. Anal Chem **76**, 3590-3598 (2004).
175. Cooper, H. J., Akbarzadeh, S., Heath, J. K. & Zeller, M. *Data-dependent electron capture dissociation FT-ICR mass spectrometry for proteomic analyses*. J Proteome Res **4**, 1538-1544 (2005).
176. Kocher, T., Savitski, M. M., Nielsen, M. L. & Zubarev, R. A. *PhosTShunter: A fast and reliable tool to detect phosphorylated peptides in liquid chromatography Fourier transform tandem mass spectrometry data sets*. J Proteome Res **5**, 659-668 (2006).
177. Klinkert, I. et al. *Tools and strategies for visualization of large image data sets in high-resolution imaging mass spectrometry*. Rev Sci Instrum **78**, 53716 (2007).

178. Romijn, E. P., Krijgsveld, J. & Heck, A. J. R. *Recent liquid chromatographic-(tandem) mass spectrometric applications in proteomics*. J Chromatogr A **1000**, 589-608 (2003).
179. Marouga, R., David, S. & Hawkins, E. *The development of the DIGE system: 2D fluorescence difference gel analysis technology*. Analytical and Bioanalytical Chemistry **382**, 669-678 (2005).
180. Old, W. M. et al. *Comparison of label-free methods for quantifying human proteins by shotgun proteomics*. Mol Cell Proteomics **4**, 1487-1502 (2005).
181. Mann, M. *Functional and quantitative proteomics using SILAC*. Nat Rev Mol Cell Bio **7**, 952-958 (2006).
182. McClatchy, D. B., Dong, M. Q., Wu, C. C., Venable, J. D. & Yates, J. R. *N-15 metabolic labeling of mammalian tissue with slow protein turnover*. J Proteome Res **6**, 2005-2010 (2007).
183. Shiio, Y., Aebersold, R. *Quantitative proteome analysis using isotope-coded affinity tags and mass spectrometry* Nat Prot **1**, 139-145 (2006).
184. Listgarten, J. & Emili, A. *Statistical and computational methods for comparative proteomic profiling using liquid chromatography-tandem mass spectrometry*. Mol Cell Proteomics **4**, 419-434 (2005).
185. Hsu, J. L., Huang, S. Y., Chow, N. H. & Chen, S. H. *Stable-isotope dimethyl labeling for quantitative proteomics*. Anal Chem **75**, 6843-6852 (2003).
186. Taban, I. M. et al. *A novel workflow control system for FTICR-MS allows for unique on-the-fly data-dependent decisions*. Rappid Commun Mass Spectrom **accepted** (2008).
187. Calero, M. et al. *Dual Prenylation Is Required for Rab Protein Localization and Function*. Mol Biol Cell **14**, 1852-1867 (2003).
188. Zaccai, M. & Lipshitz, H. D. *Role of Adducin-like (hu-li tai shao) mRNA and protein localization in regulating cytoskeletal structure and function during Drosophila oogenesis and early embryogenesis*. Dev Genet **19**, 249-257 (1996).
189. Raina, A. K. et al. *Acetylation: A novel posttranslational modification in Alzheimer disease.* J Neuropath Exp Neur **62**, 551-551 (2003).
190. Wang, J. Z., GrundkeIqbal, I. & Iqbal, K. *Glycosylation of microtubule-associated protein tau: An abnormal posttranslational modification in Alzheimer's disease*. Nat Med **2**, 871-875 (1996).
191. Guo, L., Munzberg, H., Stuart, R. C., Nillni, E. A. & Bjorbaek, C. *N-acetylation of hypothalamic {alpha}-melanocyte-stimulating hormone and regulation by leptin*. PNAS **101**, 11797-11802 (2004).
192. Dierks, T. et al. *Multiple sulfatase deficiency is caused by mutations in the gene encoding the human C-alpha-formylglycine generating enzyme*. Cell **113**, 435-444 (2003).
193. Hoozemans, J. J. M. et al. *The unfolded protein response affects neuronal cell cycle protein expression: Implications for Alzheimer's disease pathogenesis*. Experim Geront **41**, 380-386 (2006).

194. Pierson, J. et al. *Molecular profiling of experimental Parkinson's disease: Direct analysis of peptides and proteins on brain tissue sections by MALDI mass spectrometry*. J Proteome Res **3**, 289-295 (2004).
195. Pierson, J., Svenningsson, P., Caprioli, R. M. & Andren, P. E. *Increased levels of ubiquitin in the 6-OHDA-lesioned striatum of rats*. J Proteome Res **4**, 223-226 (2005).
196. Altelaar, A. F. M. et al. *Gold-Enhanced Biomolecular Surface Imaging of Cells and Tissue by SIMS and MALDI Mass Spectrometry*. Anal Chem **78**, 734-742 (2006).
197. Van Vaeck, L., Adriaens, A. & Gijbels, R. *Static secondary ion mass spectrometry: (S-SIMS) Part 1. Methodology and structural interpretation*. Mass Spectrom Rev **18**, 1-47 (1999).
198. Vickerman, J. C. & Briggs, D. e. *ToF-SIMS: Surface Analysis by Mass Spectrometry* (IM Publications, Chichester, UK, 2001).
199. Sjovall, P., Lausmaa, J. & Johansson, B. *Mass spectrometric imaging of lipids in brain tissue*. Anal Chem **76**, 4271-4278 (2004).
200. Altelaar, A. F. M., van Minnen, J., Jimenez, C. R., Heeren, R. M. A. & Piersma, S. R. *Direct molecular Imaging of Lymnaea stagnalis nervous tissue at subcellular spatial resolution by mass spectrometry*. Anal Chem **77**, 735-741 (2005).
201. Adriaensen, L., Vangaever, F., Lenaerts, J. & Gijbelsa, R. *S-SIMS and MetA-SIMS study of organic additives in thin polymer coatings.* Appl Surf Sci **252**, 6628-6631 (2006).
202. Adriaensen, L., Vangaever, F. & Gijbels, R. *Organic SIMS: the influence of time on the ion yield enhancement by silver and gold deposition*. Appl Surf Sci **231-2**, 256-260 (2004).
203. Delcorte, A., Bour, J., Aubriet, F., Muller, J. F. & Bertrand, P. *Sample metallization for performance improvement in desorption/ionization of kilodalton molecules: Quantitative evaluation, imaging secondary ion MS, and laser ablation*. Anal Chem **75**, 6875-6885 (2003).
204. Luxembourg, S. L., McDonnell, L. A., Duursma, M. C., Guo, X. H. & Heeren, R. M. A. *Effect of local matrix crystal variations in matrix-assisted ionization techniques for mass spectrometry*. Anal Chem **75**, 2333-2341 (2003).
205. McDonnell, L. A. et al. *Using matrix peaks to map topography: Increased mass resolution and enhanced sensitivity in chemical imaging*. Anal Chem **75**, 4373-4381 (2003).
206. McDonnell, L. A., Heeren, R. M. A., de Lange, R. P. J. & Fletcher, I. W. *Higher Sensitivity Secondary Ion Mass Spectrometry of Biological Molecules for High Resolution, Chemically Specific Imaging*. J Am Soc Mass Spectrom **17**, 1195-1202 (2006).
207. Nygren, H., Malmberg, P., Kriegeskotte, C. & Arlinghaus, H. F. *Bioimaging TOF-SIMS: localization of cholesterol in rat kidney sections*. FEBS Lett **566**, 291-293 (2004).
208. Paxinos, G. & Watson, C. *Rat brain steretaxic coordinates* (Academic Press, San Diego, 1998).

209. Hensel, R. R., King, R. C. & Owens, K. G. *Electrospray sample preparation for improved quantitation in matrix-assisted laser desorption/ionization time-of-flight mass spectrometry*. Rapid Commun Mass Spectrom **11**, 1785-1793 (1997).
210. Hanton, S. D., Clark, P. A. C. & Owens, K. G. *Investigations of matrix-assisted laser desorption/ionization sample preparation by time-of-flight secondary ion mass spectrometry*. J Am Soc Mass Spectr **10**, 104-111 (1999).
211. Baykut, G., Jertz, R. & Witt, M. *Matrix-assisted laser desorption/ionization Fourier transform ion cyclotron resonance mass spectrometry with pulsed in-source collision gas and in-source ion accumulation*. Rapid Commun Mass Spectrom **14**, 1238-1247 (2000).
212. Schueler, B., Sander, P. & Reed, D. A. *A Time-of-Flight Secondary Ion-Microscope*. Vacuum **41**, 1661-1664 (1990).
213. Schueler, B. W. *Microscope Imaging by Time-of-Flight Secondary Ion Mass-Spectrometry*. Microsc Microanal Microstruct **3**, 119-139 (1992).
214. Wotjak, C. T. et al. *Release of vasopressin within the rat paraventricular nucleus in response to emotional stress: A novel mechanism of regulating adrenocorticotropic hormone secretion?* J Neurosci **16**, 7725-7732 (1996).
215. Hernando, F., Schoots, O., Lolait, S. J. & Burbach, J. P. H. *Immunohistochemical localization of the vasopressin V1b receptor in the rat brain and pituitary gland: Anatomical support for its involvement in the central effects of vasopressin*. Endocrinology **142**, 1659-1668 (2001).
216. Ludwig, M. *Dendritic release of vasopressin and oxytocin*. J Neuroendocrinol **10**, 881-895 (1998).
217. Ideker, T. et al. *Integrated genomic and proteomic analyses of a systematically perturbed metabolic network*. Science **292**, 929-934 (2001).
218. Masselon, C. et al. *Targeted comparative proteomics by liquid chromatography-tandem Fourier ion cyclotron resonance mass spectrometry*. Anal Chem **77**, 400-406 (2005).
219. Heeren, R. M. A. *Proteome imaging: A closer look at life's organization*. Proteomics **5**, 4316-4326 (2005).
220. Mann, M., Meng, C. K. & Fenn, J. B. *Interpreting Mass-Spectra of Multiply Charged Ions*. Anal Chem **61**, 1702-1708 (1989).
221. Senko, M. W., Beu, S. C. & Mclafferty, F. W. *Automated Assignment of Charge States from Resolved Isotopic Peaks for Multiply-Charged Ions*. J Am Soc Mass Spectr **6**, 52-56 (1995).
222. Senko, M. W., Beu, S. C. & Mclafferty, F. W. *Determination of Monoisotopic Masses and Ion Populations for Large Biomolecules from Resolved Isotopic Distributions*. J Am Soc Mass Spectr **6**, 229-233 (1995).

223. Zhang, Z. Q. & Marshall, A. G. *A universal algorithm for fast and automated charge state deconvolution of electrospray mass-to-charge ratio spectra*. J Am Soc Mass Spectr **9**, 225-233 (1998).
224. Matthiesen, R., Trelle, M. B., Hojrup, P., Bunkenborg, J. & Jensen, O. N. *VEMS 3.0: Algorithms and computational tools for tandem mass spectrometry based identification of post-translational modifications in proteins*. J Proteome Res **4**, 2338-2347 (2005).
225. Foster, I. & Kesselman, C. *Computational grids - Invited talk (Reprinted from The Grid: Blueprint for a new computing infrastructure, 1998)*. Lect Notes Comput Sc **1981**, 3-37 (2001).
226. Carr, S. et al. *The need for guidelines in publication of peptide and protein identification data - Working group on publication guidelines for peptide and protein identification data*. Mol Cell Proteomics **3**, 531-533 (2004).
227. Amster, I. J. *Fourier transform mass spectrometry*. J Mass Spectrom **31**, 1325-1337 (1996).
228. Horn, D. M., Zubarev, R. A. & McLafferty, F. W. *Automated reduction and interpretation of high resolution electrospray mass spectra of large molecules*. J Am Soc Mass Spectr **11**, 320-332 (2000).
229. Orchard, S., Hermjakob, H. & Apweiler, R. *The proteomics standards initiative*. Proteomics **3**, 1374-1376 (2003).
230. Dekker, L. J. et al. *MALDI-TOF mass spectrometry analysis of cerebrospinal fluid tryptic peptide profiles to diagnose leptomeningeal metastases in patients with breast cancer*. Mol Cell Proteomics **4**, 1341-1349 (2005).
231. Smith, R. D. et al. *An accurate mass tag strategy for quantitative and high-throughput proteome measurements*. Proteomics **2**, 513-523 (2002).
232. Spengler, B. *De novo sequencing, peptide composition analysis, and composition-based sequencing: A new strategy employing accurate mass determination by Fourier transform ion cyclotron resonance mass spectrometry*. J Am Soc Mass Spectr **15**, 703-714 (2004).
233. Conrads, T. P. et al. *Quantitative Analysis of Bacterial and Mammalian Proteomes Using a Combination of Cysteine Affinity Tags and ^{15}N-Metabolic Labeling*. Anal Chem **73**, 2132-2139 (2001).
234. Shen, Y. et al. *High-Throughput Proteomics Using High-Efficiency Multiple-Capillary Liquid Chromatography with On-Line High-Performance ESI FTICR Mass Spectrometry*. Anal Chem **73**, 3011-3021 (2001).
235. Paša-Tolic´, L. et al. *Gene expression profiling using advanced mass spectrometric approaches*. J Mass Spectrom **37**, 1185-1198 (2002).
236. Emmet, M. R., White, F. M., Hendrickson, C. L., Shi, S. D.-H. & Marshall, A. G. *Application of micro-electrospray liquid chromatography techniques to FT-ICR MS to enable high-sensitivity biological analysis*. J Am Soc Mass Spectrom **9**, 333-340 (1998).

237. Ihling, C. et al. *Nano-high-performance liquid chromatography in combination with nano-electrospray ionization Fourier transform ion-cyclotron resonance mass spectrometry for proteome analysis*. Rapid Commun Mass Spectrom **17**, 1240-1246 (2003).
238. Palmblad, M., Tysbin, Y. O., Ramström, M., Bergquist, J. & Håkansson, P. *Liquid chromatography and electron capture dissociation in Fourier transform ion cyclotron resonance mass spectrometry*. Rapid Commun Mass Spectrom **16**, 988-992 (2002).
239. Quenzer, T. L., Emmett, M. R., Hendrickson, C. L., Kelly, P. H. & Marshall, A. G. *High Sensitivity Fourier Transform Ion Cyclotron Resonance Mass Spectrometry for Biological Analysis with Nano-LC and Microelectrospray Ionization*. Anal Chem **73**, 1721-1725 (2001).
240. Jensen, P. K. et al. *Probing proteomes using capillary isoelectric focusing-electrospray ionization Fourier transform ion cyclotron resonance mass spectrometry*. Anal Chem **71**, 2076-2084 (1999).
241. Aaserud, D. J., Prokai, L. & Simonsick Jr, W. J. *Gel permeation chromatography coupled to Fourier transform mass spectrometry for polymer characterization*. Anal Chem **71**, 4793-4799 (1999).
242. McDonnell, L. A., Derrick, P. J., Powell, B. B. & Double, P. *Sustained-off resonance irradiation collision-induced dissociation of linear, substituted and cyclic polyesters using a 9.4 T Fourier transform ion cyclotron resonance mass spectrometer*. Eur J Mass Spectrom **9**, 117-128 (2003).
243. O'Connor, P. B., Duursma, M. C., vanRooij, G. J., Heeren, R. M. A. & Boon, J. J. *Correction of time-of-flight shifted polymeric molecular weight distributions in matrix assisted laser desorption/ionization Fourier transform mass spectrometry*. Anal Chem **69**, 2751-2755 (1997).
244. Hawkridge, A. M., Zhou, L., Lee, M. L. & Muddiman, D. C. *Analytical Performance of a Venturi Device Integrated into an Electrospray Ionization Fourier Transform Ion Cyclotron Resonance Mass Spectrometer for Analysis of Nucleic Acids*. Anal Chem **76**, 4118-4122 (2004).
245. Belov, M. E. et al. *Initial implementation of an electrodynamic ion funnel with Fourier transform ion cyclotron resonance mass spectrometry*. J Am Soc Mass Spectrom **11**, 19-23 (2000).
246. O'Connor, P. B. *Considerations for design of a Fourier transform mass spectrometer in the 4.2 K cold bore of a superconducting magnet*. Rapid Commun Mass Spectrom **16**, 1160-1167 (2002).
247. Dodonov, A. et al. *A new technique for decomposition of selected ions in molecule ion reactor coupled with ortho-time-of-flight mass spectrometry*. Rapid Commun Mass Spectrom **11**, 1649-1656 (1997).
248. Belov, M. E. et al. *Design and performance of an ESI interface for selective external ion accumulation coupled to a Fourier transform ion cyclotron mass spectrometer*. Anal Chem **73**, 253-261 (2001).

249. Campbell, J. M., Collings, B. A. & Douglas, D. J. *A New Linear Ion Trap TIme-of-Flight System with Tandem Mass Spectrometry Capabilities*. Rapid Commun Mass Spectrom **12**, 1463-1474 (1998).
250. Kellerbauer, A., Kim, T., Moore, R. B. & Varfalvy, P. *Buffer gas cooling of ion beams*. Nucl Instr and Meth A **469**, 276-285 (2001).
251. Lunney, M. D. & Moore, R. B. *Cooling of mass-separated beams using a radiofrequency quadrupole ion guide*. Int J Mass Spectrom Ion Proc **190/191**, 153-160 (1999).
252. Senko, M. W., Hendrickson, C. L., Emmett, M. R., Shi, S. D. H. & Marshall, A. G. *External accumulation of ions for enhanced electrospray ionization Fourier transform ion cyclotron resonance mass spectrometry*. J Am Soc Mass Spectrom **8**, 970-976 (1997).
253. Voyksner, R. D. & Lee, H. *Investigating the Use of an Octupole Ion Guide for Ion Storage and High-pass Mass Filtering to Improve the Quantitative Performance of Electrospray Ion Trap Mass Spectrometry*. Rapid Commun Mass Spectrom **13**, 1427-1437 (1999).
254. Wang, Y., SHi, S. D. H., Hendrickson, C. L. & Marshall, A. G. *Mass-selective ion accumulation and fragmentation in a linear octopole ion trap external to a Fourier transform ion cyclotron resonance mass spectrometer*. Int J Mass Spectrom **198**, 113-120 (2000).
255. Belov, M. E., Nikolaev, E. N., Alving, K. & SMith, R. D. *A new technique for unbiased external ion accumulation in a quadrupole two-dimensional ion trap for electrospray ionization Fourier transform ion cyclotron resonance mass spectrometry*. Rapid Commun Mass Spectrom **15**, 1172-1180 (2001).
256. Håkansson, K., Axelsson, J., Palmblad, M. & Håkansson, P. *Mechanistic studies of multipole storage assisted dissociation*. J Am Soc Mass Spectrom **11**, 210-217 (2000).
257. McDonnell, L. A., Giannakopulos, A. E., Derrick, P. J., Tsybin, Y. O. & Håkansson, P. *A theoretical investigation of the kinetic energy of ions trapped in a radio-frequency hexapole ion trap*. Eur J Mass Spectrom **8**, 181-189 (2002).
258. Sannes-Lowery, K., Griffey, R. H., Kruppa, G. H., P, S. J. & Hofstadler, S. A. *Multipole storage assisted dissociation, a novel in-source dissociation technique for electrospray ionization generated ions*. Rapid Commun Mass Spectrom **12**, 1957-1961 (1998).
259. Sannes-Lowery, K. A. & Hofstadler, S. A. *Characterization of multipole storage assisted dissociation: Implications for electrospray ionization mass spectrometry characterization of biomolecules*. J Am Soc Mass Spectrom **11**, 1-9 (2000).
260. Chernushevich, I. V. & Thomson, B. A. *Collisional cooling of large ions in electrospray mass spectrometry*. Anal Chem **76**, 1754-1760 (2004).
261. Loboda, A. et al. *Novel Linac II electrode geometry for creating an axial field in a multipole ion guide*. Europ J Mass Spectrom **6**, 531-536 (2000).

262. Herfurth, F. et al. *A linear radiofrequency ion trap for accumulation, bunching, and emittance improvement of radioactive ion beams*. Nucl Instr and Meth A **469**, 254-275 (2001).
263. Thomson, B., Jolliffe, C. & Javahery, R. in *Proc 44th ASMS Conf Mass Spectrom and Allied Topics* 1155 (Portland, USA, 1996).
264. Mansoori, B. A. et al. *Analytical performance of a high-pressure radio frequency-only quadrupole collision cell with an axial field applied by using conical rods*. J Am Soc Mass Spectrom **9**, 775 (1998).
265. Wilcox, B. E., Hendrickson, C. L. & A.G. Marshall. *Improved ion extraction from a linear octopole ion trap: SIMION analysis and experimental demonstration, 2002. p. 1304-1312.* J Am Soc Mass Spectrom **13**, 1304-1312 (2002).
266. Hägg, C. & Szabo, I. *New ion-optical devices utilizing oscillatory electric fields. II. Stability of ion motion in a two-dimensional hexapole field.* Int J Mass Spectrom Ion Proc **73**, 237-275 (1986).
267. Tolmachev, A. V., Udseth, H. R. & Smith, R. D. *Modeling the ion density distribution in collisional cooling RF multipole ion guides*. Int J Mass Spectrom **222**, 155-174 (2003).
268. Dawson, P. H. *Quadrupole mass spectrometry and its applications* (ed. Scientific, E.) (New York, 1976).
269. Rama Rao, V. V. K. & Bhutani, A. *Electric hexapoles and octopoles with optimized circular section rods*. Int J Mass Spectrom **202**, 31-36 (2000).
270. Dahl, D. A. *SIMION for the personal computer in reflection*. Int J Mass Spectrom **200**, 3 (2000).
271. Jarrold, M. F. *Peptides and proteins in the vapor phase*. Annu Rev Phys Chem **51**, 179-207 (2000).
272. Tolmachev, A. V., Udseth, H. R. & Smith, R. D. *Radial stratification of ions as a function of mass to charge ratio in collisional cooling radio frequency multipoles used as ion guides or ion traps*. Rapid Commun Mass Spectrom **14**, 1907-1913 (2000).

Summary

Understanding a living biological system requires understanding of knowing how different biomolecules work together in the organism. In order to understand the ongoing processes that take place in a biological system, an experiment that provides chemical, spatial as well as temporal information would be ideal. However, at this moment there is no instrument or method that gives this information in an one-step experiment.

Currently, fluorescent microscopy is the most used technique to localize biomolecules. Antibodies labelled with a fluorophore or colorant bind to the molecules of interest, which can then be localized by optical microscopy. Combining the chemical specificity provided by the label with the very high spatial resolution and sensitivity of optical microscopy allows localization of different molecular species in cells and tissue sections.

Although fluorescence microscopy is a widely used technique, in imaging experiments it has a major drawback, which is the limited amount of known molecules that can be analysed in a single experiment. Furthermore, using labels to obtain chemical specificity makes it difficult to specifically target posttranslational modifications and these labels might interfere with the natural behaviour, and thus localization, of the molecules under investigation.

Imaging mass spectrometry (IMS) provides unique chemical specificity and the possibility to map the distribution of multiple, unknown compounds in a single experiment without labelling. As any technique, IMS has its own challenges. Significant progress has been made in improving the speed and spatial resolution of IMS. Now, methodological and instrumental improvements are moving towards developments that give not only information about chemical specification but also chemical identification. In this context, new instrumentation and methods for IMS are described in this thesis.

Summary

Chapter 1 introduces imaging mass spectrometry as an alternative technique to the traditional imaging techniques for the study of different compounds in biological tissue sections. Proteins represent an important class of molecules in any biological system. In order to gain understanding of many biological processes it is necessary to obtain information about the structure, function, identity, quantity, spatial localization and temporal changes of proteins. Mass spectrometry established itself as an important tool in proteomics. Now, the development of spatially resolved mass spectrometry combined with compound identification could answer new biological questions. Nevertheless, new challenges have to be further addressed.

To introduce IMS, ionisation techniques and instruments related to IMS are described in this chapter. Different ionisation techniques are used depending on the type of application. In IMS, matrix-assisted laser desorption ionisation (MALDI) and secondary ion mass spectrometry (SIMS) are the methods mainly used. In SIMS, the sample is bombarded with high-energy primary ions resulting in ion desorption. The primary ion beam is rastered over de sample surface, recording a mass spectrum at every point (microprobe mode). The resulting high-resolution image (50 – 100 nm) is constructed after the data acquisition. SIMS is limited to imaging of low molecular weight species due to the extensive fragmentation that takes place during the bombardment with high-energy ions. To increase the mass range, different techniques, briefly discussed in this chapter, have been developed.

MALDI is a soft ionisation technique. The analyte is dissolved in a suitable matrix that absorbs the energy of the laser used to illuminate the sample. For MALDI imaging experiments not the laser is rastered over the surface but the sample stage is moved in the laser field. The spot size of the laser can be between 50 to 200 µm resulting in an image resolution significantly lower than in SIMS experiments. In order to improve the obtainable spatial resolution in MALDI, microscope mode experiments are performed. In this stigmatic ion imaging mode, specially modified ion optics are used to retain the original spatial distribution of the ions during time of flight analysis, after which

the ions arrive at their conjugate image points on a 2D position sensitive detector. In microscope mode imaging, the spatial resolution depends on the quality of the ion optics and the detector.

Another (new) ionisation technique which is used in this thesis is desorption electrospray ionisation (DESI). DESI in principle requires no sample preparation and is used under ambient conditions. Here, charged droplets and ions of solvent are electrosprayed onto the sample surface resulting in desorption and ionising of analyte molecules.

In IMS, the need for analyte identification becomes more and more important. Currently there are several different approaches for chemical identification. In this regard, mass accuracy and the possibility to perform different forms of ion fragmentation is important. Time-of-flight (TOF) instruments are mainly used in IMS because of their speed and high spatial resolution capabilities. In this thesis, Fourier transform ion cyclotron mass spectrometry (FTICR-MS) is introduced as an IMS technique. FTICR-MS is shown to be important in IMS because of the added information obtained about the compounds of interest. In this respect the FTICR-IMS data acquisition and analysis is as important as instrumental developments and improvements in this direction are discussed.

Chapter 2 is dedicated to FTICR-MS mass spectrometry. Principles of operation and how this instrument can position itself in IMS are described. FTICR-MS provides a very good mass resolution and accuracy as well as many different types of fragmentation. FTICR-MS cannot provide the spatial resolution as is obtained with TOF instruments, however it can be used as a complementary technique in IMS. The benefits and the drawbacks of this instrument in IMS are discussed in this chapter.

In order to achieve our goal, a novel workflow-based data acquisition and control system for FTICR-MS was developed. In **Chapter 3** new software is presented, which allows flexibility in experimental design and decisions to be made on-the-fly. Sequence, evaluation, decision and visual viewer modules are presented. To demonstrate the benefit of the modular build software, different

experiments with standard peptides are performed. An advantage of the modular build software is that it allows external control, such as the movement of the sample stage, by implementing a module that reads the external output. A desorption electrospray ionisation (DESI) experiment was described showing the use of this method in imaging experiments. Furthermore, novel experiments were implemented in the workflow where on-the-fly decisions are made in order to switch dynamically between different fragmentation techniques. Using complementary fragmentation techniques increased the chance of compound identification. A last example shows that our software allows on-the-fly decisions in LC-MS-based quantitative proteomics, e.g. the selection of labeled peptides followed by targeted fragmentation of the peptides that exceed a user-defined abundance ratio.

In **Chapter 4**, an FTICR-IMS experiment on rat brain tissue is described. An evaluation of the use of FTICR is made and possible improvements are assessed. A comparison between an FTICR-MS and stigmatic TOF imaging experiment is shown. The high mass resolution of FTICR-MS allowed to differentially localize compounds with very small mass difference. This could not be done using the lower mass resolution TOF instrument. To reduce the measuring time, FTICR-MS imaging should be restricted to analysis of areas of interest that can be pre-selected after an imaging measurement with faster imaging techniques. Imaging of small areas of interest combined with MS/MS analysis makes this approach valuable, thus complementing the high spatial resolution stigmatic TOF imaging approach.

Running an imaging experiment with FTICR-MS creates a very large amount of data. The higher the mass resolution of the experiment, the longer the acquisition and post-processing time. To deal with gigabytes of raw data a new approach for automatic parallel processing in a distributed computing environment is developed. In **Chapter 5** this approach is demonstrated for large nanoLC (liquid chromatography)-FTICR-MS datasets. The speed benefits are not the only advantage of using this approach. The storage of raw data combined with the use of the parallel processing strategy allows the reprocessing of the

same set of data with different parameters (e.g. noise reduction, apodisation, calibration). This strategy, shown for LC-FTICR-MS data sets of cerebral spinal fluid samples, is also applicable for FTICR imaging experiments.

The final result of all the described developments will be the implementation of a switchable double source (ESI/MALDI) on the FTICR-MS instrument for combined high throughput proteomics and IMS. In **Appendix 1** the design and the results of a high performance linear accumulation octopole with enhanced ejection capabilities is presented. The octopole designed presented here, increased the measurement sensitivity by a factor of two. The implementation of the octopole was the first step in the development of our instrument in order to combine the existing ESI (electrospray) with imaging FTICR-MS.

De samenvatting

Het begrijpen van een levend biologisch systeem vereist begrip van hoe verschillend biomoleculen in het organisme samenwerken. Om de aanhoudende processen te begrijpen die plaats vinden in een biologisch systeem, zou een enkel experiment dat zowel de chemische compositie, de ruimtelijke informatie als de veranderingen in de tijd weergeeft ideaal zijn. Nochtans, is er geen instrument of methode die deze informatie in een een-stapexperiment geeft.

Momenteel is fluorescentie microscopie de meest gebruikte techniek om biomoleculen te lokaliseren. Antistoffen etiketteren met een fluorophore of kleurstof binden met de moleculen van belang, die dan door optische microscopie kunnen worden gelokaliseerd. Het combineren van de chemische specificiteit van het etiket met de zeer hoge ruimtelijke resolutie en gevoeligheid van optische microscopie maakt de lokalisatie van verschillende moleculen in cellen en weefsel mogelijk.

Hoewel fluorescentiemicroscopie een veel gebruikte techniek is in beeldexperimenten heeft het een aantal belangrijke nadelen. Ten eerste moeten de te onderzoeken moleculen bekend zijn en kunnen er maar een beperkt aantal in een enkel experiment worden geanalyseerd. Daarnaast is het moeilijk om posttranslationele wijzigingen te detecteren en zouden de etiketten het natuurlijke gedrag en dus de lokalisatie, van de moleculen onder onderzoek kunnen beïnvloeden.

Beeldmassaspectrometrie (IMS) verzorgt unieke chemische specificiteit en de mogelijkheid om de distributie van een veelvoud aan onbekende moleculen in een enkel experiment in kaart te brengen zonder te etiketteren. Als techniek heeft IMS zijn eigen uitdagingen. Beduidende vooruitgang is al gemaakt in het verbeteren van de snelheid en ruimtelijke resolutie van IMS. Momenteel bewegen methodologische en instrumentale verbeteringen richting ontwikkelingen die niet alleen informatie over chemische specificatie geven maar

ook chemische identificatie. In deze context worden nieuwe instrumentatie en methoden voor IMS beschreven in dit proefschrift.

Hoofdstuk 1 stelt beeldmassaspectrometrie voor als een alternatieve techniek voor de de studie van verschillende moleculen in biologische weefsels. Eiwitten vertegenwoordigen een belangrijke klasse moleculen in biologische systemen. Om de vele biologische processen te kunnen begrijpen is het noodzakelijk om informatie over de structuur, functie, identiteit, hoeveelheid, ruimtelijke lokalisatie en veranderingen in de tijd van eiwitten te verkrijgen. Massa spectrometrie heeft zichzelf gevestigd als een belangrijk werktuig in proteomics. Nu wordt met de ontwikkeling van ruimtelijk opgeloste massa spectrometrie plaats bepaling gecombineerd met moleculaire identificatie wat nieuwe wegen opent om biologische vragen te beantwoorden. Niettemin moeten nog altijd veel uitdagingen aangepakt worden.

Om IMS voor te stellen worden ionisatietechnieken en instrumentatie welke betrekking hebben op IMS beschreven in dit hoofdstuk. Verschillende ionisatietechnieken worden gebruikt, afhankelijk van het soort toepassing. In IMS matrix-geassisteerde laser desorptie ionisatie (MALDI) en secundaire ionen massa spectrometrie (SIMS) zijn de meest gebruikte methoden. In SIMS wordt het monster gebombardeerd met hoog energetische primaire ionen wat resulteert in ion desorption. De primaire ionenbundel wordt over het monsteroppervlak gerasterd, en registreert een massa spectrum op ieder punt (microprobe modus). Het resulterende hoge resolutiebeeld (50 – 100 nm) wordt opgebouwd na het verzamelen van al de gegevens. SIMS is gelimiteerd tot de analyse van moleculen met een laag moleculaire gewicht, tengevolge van de extreme fragmentatie die plaats heeft tijdens het bombardement met hoog energetische ionen. Om het massabereik toe te laten nemen zijn verschillende technieken ontwikkeld welke kort worden besproken in dit hoofdstuk..

MALDI is een zachte ionisatietechniek. Het monster wordt in een geschikte matrix opgelost om de energie van de laser te absorberen. Voor MALDI beeldexperimenten wordt niet de laser gerasterd over het oppervlakte, maar wordt het monster oppervlak door het laserveld bewogen. De afmeting

van de laserspot kan tussen de 50 en 200 µm zijn, wat resulteert in een beeldresolutie beduidend lager dan in SIMS experimenten. Om de ruimtelijke resolutie in MALDI te verbeteren, worden microscoopmodus experimenten verricht. In deze gestigmatiseerde ion beeldmodus wordt speciale ionen-optiek gebruikt welke de oorspronkelijke ruimtelijke distributie van de ionen tijdens de vluchtanalyse, intact houdt en de ionen aan hun gekoppelde beeldpunt op een 2D positie gevoelige detector afbeeldt. In microscoopmodus, hangt de ruimtelijke resolutie af van de kwaliteit van de ionen optiek en de detector.

Een andere (nieuwe) ionisatietechniek die in dit proefschrift wordt gebruikt is desorptie electrospray ionisatie (DESI). DESI vereist in principe geen monstervoorbereiding en wordt onder omgevings omstandigheden gebruikt. Hier worden geladen druppeltjes en ionen van oplosmiddel op het monsteroppervlakte gesprayed wat in desorptie en ionisatie van monster moleculen resulteert.

In IMS wordt de noodzaak aan molecuul identificatie steeds belangrijker. Momenteel zijn er enkele verschillende benaderingen voor chemische identificatie. Hier is massa nauwkeurigheid en de mogelijkheid om verschillende manieren van ionen fragmentatie te verrichten belangrijk. Vluchttijd (TOF) instrumenten worden hoofdzakelijk gebruikt in IMS wegens hun snelheid en hoge ruimtelijke resolutiecapaciteiten. In dit proefschrift wordt transformatie Fourier ioncyclotron massa spectrometrie (FTICR-MS) geïntroduceerd als een IMS techniek. Aangetoond wordt dat FTICR-MS belangrijk is in IMS vanwege de aanvullende moleculaire informatie die verkregen wordt. In dit geval is de FTICR-IMS gegevensverzameling en analyse even belangrijk als instrumentele ontwikkelingen en verbeteringen in deze richting worden besproken.

Hoofdstuk 2 wordt aan FTICR-MS gewijd. Principes van operatie en de plaats van dit instrument in IMS worden beschreven. FTICR-MS heeft een heel goede massaresolutie en massa nauwkeurigheid evenals vele verschillende soorten fragmentatie. Met FTICR-MS kan niet dezelfde ruimtelijke resolutie worden verkregen als met TOF instrumenten, echter het kan worden gebruikt

als een complementaire techniek in IMS. De voordelen en de nadelen van dit instrument in IMS worden in dit hoofdstuk besproken.

Om ons doel te bereiken hebben we een nieuwe workflow gebaseerde gegevensverzameling en controlesysteem voor FTICR-MS ontwikkeld. In **Hoofdstuk 3** wordt nieuwe software geïntroduceerd, met hoge mate van flexibiliteit in experimenteel ontwerp en die toestaat beslissingen 'on-the-fly' te maken. Sequentie, evaluatie, beslissing en visuele modules worden beschreven. Om het voordeel van de modulaire software te demonstreren worden verschillende experimenten met standaard peptides verricht. Een voordeel van de modulaire software is dat het controle van buiten, zoals de beweging van het monster oppervlak, toestaat door een module die de uitwendige output leest. Een desorptie electrospray ionisatie (DESI) experiment wordt beschreven om het gebruik van deze methode in beeldexperimenten aan te tonen. Verder worden nieuwe experimenten in de workflow uitgevoerd waar 'on-the-fly' beslissingen worden gemaakt om dynamisch tussen verschillende fragmentatie technieken te schakelen. Met complementaire fragmentatie technieken neemt de kans op molecuul identificatie aanzienlijk toe. Een laatste voorbeeld toont aan dat de software 'on-the-fly' beslissingen in LC-MS gebaseerde kwantitatieve proteomics toestaat. Hier worden alleen de geëtiketteerde peptiden die een vooraf opgegeven abundantie verhouding overschrijden geselecteerd voor fragmentatie.

In **Hoofdstuk 4** wordt een FTICR-IMS experiment op rattenbrein weefsel beschreven. Een evaluatie van het gebruik van FTICR wordt gemaakt en mogelijke verbeteringen worden bepaald. Een vergelijking tussen een FTICR-MS en gestigmatiseerd TOF-MS beeldexperiment wordt getoond. De hoge massa resolutie van FTICR-MS stond differentie toe van verschillende moleculen met een heel klein massaverschil. Dit zou niet kunnen worden gedaan met de lagere massaresolutie van een TOF instrument. Om de meettijd te verminderen, zou FTICR-MS in beeldexperimenten moeten worden beperkt tot kleine gebieden van belang die worden geselecteerd na een volledig beeldexperiment met een snellere techniek. Beelden van kleine gebieden van belang gecombineerd met

MS/MS analyse maakt deze techniek zeer interessant en is een aanvulling op de hoge ruimtelijke resolutie gestigmatiseerde TOF beeldbenadering.

Het uitvoeren van een beeldexperiment met FTICR-MS creëert een heel grote hoeveelheid gegevens. Hoe hoger de massaresolutie van het experiment, hoe langer de data acquisitie en verwerking tijd. Om met gigabytes aan ruwe data om te kunnen gaan is een nieuwe benadering voor automatisch parallelprocessing in een verdeelde berekenomgeving ontwikkeld. In **Hoofdstuk 5** wordt deze benadering voor grote nanoLC (vloeibare chromatografie) FTICR-MS datasets gedemonstreerd. De toegenome snelheid is niet het enige voordeel van gebruik van deze benadering. De opslag van ruwe data gecombineerd met het gebruik van de parallelprocessing strategie staat het opnieuw porcessen van dezelfde gegevens met veranderde parameters (b.v. geluidreductie, of calibratie) toe. Deze strategie, aangetoond aan de hand van LC-FTICR-MS data van cerebraal ruggegraat vloeistof monsters, is ook toepasbaar voor FTICR beeldexperimenten.

Het eindresultaat van al de beschreven ontwikkelingen zal de implementatie van een verwisselbare dubbele ionisatiebron (ESI/MALDI) op het FTICR-MS instrument, voor gecombineerde hoge verwerkingscapaciteit proteomics en IMS, zijn. In **Aanhangsel 1** wordt het ontwerp en de resultaten van een hoge prestatie lineaire accumulatie octopole met versterkte uitstoot capaciteiten voorgesteld. Het octopole ontwerp hier gepresenteerd, vergrootte de gevoeligheid met een factor van twee. De uitvoering van de octopole was de eerste stap in de ontwikkeling van ons instrument om de bestaande ESI (electrospray) met beeld FTICR-MS te combineren.

Acknowledgments

In the end, I would like to thank many people for their support during my PhD. I do not know what this thesis and my life during PhD would have been without you all. I remember every one of you as I write this final piece. I feel very emotional now when so many memories are running in front of my eyes. I will try to thank all the people who meant something to me in the last 4-5 years at AMOLF. I hope I do not forget any of you here.

Firstly, I would like to thank my promoter, Ron. I would not be where I am now without you. Ron, you are a very positive person, full of ideas and enthusiasm. This was very important for me and not only for my work. Whenever somebody needs to learn more, start, change or drop projects you have shown flexibility and trust. And this was great. This is the way in which science benefits and people discover who they are. Working here has helped me discover myself and to improve my knowledge. For all these I thank you.

A group doesn't mean anything without its members. Thus, I want to thank here many people I worked with. I will start by thanking Liam, who was more than just a co promoter of my thesis. He was here from my first workday. He helped me with almost all the projects I was involved in. His scientific and English knowledge was very important for me and I do not want to count in percentages how much he meant for my development here in AMOLF, but it is a LOT.. Liam was not only my colleague but also my friend. Living in Amsterdam was not always easy for me. I have to thank a few people (most of them not here anymore) for making my life what it is now. And I want to say: you are one of them. Thank you Liam for everything.

I realize now, if I go on with acknowledging everyone on my list in every paragraph, I'll need to write another thesis! Hence I'll continue as follows.

Yuri and Andreas. Another two people I was working closely with during my PhD. We had projects and tasks to share and many times it was not easy ☺. Although you are not here in AMOLF anymore, we are still in contact and not

only for work reasons. This means that in the end everything was a SUCCESS. Part of the work we three shared, involved Theo and Lennard from Erasmus MS in Rotterdam who provided us with biological samples, data, advice.... So, here I take the opportunity to acknowledge the people from Rotterdam. I also want to thank some people from Bruker, especially to Goekhan and Jens, whom I'm indebted to for spending sleepless nights to help me finish the imaging experiments. Because I am acknowledging our collaborators, I also have to mention here all the visitors from Moscow we were working with. Although none of those results is presented in this thesis, I would like to say that it was a very useful experience for me. I learnt a lot and I had a good time with you all. I also want to thank Zoltan Takats who spent a few weeks with us to set the DESI experiments. Furthermore, I would like to thank Pete O'Conner for the advice he gave us regarding our AWG software and the building of the MALDI/ESI source and for providing us with the parts of this source.

Now my special thanks to Marc. I can say that you really helped me in all my projects. People were coming and leaving AMOLF, but you were always in the FTMS lab. It was a pleasure to work with you. When so many times I was upset and not feeling like going on, the fact that you were there, talking or only listening to me, calmed me down. I think that working with you was very productive. Also many thanks for agreeing to be my paranimf at my thesis defence, together with Janne. Further, I also want to thank Frans. Working with Frans in building instruments is a useful lesson. It is good to have around people so organized and precise as Frans.

People from the design department, E&I and workshop were also very important in my work. Ilya and Dirk-Jan, thank you for advising and helping in designing so many parts of the FTICR for us. I also want to thank ALL the people from the workshop for making our impossible designs take shape into reality. I have to thank many people at the E&I for helping me in my work and especially to Duncan, Idsart, Ton and Ronald for advising, designing and building all the electronics we needed to bring our instruments to life. The two Marcos and Ivo - I especially thank you for developing our software and being so patient with me

bothering them so many times - especially Marco S. Without your help, a lot of what I was working on would have not been possible.

I have to thank many other people from personnel department, the secretaries, actually to all the support departments, which made things go so smooth. And if I do not write your names here is not because I forgot you but you are too many! I also thank the group: Todd, Katrien, Jerre, Gert, Martin, Romulus, Anne, Annelies, Beatrice, Georgiana, Piet, Xinghua, Frank, Lennaert (thanks to you and Avi for helping me in the evening before sending the thesis to the printer), Jaap, Lidwien, Bas, Olga, Aleksey, Luck, Els, Basak, Erika, Ester (not only for being the greatest officemate ever ☺), Andrey, Jonnatan, Liam, Andreas, Yuri, Frans, Maarten and Marc for making my time here not only productive but also enjoyable during coffee breaks, lunches, borrels and outside AMOLF activities. I also want to thank the people from PV for the good time spent together during meetings and all events we organized. And there are more people other than those in the PV and in our group, whom I would like to mention, but due to space constraints I HAVE to keep the list short. I do thank you all for knowing me and for making my life enjoyable here.

I thank my parents, my sister Andreea, my grandparents and all my friends outside AMOLF for bringing colour to my life in Amsterdam and offering me support when I needed it. I want to especially thank Gabriel, who always supported me during all these years in the Netherlands. Thanks for the time we spent together, thanks for everything.

Le multumesc parintilor mei, sorei mele Andreea si bunicilor mei care m-au sustinut in tot ceea ce fac. Le multumesc deasemenea prietenilor mei romani care m-au ajutat de multe ori sa ma simt mai aproape de casa.

Finally, I want to thank Maarten. Thanks for all good discussions we had (not only about work), for your patience and love. I have many things to thank you for and "thank" is not enough or the appropriate word if I refer to you but to be short (I learnt here what efficiency means ☺) and to include as much as I can in one sentence. I thank you for what YOU are and that YOU are.

Ioana

Curriculum Vitae

Ioana Mihaela Barbu was born on 10th of January in 1979 in Calarasi, Romania. She received her baccalaureate degree at theoretical high school Mihai Eminescu in the same town in 1997. She went to study physics at Faculty of Physics, University of Bucharest. In 2001 she completed her education with the research project on comparison of light curves in visible of two supernovae, supervised by Prof. Dr. Mircea Rusu. In 2001 she joined the astrochemistry group, Raymond and Beverly Sackler Laboratory, Leiden University, The Netherlands with an Erasmus international scholarship. Here, under the supervision of Dr. Willem Schutte she worked on laboratory measurements in-situ near infrared and midinfrared spectra of analogs ices for comparison to spectra provided by astronomical objects. In 2002 she started the PhD research on development of both instrumentation and methodology for imaging of (bio)-molecules using Fourier Transform Ion Cyclotron Resonance mass spectrometry at FOM Institute for atomic and molecular physics (AMOLF). This thesis contains the most important results from her research.

This thesis is based on following publications

I.M. Taban, L.A. McDonnell, A. Rompp, I. Cerjak and R.M.A. Heeren, *SIMION analysis of a high performance linear accumulation octopole with enhanced ejection capabilities*, International Journal of Mass Spectrometry, 2005, 244 (2-3), 135-143 (**Appendix 1**)

Y.E.M. van der Burgt, I.M. Taban, M. Konijnenburg, M. Biskup, M.C. Duursma, R.M.A. Heeren, A. Römpp, R.V. van Nieuwpoort and H.E. Bal, *Parallel Processing of Large Datasets from NanoLC-FTICR-MS Measurements*, Journal of American Society of Mass Spectrometry, 2007, 18, 145-151 (**Chapter 5**)

I.M. Taban, A.F.M. Altelaar, Y.E.M. van der Burgt, L.A. McDonnell, R.M.A. Heeren, J. Fuchser and G. Baykut, *Imaging of Peptides in the Rat Brain Using MALDI-FTICR Mass Spectrometry*, Journal of American Society of Mass Spectrometry, 2007, 18, 152-161 (**Chapter 4**)

I.M. Taban, Y.E.M. van der Burgt, M. Duursma, Z. Takáts, M. Seynen, M. Konijnenburg, A. Vijftigschild, I. Attema and R.M.A. Heeren, *A novel workflow control system for FTICR-MS allows for unique on-the-fly data-dependent decisions*, Rapid Communication in Mass spectrometry, 2008, accepted (**Chapter 3**)

I.M. Taban, Bas van Breukelen, Y.E.M. van der Burgt, M. Duursma, A J.R. Heck, Jeroen Krijgsveld and R.M.A. Heeren*, On-the-fly data-dependent decisions in* quantitative proteomic studies, in preparation, 2008 (**Chapter 3**)

Other publications

A.F. Maarten Altelaar, I.M. Taban, L.A. McDonnell, P.D.E.M. Verhaert, R. P.J. de Lange, R.A.H. Adan, W.J. Mooi, R.M.A. Heeren and S.R. Piersma, *High-resolution MALDI imaging mass spectrometry allows localization of peptide distributions at cellular length scales in pituitary tissue sections* International Journal of Mass Spectrometry, 2007, 260 (2-3), 203-211

T.H. Mize, I. Taban, M. Duursma, M. Seynen, M. Konijnenburg, A. Vijftigschild, C.V. Doornik, G.V. Rooij and R.M.A. Heeren, *A modular data and control system to improve sensitivity, selectivity, speed of analysis, ease of use, and transient duration in an external source FTICR-MS*, International Journal of Mass Spectrometry, 2004, 235 (3), 243-253

A. Rompp, I.M. Taban, R. Mihalca, M.C. Duursma, T.H. Mize, McDonnell LA and R.M.A. Heeren, *Examples of Fourier transform ion cyclotron resonance mass spectrometry developments: from ion physics to remote access biochemical mass* spectrometry, European Journal of Mass Spectrometry, 2005, 11 (5), 443-456

A. Römpp, L. Dekker, I. Taban, G. Jenster, W. Boogerd, H. Bonfrer, B. Spengler, R.M.A. Heeren, P.S. Smitt and T.M. Luider, *Identification of leptomeningeal metastasis-related proteins in cerebrospinal fluid of patients with breast cancer by a combination of MALDI-TOF, MALDI-FTICR and nano LC-FTICR MSPROTEOMICS*, Proteomics, 2007, 7 (3), 474-481

R.M.A. Heeren, B. Kaletas, I. M. Taban, L. MacAleese and L. A. McDonnell, *Quality of surface: The influence of sample preparation on MS based biomolecular tissue imaging with MALDI-MS and (ME-)SIMS*, Applied Surface Science, 2008, accepted